TECHNISCHE UNIVERSITÄT MÜNCHEN

Lehrstuhl für Experimentelle Genetik

Development of an osteoblast cell culture system for functional characterization and comparative analyses of mouse models with bone phenotypes and systemic investigation of an *Osteogenesis imperfecta* disease model

Frank Thiele

Vollständiger Abdruck der von der Fakultät Wissenschaftszentrum Weihenstephan für Ernährung, Landnutzung und Umwelt der Technischen Universität München zur Erlangung des akademischen Grades eines

Doktors der Naturwissenschaften

genehmigten Dissertation.

Für

Käte und Erich,

Gudrun, Peter, Monique und Alexander

I. Table of contents

II. Figures and tables

II.I. Figures

II.II. Supplemental Figures

II.III. Tables

II.IV. Supplemental Tables

III. Abbreviation list

Aga2	Abnormal gait 2 (mouse mutant with *Col1a1* mutation)
Aga2^{mild}	*Aga2* mutant with mild phenotype
Aga2^{severe}	*Aga2* mutant with severe phenotype
ABE2	Abnormal behavior 2 (mouse mutant with *Jag1* mutation)
ALP	Alkaline phosphatase
α-MEM	Minimal essential medium alpha
AMP	Adenosine monophosphate
ANOVA	Analysis of variance
ATP	Adenosine triphosphate
AVF	Augmented vector foot
AVL	Augmented vector left
AVR	Augmented vector right
BMC	Bone mineral content
BMD	Bone mineral density
BMU	Basic multicellular unit (bone multicellular / metabolic unit)
bp	Base pairs
BSA	Bovine serum albumin
CMCM	CellyticM reagent with Complete Mini Protease Inhibitor
Col1a1^{Aga2}	Mutated *Col1a1* allele
Col1a1^{WT}	Wild type *Col1a1* allele
CQBM	CellQuanti-Blue reagent with culture medium A
CRTAP	Cartilage associated protein
C_t	Crossing point (cycle threshold)
DAB	3,3'-Diaminobenzidine
DAPI	4'6-diamidino-2'-phenylindole
DMEM	Dulbecco's modified eagle medium
DPD	Deoxypyridinoline
DXA	Dual energy X-ray absorptiometry
ECG	Electrocardiography
ECM	Extracellular matrix
EDTA	Ethylene diamine tetraacetic acid
EF	Ejaction fraction

EGF	Epidermal growth factor
ENU	*N*-ethyl-*N*-nitrosourea
ER	Endoplasmic reticulum
FCS	Fetal calf serum
FDR	False discovery rate
FGF	Fibroblast growth factor
FS	Fractional shortening
GAGs	Glycosaminoglycans
GEO	Gene Expression Omnibus
GMC	German Mouse Clinic
GO	Gene ontology
HBSS	Hank's balanced salt solution
H&E	Haematoxylin and eosin
HSC	Haematopoietic stem cells
HTC	Hypertrophic chondrocytes
ICC	Immunocytochemistry
IGF	Insulin-like growth factor
IHC	Immunohistochemistry
ILD	Interstitial lung disease
LEPRE1	Leprecan
LVEDD	Left ventricular end-diastolic internal diameter
LVESD	Left ventricular end-systolic internal diameter
M-CSF	Macrophage colony-stimulating factor
µCT	Micro computed tomography
MGI	Mouse Genome Informatics
MSC	Mesenchymal stem cells
MV	Matrix vesicle
NCP	Non-collagenous proteins
NTPPPH	Nucleoside triphosphate pyrophosphohydrolase
NTPs	Nucleoside triphosphates
OA	Osteoarthritis
OD	Optical density
OI	*Osteogenesis imperfecta*
pBMD	Partial BMD (excluding skull)

PBS	Phosphate buffered saline
PCR	Polymerase Chain Reaction
PFA	Paraformaldehyde
P_i	Orthophosphate
PNPP	4-Nitrophenylphosphate
pO_2	Oxygen partial pressure
PP_i	Pyrophosphate
pQCT	Peripheral quantitative computed tomography
PTH	Parathyroid hormone
qRT-PCR	Quantitative Reverse Transcriptase Polymerase Chain Reaction
RA	Rheumatoid Arthritis
RANKL	Receptor Activator for Nuclear Factor kappaB Ligand
RFU	Raw fluorescence value
RGD	Amino acid sequence Arg-Gly-Asp
rpm	Rounds per minute
RT	Room temperature
sBMD	Specific BMD (BMD related to body weight)
SD	Standard deviation
SDS	Sodium dodecyl sulfate
SEM	Scanning electron microscopy
SEM	Standard error of the mean
SNP	Single nucleotide polymorphism
SOP	Standard operating procedure
SSC	Standard saline citrate
TEM	Transmission electron microscopy
TGF-β	Transforming growth factor beta
TRAP	Tartrate resistant acid phosphatase
Tris	Tris (hydroxymethyl) aminomethane
VEGF	Vascular endothelial growth factor
WS	Working solution

1. Introduction

Although characterized by a hard and rigid nature, bone is a living organ that, together with cartilage, builds up the vertebrate endoskeleton that is supplemented by ligaments, tendons and muscles. In adult humans, the skeleton consists of 206 bones making up about 12% of total body weight.

1.1. Bone function

Bone is a versatile organ possessing multiple mechanical and metabolic functions [1]. Based on its stiffness and strength, bones hold up the body, provide mechanical integrity for locomotion and serves for attachment of muscles, ligaments and tendons. It protects internal organs (brain, spinal cord, heart and lung as well as pelvic viscera) and is furthermore important to support breathing and for the mechanical aspect of hearing - sound transduction. Due to its composition, bone supports haematopoiesis and regulates mineral homeostasis as it contains 99% of body calcium, 88% of body phosphate and 40-60% total body sodium and magnesium. By serving as a reservoir for these ions, the inorganic matrix helps to maintain their extracellular fluid concentrations within the ranges necessary for physiologic functions, including nerve conduction and muscle contractions as well as important biochemical reactions. Bone furthermore stores fat, regulates acid-base balance by absorbing or releasing alkaline mineral salts and influences detoxification by storing heavy metals and other foreign elements after their removal from the blood.

1.2. Classification of bones

According to their shape, bones can be classified in 5 different types (figure 1) [2]. As implied by the name, (1) long bones appear longish and straight. They are rationed in a mid section termed the diaphysis, followed by a short metaphysis and the ephiphysis are the rounded ends of the long bones. The metaphysis emanates from the ephiphyseal plate (growth plate), which regulates bone growth and becomes ossified after adolescence. Long bones are composed of a pronounced shell of compact bones that are covered with the periosteum. The trabecular portion inside

the bone disappears in the diaphysis during the process of bone growth (described below), leaving behind the central cavity, referred to as medullary cavity, containing the marrow with only walls of spongy bone. Thus, trabecular tissue can only be found inside the epiphysis of adult long bones. Long bones include femur, tibia and fibula of the legs, humeri, radii and ulna of the arms, metacarpals and metatarsals of the hand and feet as well as the phalanges of the fingers and toes.
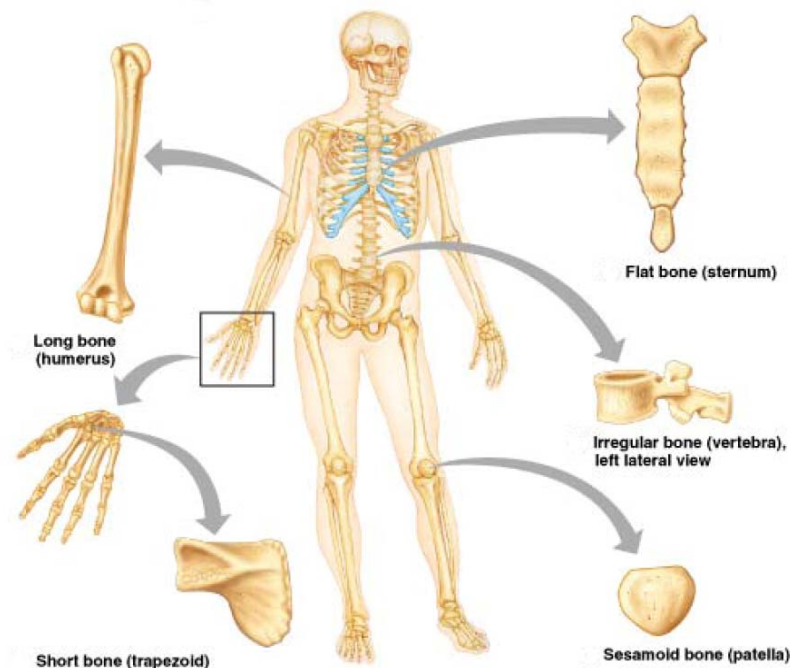
Figure 1. Classification of bones. A sample for each of the 5 different bone types that are classified on the basis of their shape is illustrated. Copyright © 2001 Benjamin Cummings, an imprint of Addison Wesley Longman, Inc.

(2) Short bones (os breve) are nearly cube-shaped and consist of a spongy interior enclosed by a thin layer of compact bone. They are found in the carpals of the wrist and tarsus of the ankle.

Corresponding to their constitution, (3) sesamoid bones are also considered as short bones. However, they feature the characteristic of being embedded in tendons. Thus, they protect the tendon, force its mechanical effect by keeping it more away from the joint to increase the moment arm and prevent the tendon from flattening into the joint. Sesamoid bones can be found in skeletal parts where a tendon passes over a joint, like in the knee (patella), hand (distal of first and second metacarpal bone as well as the pisiform of the wrist) and in the foot (distal of first metatarsal bone).

(4) Flat bones (os planum) are generally curved and appear as broad and flat plates. They are part of the skeleton where extensive protection or broad contact surface for muscle attachment are needed and are composed of two layers of compact bone

tissue enclosing the trabecular portion with the marrow (red bone marrow). Flat bones are the occipital, parietal, frontal, nasal, lacrimal and vomer bones of the skull as well as the hip bone of the pelvis, scapula, sternum and ribs. In the flat bones of the skull, the outer layer of compact bone is thick and robust while the inner layer is thin and more brittle. Moreover, the intervening trabecular bone becomes absorbed, similar to the medullary cavity in long bones.

(5) Irregular bones have a complicated, peculiar shape and can not be grouped into the categories mentioned above. Vertebrae, sacrum and coccyx of the pelvis as well as some bones of the skull (temporal, sphenoid, ethmoid, zygomatic, maxilla, mandible, palatine, inferior nasal concha and hyoid) are classified as irregular bones. They consist of trabecular tissue enclosed with a thin layer of compact bone and fulfil various functions such as protection of the spinal cord (vertebrae) or enable multiple anchor points for skeletal muscle attachment (sacrum).

1.3. Composition and structure of bone

A major part of the bone organ is the mineralized extracellular matrix, termed osseous tissue. Further components are the periosteum and endosteum as well as marrow, blood vessels and nerves [3]. A schematic representation of the macroscopic bone structure is shown in figure 2.

Osseous tissue, also referred to as bone tissue, is a specialized connective tissue that forms the rigid part of the bone and confers stiffness and stability. It consists of an organic matrix (osteoid) that becomes mineralized (see later). Organic components make up ~ 35% and inorganic elements account for ~ 65%. Depending on the texture and overall structure of the bone tissue, two major types can be distinguished. First, cortical bone (compact bone) is formed of multiple stacked layers with few gaps and account for the dense and extremely hard exterior part of the bone organ, making up 80% of total bone mass [3]. Within the cortical bone, osteocytes (see later) are interdispersed in small lacunae and are interconnected via a network of narrow canals (canaliculi). Cortical bone is structurally arranged in small functional units termed osteons (Haversian system), which are arranged in parallel to the long axis of the bone. Each osteon is composed of 4 to 20 concentric lamellae of compact bone tissue arranged around a central canal (Haversian canal) [4]. The area between osteons is occupied by interstitial lamellae, the vestige of resorbed osteons during

bone remodeling. Interconnection of the osteons among each other (between Haversian canals) and with the periosteum is permitted by so called Volkmann's canals, which are perpendicular arranged to the osteons and by canaliculi, which further provide communication between the Haversian canals and the osteocytes [4]. The second type of bone tissue, trabecular bone (cancellous bone or substantia spongiosa), is composed of a network of rod- and plate-like elements and possesses low density and strength but a high surface area. Given the low density, the inner part of the bone forms a central cavity with only walls of spongy bone, thus providing space for blood vessels and marrow. It fills the interior of the bone organ, accounting for the remaining 20% of total bone mass [3].
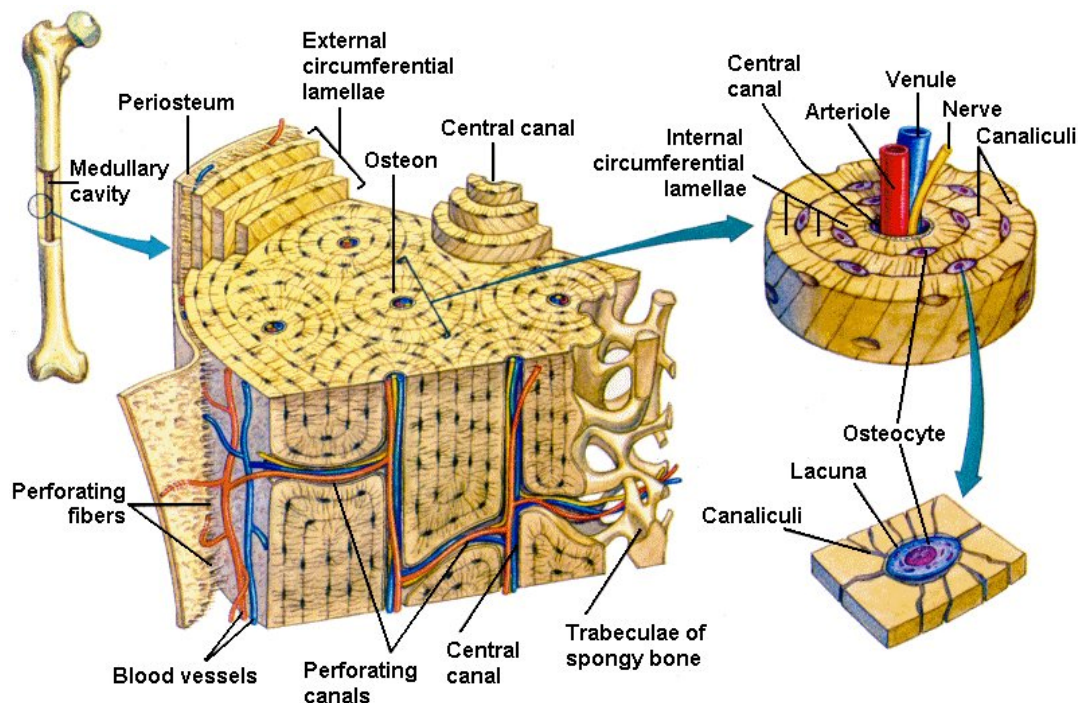
Figure 2. Structural organization of long bones. The cortical part is composed of dense and parallel arranged osteon providing the hard exterior part of the bone. The trabecular area consistes of rod- and plate like elements with low density and strength but high surface area harboring the marrow cavity inside the bone. Osteocytes reside in small lacunae in the bone tissue. The bone is pervaded with blood vessels and nerves. Taken from http://people.uleth.ca/~s.simard/knes2110/Fuzzyimages/osteon%202.jpg.

The bone marrow is stored in between the central cavity of the trabecular portion. It can be classified into (1) red marrow containing the myeloid tissue with haematopoietic stem cells (HSC), (2) yellow marrow mainly consisting of fat and (3) marrow stroma with fibroblasts as well as mesenchymal stem cells (MSC) including developing bone cells.

The outer surface of bones is covered with a vascular membrane termed periosteum, except at joint surfaces, where it is covered with cartilage. Periosteum consists of dense irregular connective tissue divided into an outer fibrous layer containing fibroblasts and an inner cambium layer (osteogenic layer) with progenitor cells developing in bone cells [5]. Similar in morphology and function to the periosteum, the medullary cavity inside the bone is lined with the endosteum. The bone is innervated with nerves and pervaded with blood vessels running in the medullary cavity (trabecular bone) as well as the Haversian canals (Haversian capillaries) and Volkmann's canals in the cortical bone [6].

1.4. Bone cells

There are four different cell types constituting the bone (figure 3). (1) Osteoblasts, (2) osteocytes and (3) bone lining cells account for bone formation. They originate in a linear sequence from mesenchymal stem cells (MSC) via osteoprogenitor and preosteoblast stage to mature osteoblasts, bone lining cells and osteocytes. In contrast, (4) osteoclasts are responsible for bone resorption and descend from haematopoietic stem cells. Development, stimulation and maturation of these bone cells are regulated by cell-cell and cell-matrix interactions, cytokines and growth factors (figure 4 and 5).
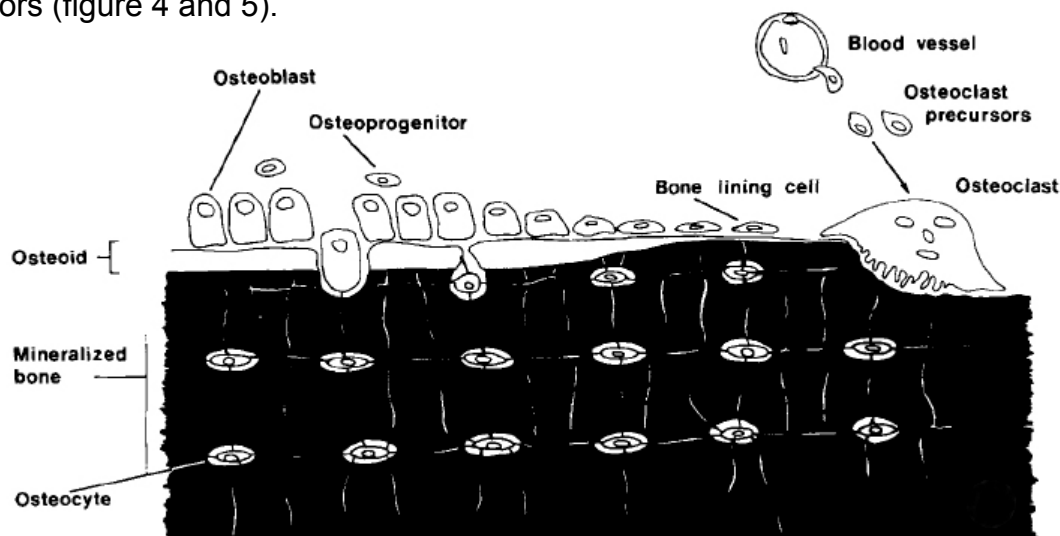
Figure 3. Topographic relationships among bone cells. The bone surface is covered with different cell types. Osteoblasts are responsible for new matrix formation. Bone lining cells are quiescent osteoblasts and osteoclasts are the bone resorbing cells. Inside the mineralized matrix reside osteocytes in small lacune. Taken from [7].

(1) Osteoblasts are fully differentiated cells present on the surface of the osteoid and responsible for matrix production. Hence, osteoblasts possess a typical protein producing cytoplasmic structure with prominent Golgi apparatus and a well developed ER. They secrete different types of collagen (mainly type I) and non-collageneous matrix proteins. Moreover, osteoblasts regulate mineralization of the osteoid by producing ALP, an enzyme important for initiation and regulation of the mineralization process. Many transcription and growth factors mediate commitment, proliferation and differentiation of osteoblasts [8-10]. Figure 4 illustrates the development of osteoblasts from their precursor cells.

Figure 4. Osteoblast differentiation from mesenchymal progenitor cells. Osteoblasts originate from mesenchymal progenitor cells that also give rise to myocytes, adipocytes and chondrocytes depending on stimulation and differentiation factors. MRFs - myogenic regulatory factors (including MyoD, myogenin, myogenic factor 5 and myogenic regulatory factor 4); MEF2 - myocyte enhancer factor 2; C/EBP - CCAAT enhancer binding protein; PPARG - peroxisome proliferator activated receptor g; STAT1 - signal transducers and activators of transcription 1; Runx2 – runt related transcription factor 2; Col I/II/X - type I/II/X collagen; Ihh - Indian hedgehog; BSP - bone sialoprotein; OC - osteocalcin. Taken from [11].

Matrix deposition is normally polarized toward the osteoid surface, but during the process of bone formation, some osteoblasts become trapped and surrounded by the matrix. These cells differentiate into (2) osteocytes, the most abundant cell type of the bone [12, 13]. As mineralization proceeds, they get embedded into the calcified matrix and reside in small lacunae in the bone tissue. They are connected with each other via cellular processes and gap junctions proceeding in small canals termed canaliculi, further connecting them with osteoblasts and vessels. Osteocytes do not entirely fill up the canaliculi and the remaining space is known as periosteocytic space filled with periosteocytic fluid, facilitating exchange of nutrients and metabolic waste. Beside matrix maintenance and calcium homeostasis, osteocytes are also

important for mechanosensing and mechanotransduction, i.e. regulating the response to stress and mechanical load to the bone.

Bone surfaces that undergo neither formation nor resorption are covered with (3) bone lining cells. Considered as inactive osteoblasts, these cells appear flat and elongated with few cytoplasmic organelles. They separate the bone fluids from the interstitial fluids and function as barrier for certain ions [14]. They are thought to regulate the movement of calcium and phosphate into and out of the bone. There is evidence that bone lining cells are precursors for osteoblasts and furthermore, their retraction is a mandatory step in starting osteoclastic bone resorption.

(4) Osteoclasts are as well located at the bone surface but function as bone resorbing cells. As drawn in figure 5, they originate from the monocyte/macrophage lineage after M-CSF and RANKL induced differentiation [15, 16]. Osteoclasts are large and multinucleated cells containing multiple circumnuclear Golgi stacks, a high density of mitochondria and abundant lysosomal vesicles. A high expression of tartrate resistant acid phosphatase (TRAP) and cathepsin K is characteristic for osteoclasts. After attachment to the bone surface, a leakproof membrane compartment for tight surface binding is formed. This sealing zone encases the so-called ruffled border, a specialized infolded membrane domain were resorption takes place, thereby generating resorption pits in the matrix (Howship's lacunae). The ruffled border is composed of microvilli enriched with V-type H^+-ATP_{ases} and chloride channels to secrete hydrochloric acid for dissolving calcium phosphate crystals. Collagens and other organic components are digested by proteolytic enzymes like cathepsin K [17].
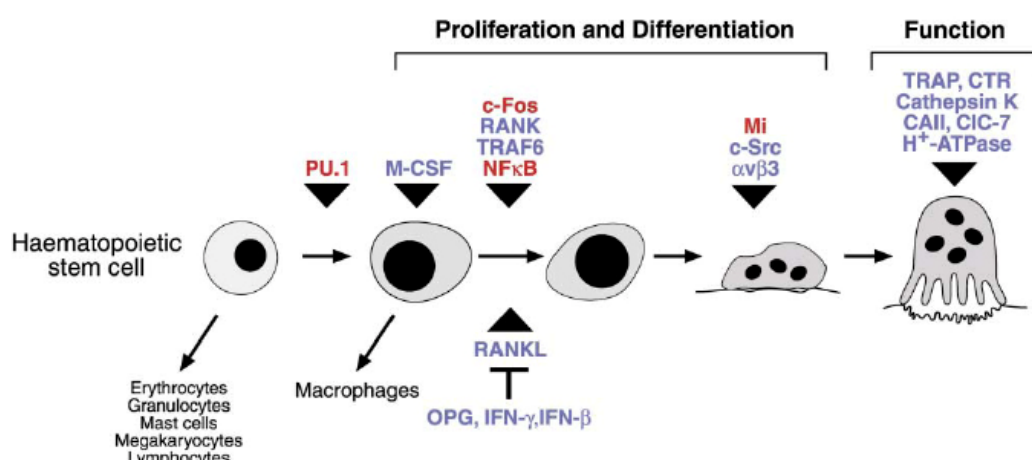
Figure 5. Osteoclast differentiation from haematopoietic stem cells. The individual molecules acting at different stages during precursor development are depicted with transcription factors in red and signaling molecules in blue. CTR - calcitonin receptor; CAII - carbonic anhydrase II; ClC 7 - chloride channel 7. Taken from [18].

1.5. ECM and mineralization of bone

The organic matrix of the bone (osteoid) is composed predominantly of type I collagen (90%) as well as a small amount of non-collagenous proteins (NCP) to about 10% [3]. Type I collagen is essential for bone strength and serves as scaffold for binding other proteins that nucleate hydroxyapatite deposition (mineralization). Non-collagenous proteins can be classified according to their structural basis [19, 20]. (1) Proteoglycans are a special class of glycoproteins consisting of a core protein with covalently attached polysaccharide side chains (glycosaminoglycans – GAGs) that are in most cases sulphated [6]. Four subclasses of proteoglycans are characterized by the nature of the protein core and the GAG side chain. (1a) Chondroitin sulphate side chains are found in biglycan, decorin and versican. (1b) Keratan sulphate side chains occur in fibromodulin and (1c) heparin sulphate side chains in membrane associated proteoglycans like the receptors for TGF-β and FGFs. The (1d) glycosaminoglycan hyaluron belongs to the fourth subclass and is neither sulphated nor attached to a protein core. (2) Gamma carboxy glutamate containing proteins are also major constituents of bone matrix like osteocalcin, matrix Gla protein or protein S. (3) Glycoproteins are posttranslationally modified proteins containing either N- or O-linked oligosaccharides like alkaline phosphatase (ALP), osteonectin or tetranectin. Some of them possess the amino acid sequence Arg-Gly-Asp (RGD) and are therefore termed RGD-containing glycoproteins like thrombospondin, fibronectin, vitronectin, fibrillin or sialoproteins (containing sialic acid like osteopontin (SPP1 / BSP-I), bone sialoprotein (IBSP / BSP-II) or BAG-75). The RGD sequence confers the ability to bind to integrin cell surface receptors, the basis for cell-matrix interactions. (4) Finally, several other NCPs can be found in variable amounts in the bone matrix including serum proteins (e.g. albumin, α-2HS glycoprotein, immunoglobulins), cytokines, chemokines, growth factors, proteolipids as well as enzymes and their inhibitors. The non-collagenous proteins adhere to the matrix and regulate cell attachment, cell proliferation, collagen fibrillogenesis and bone resorption, function as calcium binding proteins and initiate and mediate mineralization [19, 20].

Incorporation of calcium phosphate as hydroxyapatite $Ca_{10}(PO_4)_6(OH)_2$ into the organic matrix lead to mineralization of the osteoid. The crystals are spindle or platelet shaped up to 200 nm in length. Because of the small crystal size and

therefore large surface per weight ratio (10 m^2/g bone), a high proportion of the mineral particles can be exchanged and react with other ions similar in size and charge to Ca^{2+}, PO$_4^{3-}$, OH$^-$. Thus, bone has the ability to incorporate ions as Mg^{2+}, Sr^{2+} or replace OH$^-$ with F$^-$, Cl$^-$ or CO$_3^{2-}$. Indeed, many investigators refer to hydroxyapatite as carbonate-apatite, since carbonate is the most prevalent bone mineral constituent [21]. Other components include calcium carbonate, calcium fluoride and magnesium fluoride. The process of mineralization takes place in distinct stages. The first step comprises an increase of extracellular Ca^{2+} and P$_i$ concentration as well as the amount of NCP and enzymes important for the mineralization process like ALP. ALP hydrolyzes pyrophosphate (PP$_i$) into orthophosphate (P$_i$). It thereby reduces the amount of inhibitory pyrophosphate that antagonizes hydroxyapatite formation and concomitantly increases the amount of P$_i$ needed for the mineralization process [22-24] (figure 6). Extracellular matrix vesicles (MV) rich in ALP bud from the osteoblasts and a milieu conducive for initiation of mineralization is provided. Hydroxyapatite is deposited on initially formed calcium phosphate crystals (nucleation) and additional hydroxyapatite crystals grow on their surface. The organization of the collagenous matrix and NCP determines the orientation and size of the crystal deposition [21].
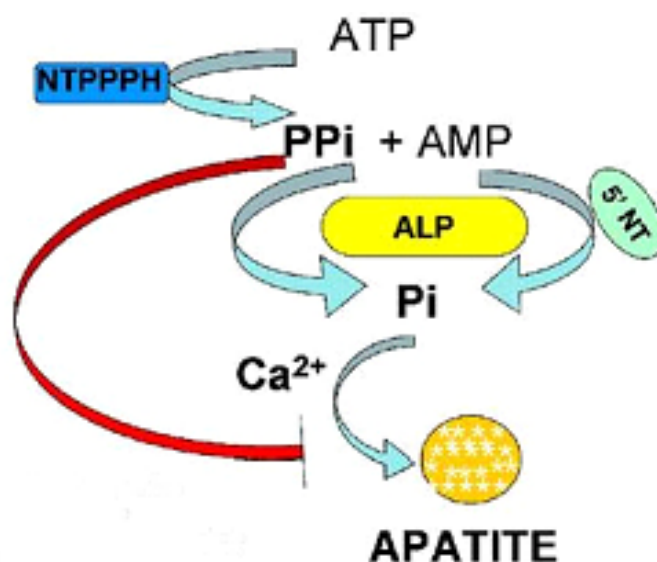
Figure 6. ALP activity for hydroxyapatite formation. Nucleoside triphosphate pyrophosphohydrolase (NTPPPH) catalyzes the hydrolysis of NTPs (for example ATP), thereby producing pyrophosphate (PP$_i$) that antagonizes apatite production. Alkaline phosphatese (ALP) boost the formation of hydroxyapatite by hydrolyzing pyrophosphate and concomitantly provide orthophosphate (P$_i$) which is needed together with Ca^{2+} for mineralization to occur. Taken from [25].

According to the structural organisation of the collagen fibres and the osteocyte ratio, bone matrix can be distinguished as either woven or lamellar [26]. Woven bone is initially laid down during osteogenesis and afterwards gradually replaced by the lamellar structure. Therefore, lamellar organisation occurs in both trabecular and cortical bone. Woven bone (primary, immature bone tissue) forms quickly, but contains a high proportion of osteocytes and a disorganized structure with few randomly oriented collagen fibres making it weak. It is observed in fetal skeleton and in pathological situations like fractures in adults. Lamellar bone (secondary bone tissue) is stronger, possesses a low proportion of osteocytes and is highly organized in osteons containing many parallel arranged collagen fibres. Almost all bones in adults are of lamellar structure, except few places like the sutures of flat bones of the skull.

1.6. Development and formation of bone

Development and formation of bone (ossification) results by either a direct (intramembranous) or indirect (endochondral) process (figure 7). Intramembraneous ossification is characterized by the direct transformation of mesenchymal cells into osteoblasts without prior formation of cartilage [26, 27]. It occurs during fetal development of the skeleton and is also essential during formation of the skull (calvaria, some facial bones and parts of mandible and clavicle) and the initial phase of fracture healing. It leads to the deposition of woven bone, which is later replaced by lamellar bone. Intramembraneous ossification is initiated by replication of MSC that derive from the mesenchyme (embryonal bone formation) or medullary cavity (fracture healing) and aggregate into nodule-like structures (mesenchymal condensation). Once a nodule has been formed, MSCs stop replicating and develop into osteoprogenitor cells with changes in morphology, enlargement of the cell body and increasing amounts of Golgi and ER. The cells begin to synthesize the ECM consisting mainly of type I collagen (osteoid). At this stage, they are referred to as osteoblasts and continue to produce the matrix at the periphery of the nodules or develop into osteocytes when they become incorporated into the osteoid. Mineralization of the growing nodules leads to formation of rudimentary bone tissue that aggregates to build up bone spicules. Bone growth proceeds at the surface of

the spicule by ECM secreting osteoblasts and as the size of the spicule increases, they fuse with each other and become trabeculae.

Interconnection of increasing trabeculae lead to formation of woven bone (primary spongiosa) and the periosteum is formed by differentiating MSCs around the trabeculae. As woven bone is weaker, it can be replaced by lamellar bone at the primary center of ossification between the periosteum and the primary spongiosa, where osteogenic cells increase appositional growth and a bone collar is formed. When the bone collar is mineralized, lamellar bone arise.
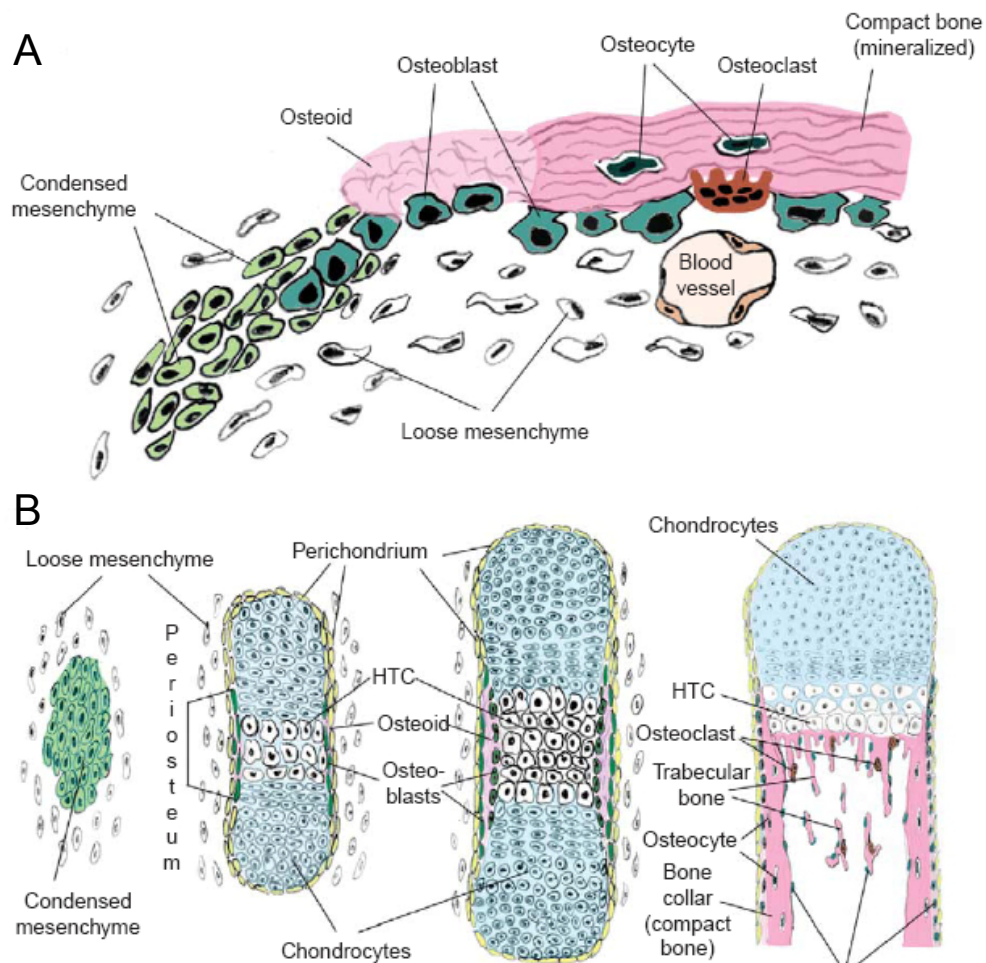
Figure 7. Schematic representation of intramembranous and endochondral bone formation. **A** Intramembranous ossification. Within mesenchymal condensations, osteoblasts differentiate and produce nonmineralized matrix that becomes organized in compact bone with osteocytes entrapped in the mineralized bone matrix. **B** Endochondral ossification. Condensed mesenchyme forms the hyaline cartilage model made of chondrocytes. The perichondrium is formed by mesenchymal cells on the outside and in the middle of this cartilage "anlage" adjacent to hypertrophic chondrocytes (HTC), the first osteoblast precursors differentiate from mesenchymal progenitor cells and form the periosteum. Osteoblasts secrete a non-mineralized ECM (osteoid) that becomes organized into mineralized compact bone. Osteoclasts are required for the formation of the trabecular bone. The cartilage is replaced by bone from the middle of the diaphysis towards the epiphysis. Later, the cartilage of the epiphysis becomes also replaced by trabecular bone. Taken from [28].

During the second type of ossification (endochondral), bone is formed through a cartilage intermediate [26, 27, 29, 30]. It occurs during fetal development of diaphysis from long bones, short bones and irregular bones (primary ossification) and after birth for epiphysis of long bones (secondary ossification). Furthermore, it is important for the replacement of woven bone in the process of fracture healing. As with intramembranous ossification, woven bone is first laid down and replaced by lamellar bone. The initial step is the development of a hyaline cartilage "model" from mesenchymal condensation, which grows in length by replication of chondrocytes, accompanied by secretion of cartilage ECM (interstitial growth). Appositional growth in thickness occurs with development of new chondroblasts from the perichondrium surrounding the cartilage and further deposition of ECM on the periphery. Ossification of the cartilage model occurs in the middle of the cartilage shaft (later diaphysis), the primary ossification center. On the outside, the perichondrium becomes vascularized and develops into the periosteum, containing osteoprogenitor cells that turn into osteoblasts to secrete the osteoid against the shaft of the cartilage model. This appositional growth forms a bone collar which gives rise to cortical bone that is first laid down as woven bone and later replaced by lamellar structure. Inside the primary ossification center, chondrocytes begin to grow (hypertrophic chondrocytes) and secrete ALP, an enzyme essential for matrix mineralization, as well as VEGF (vascular endothelial growth factor), important for vessel formation. After onset of calcification, the hypertrophic chondrocytes undergo apoptosis. Blood vessels sprout out from the perichondrium and invade the cavity left by apoptotic chondrocytes, thereby carrying haematopoietic and mesenchymal stem cells inside the cavity to later form the bone marrow. Migrating osteoprogenitor cells develop to osteoblasts, which use the calcified cartilage as scaffold to secrete osteoid, thereby forming the bone trabecula as woven bone, which becomes later replaced by lamellar structure. Concomitantly, osteoclasts proteolyse the cartilage matrix and degrade the spongy bone to form the medullary cavity. During the progression of the endochondral ossification, the cartilage is replaced by bone from the middle of the diaphysis towards the epiphysis. When the secondary ossification center is formed in the epiphysis, the cartilage - according to the process of primary ossification - is replaced by bone, with spongy bone surrounded by a thin layer of articular cartilage. In contrast to the diaphysis, the spongy bone inside is not degraded but completely fills the epiphysis. Remaining cartilage stays between diaphysis and epiphysis in the

so-called epiphyseal plate (growth plate, growth zone), where growth in length takes place. After the growth period, when skeletal maturity has been completed, proliferation of hypertrophic chondrocytes in the epiphyseal plate also stops and the continuous replacement with bone results in the obliteration of the epiphyseal plate, the closure of the epiphysis. Growth in diameter occurs by deposition of bone beneath the periosteum while osteoclasts in the interior cavity resorb bone until its ultimate thickness is obtained.

1.7. Bone modeling and homeostasis

Once bone has been made, it is not a rigid structure but rebuilt throughout the life, where old bone is removed and replaced with new bone. The factors and parameters determining bone formation and resorption are illustrated in figure 8.
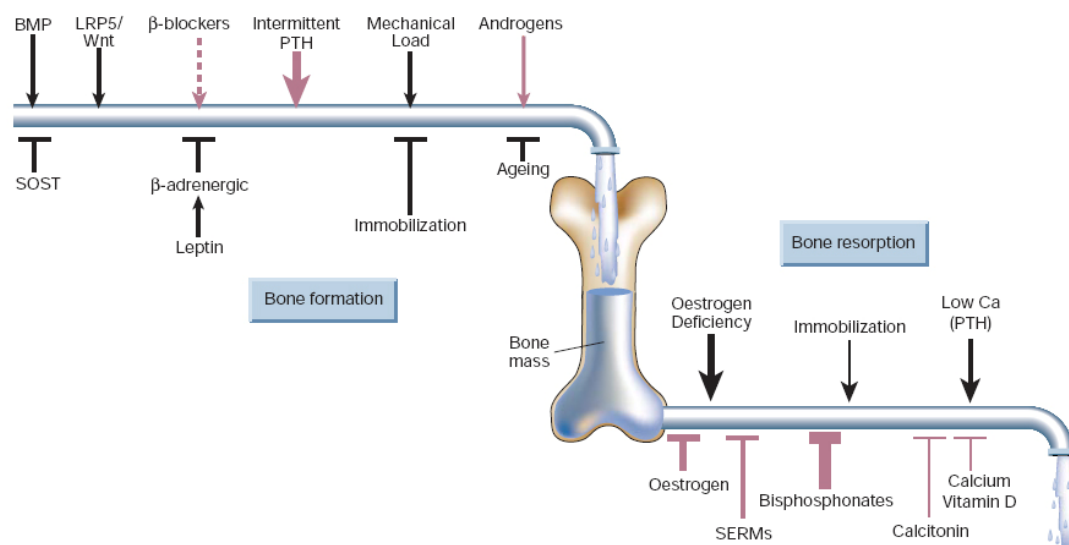
Figure 8. Skeletal homeostasis. Determinants of skeletal homeostasis and bone mass are shown with physiological (black) and pharmacological (red) stimulators and inhibitors. The relativ impact is indicated by the thickness of the arrows. BMP - bone morphogenetic protein(s); SOST - sclerostin; LRP5 - low density lipoprotein (LDL) receptor related protein 5; PTH - parathyroid hormone; SERM - selective oestrogen receptor modulator. Taken from [11].

During childhood and adolescence, this process is called modeling and leads in sum to new net bone formation. In the first year of life, almost all the skeleton is replaced. It enables long bones to increase in diameter, changing shape and developing the marrow cavity. Modeling continues throughout the growth period until peak bone mass has been achieved. Afterwards, during adulthood, the process of bone maintenance is referred to as remodeling (homeostasis) and bone resorption is

equally and optimally balanced by bone formation in healthy skeleton. Approximately 0.7% of human skeleton is resorbed daily and replaced by new bone [31]. It is important for regulation of calcium homeostasis and mineral metabolism, repair of microdamaged bones, replacement and reshaping of bone after injuries and response to functional demands and muscle attachment. Imbalances in regulation of the remodeling process result in many metabolic bone diseases such as osteoporosis. Bone remodeling has important genetic determinants and is furthermore influenced by other factors like hormones, nutritional intake, mechanical forces and diseases. For example, the influence of mechanical load on remodeling is explained by Wolff's law, which states that bone will adapt to increasing load with remodeling to become stronger and more resistant [32]. In the process of bone homeostasis, bone cells are functionally linked via complex regulatory networks in a "basic multicellular unit" (BMU – also termed "bone multicellular unit" or "bone metabolic units") [33, 34]. The skeleton contains millions of these units, which are not permanent structures but forms after stimulation and always undergo the same sequence of function. (1) BMU formation is triggered by mechanical stress or injury and originate in response to hormones and cytokines including PTH, 1,25-dihydroxy-vitamin D, interleukin 6 and 11, estrogens, androgens and prostaglandins. (2) As a single BMU can exist for months but the lifespan of individual cells in between a BMU is much shorter, new cells must be continuously recruited and activated, a process that occurs at the edge of the BMU. The signals come from existing BMU cells, although bone lining cells and osteocytes may participate. (3) Resorption takes place after bone lining cells change their shape and secrete collagenase to expose the collagen matrix and the bone mineral. Thereafter, they attract pre-osteoclasts which fuse into multinucleated osteoclasts and resorb bone. During resorption, bone-derived growth factors that were deposited into the matrix by previous generation of osteoblasts are released like TGF-β, IGF and FGF. These factors recruit osteoblasts which are responsible for (4) new bone formation. Osteoblasts converge at the bottom of the cavity and form the osteoid which becomes (5) mineralized. The osteoblasts continue to form and mineralize osteoid until the cavity is filled and thereafter begin to flatten and cover the surface as quiescent lining cells or differentiate to osteocytes if remaining in the matrix. Figure 9 depicts schematically the process of bone remodeling.
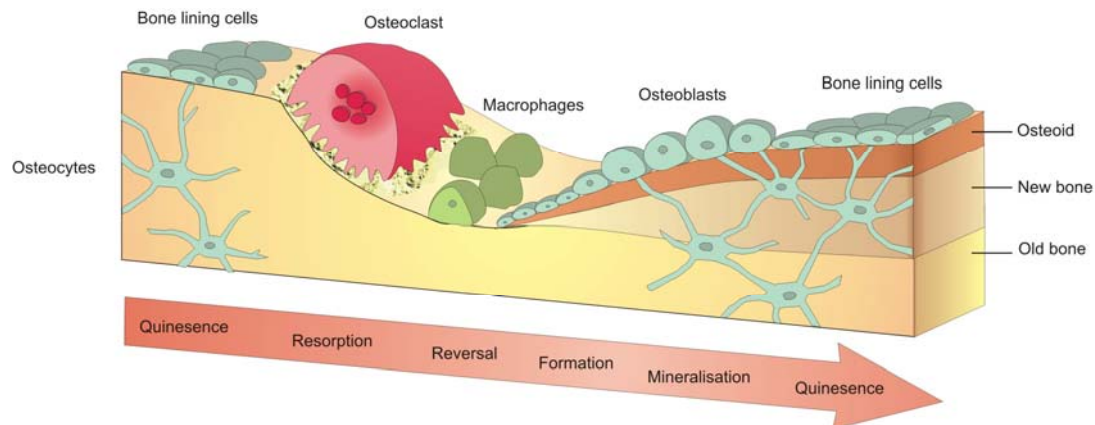
Figure 9. Osteoblasts and osteoclasts during bone remodeling. Bone is continuously remodeled at discrete sites in the skeleton with the involved cells organized in "basic multicellular units" (BMUs). After initiation of the remodeling process, old bone is resorbed by osteoclasts. Thereafter, osteoblast precursors are recruited, proliferate and differentiate into mature osteoblasts to secrete the unmineralized matrix (osteoid). Osteoblasts that become embedded into the newly synthesized matrix differentiate to osteocytes and the surface is covered by new bone lining cells. The matrix mineralizes to generate new bone and this completes the remodeling process. Copyright BTR ©.

1.8. Bone diseases

Given the complex structure and diverse functions of the bone organ, various diseases of the skeletal system are known. Bone disorders can become noticeable by radiographic assessments and morphological alterations or by biochemical, metabolic and hormonal anomalies. They can be acquired or genetically entailed. To cope with the large number of disorders, different classifications have been proposed. For instance, a classification of genetic disorders of the skeleton based on the structure and function of the causative genes and proteins has been suggested [35].The categories encompass defects in (1) extracellular structural proteins, (2) metabolic pathways (including enzymes, ion channels, transporters), (3) folding and degradation of macromolecules, (4) hormones and signal transduction, (5) nuclear proteins and transcription factors, (6) oncogenes and tumor-suppressor genes as well as (7) RNA/DNA processing and metabolism. A more generalized classification of bone diseases [36] distinguishes four categories including alterations in:

(1) patterning (Polydactyly, Syndactyly, Brachydactyly)

(2) metabolism and growth (Rickets, Osteomalacia, OI, Achondroplasia)

(3) modeling and remodeling (Osteopenia, Osteoporosis, Osteopetrosis)

(4) aging and immune system defects (Arthritis, ruptured disks).

(1) Defects in developmental patterning entail malformations of the fingers or toes with supernumerary digits in polydactyly, fusion of digits in syndactyly or shortness of digits in brachydactyly. (2) Alterations in metabolism and growth / mineralization result in growth retardation and bending or fractures of bone. Softening of bone tissue due to defective mineralization is characteristic for patients with a lack of vitamin D or its metabolism and occurs in rickets (childhood) and osteomalacia (adult age). Abnormal collagen metabolism accounts for increased fracture rate and bone deformities in *Osteogenesis imperfecta* (OI), and bone growth anomalies with defects in the growth plate causes Achondrodysplasia, a major cause of dwarfism. (3) Imbalance in bone modeling / remodeling processes causes alterations in bone mass and bone mineral density (BMD), respectively. The bone mineral density T score relates the BMD of a patient to the mean value of healthy control. A decrease of the BMD with a score between -1.0 and -2.5 (SD to control) is considered as osteopenia and a further decrease with scores below -2.5 characterizes osteoporosis. Reduced BMD is either caused by decreased bone formation or increased resorption, leading to a less stable skeleton with pronounced fracture risk. Osteopetrosis is also a bone disease with a dysfunction of the remodeling process, but contrariwise, it is characterized by higher BMD due to functional impairment of osteoclasts with decreased bone resorption. (4) Inflammatory processes that affect the bone are seen in Osteoarthritis (OA) and Rheumatoid Arthritis (RA), the most frequent joint diseases in the world with prevalence of 50% in people over 65 years. OA is a degenerative disease affecting the articular cartilage and subchondral bone, leading to degeneration of the synovium and cartilage in joints of mostly hip and knee, which results in joint pain, tenderness, stiffness and inflammation amongst other symptoms. RA is a chronic, systemic inflammatory disorder affecting many organs but primarily targets multiple joints of hands, feet, wrists, elbows, ankles, shoulders and knees. It results in inflammation of the synovial membrane (synovitis) that often leads to destruction of the articular cartilage and ankylosis of the joints. Cartilage destruction, bone erosion, joint deformity and loss of joint function are common features in RA.

Many skeletal diseases cause long term complications and as the population ages, the economic toll of medical treatment is predicted to increase in the future. Therefore, bone diseases gain importance in research and medicine and a raise of awareness for musculo-skeletal disorders in the society has to be achieved.

1.9. *Osteogenesis imperfecta* – the "brittle bone disease"

Osteogenesis imperfecta is a group of inherited connective tissue disorders also referred to as "brittle bone disease". Skeletal symptoms comprise bone deformities, brittle bones, fractures, low bone mass and osteoporosis (figure 10).
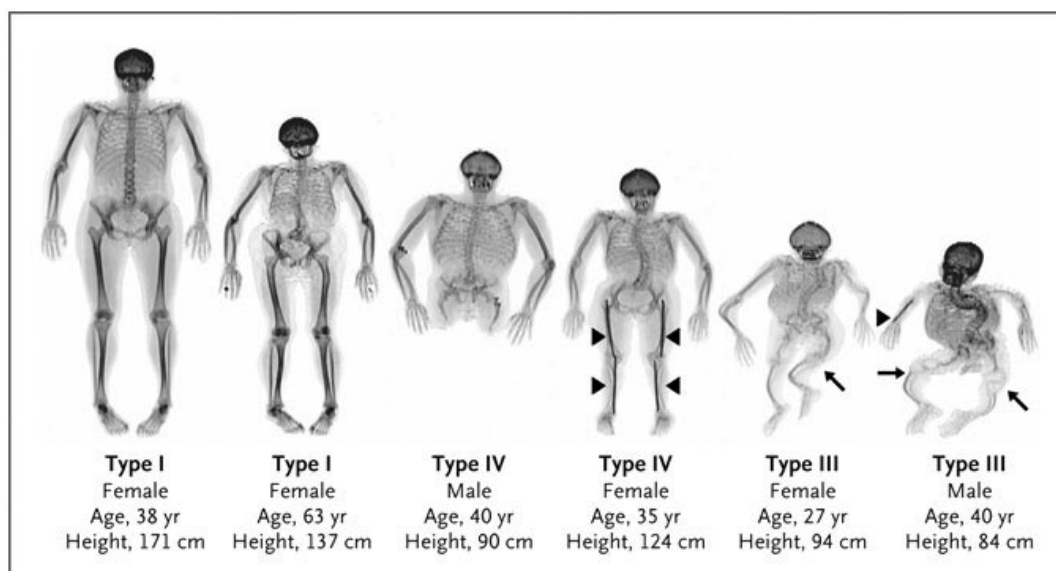
Figure 10. Whole body DXA images of OI patients. The skeletal manifestations varying between the different subtypes of OI from mild abnormalities in type I OI (the 38-year-old female on the left) to severe deformities in type III OI (the 40-year-old man on the right). Most of the patients suffer from scoliosis, one has orthopedic rods in femur and tibia and another has a rod in the radius (arrowheads). Owing to multiple fractures, one underwent the amputation of both legs and typical fragmentation of the epiphyseal growth plates ("popcorn epiphyses") at the knees are evident in two patients (arrows). Type II OI is not shown as it is perinatal lethal. Taken from [37].

Although primarily seen as a bone disorder, further extraskeletal manifestations are associated with the disease. Corneal alterations with blue sclera, joint laxity, hearing loss and *Dentinogenesis imperfecta* (brittle teeth) amongst others point out OI as a more systemic disease [38, 39]. It is the most common heritable cause of skeletal fractures and deformities in humans and in most cases is entailed by autosomal dominant mutations in one of the two genes encoding type I collagen (*Col1a1 / Col1a2*), the most abundantly expressed protein of the extracellular matrix in connective tissues [40, 41].

Recently, mutations in the cartilage associated protein (CRTAP) and leprecan (LEPRE1), two proteins involved in posttranslational modifications of collagen fibrils (3-hydroxylation collagen prolyl residues), have been identified to be associated with recessive forms of OI [38, 42].

Depending on symptoms and severity, human cases are classified in 8 subtypes ranging from mild onset with few fractures in one's lifetime to severe forms with intrauterine fractures and perinatal lethality [42, 43]. Table 1 summarizes typical features and clinical severity of the subtypes including inheritance and known associated mutations. Severity of clinical phenotypes is partly related to the type of mutation, its location in the alpha chains of the type I collagen, the surrounding amino acid sequences and genetic interactions [44]. Generally, N-terminal mutations in *Col1a1 / Col1a2* lead to mild symptoms while core and C-terminal defects result in severe OI phenotypes.

Type	Inheritance	Clinical severity	Typical features	Associated mutations
I	AD	mild	non-deforming, normal height, blue sclera, no DI	null α1(I) allele
II	AD	perinatal lethal	rib and long-bone fractures at birth, pronounced deformities, broad long bones, low density of skull bones, dark sclera	structural defects type I collagen
III	AD	severe	very short, triangular face, severe scoliosis, greyish sclera, DI	structural defects type I collagen
IV	AD	moderate	moderately short, scoliosis, greyish or white sclera, DI (clinically most diverse group)	structural defects type I collagen
V	AD	moderate	mild to moderate short, dislocation of radial head, scoliosis, mineralised interosseous membrane, hypertrophic callus, white sclera, no DI	unknown
VI	AR	moderate to severe	moderately short, scoliosis, mineralization defect (accumulation of osteoid in bone), "fish-scale" lamellae, white sclera, no DI	unknown
VII	AR	severe to lethal	mild short stature, scoliosis, short humeri and femora, coxa vara, white sclera, no DI	CRTAP
VIII	AR	severe to lethal	severe growth deficiency, white sclera, extreme skeletal undermineralization, bulbous metaphyses	LEPRE1

Table 1. *Osteogenesis imperfecta* - Nosology. AD (autosomal dominant), AR (autosomal recessiv), DI (*Dentinogenesis imperfecta*). Adapted from [40] and [42].

As well as the clinical outcome, the mortality varies between the different subtypes. Except for type I, all subtypes of OI are characterized by an increase of the lethality rate with even 100% of intraurine or perinatal mortality in the most severe type II OI [45]. Several studies have been conducted to point out the causes of death in patients with OI and different reasons were found, whereas respiratory and cardiovascular related effects are the most prominent [46]. Pulmonary compromise is the leading cause of death [47], with loss of lung capacity, acute and chronic respiratory failure, pneumonia, bronchitis and other respiratory problems as common

features in patients with OI. Although type I collagen is one of the major collagens in lung and abnormal lung collagen has been thought to provoke respiratory problems, large studies concerning this matter are missing and its involvement is poorly understood. So far, lung problems are considered as secondary effects due to rib fractures and scoliosis [40, 46, 47]. One study suggested effects of abnormal collagen on the lung function in OI, but primary dermal fibroblasts were used for the investigation of the type I collagen synthesis and the lung has not been studied systematically [48].

Also cardiovascular disorders are known complications associated with OI and clinical studies refer to pathological alterations such as aortic root dilatation, valvular insufficiency and atrial septal defects. However, an explanation about the onset of heart failure in patients with OI is wanting or, comparable to lung problems, cardiovascular alterations are thought to be side effects due to skeletal abnormalities like *Kyphoscoliosis* [46]. Type I collagen alterations in heart were previously described in an OI mouse model and type II OI affected fetuses respectively [49, 50], but an association of the encountered collagen defects with the development of heart failure and the higher mortality in OI is missing.

To date, although substantial findings concerning lethality in OI were made, defects in heart and lung are not directly linked to the underlying collagen mutation. Moreover it is important to mention that the causes of death – if described – are considered as asymptomatic and secondary, mostly due to an abnormity of the skeletal phenotype.

1.10. Mouse models for human diseases

Model organisms are widely used to study human diseases and reveal insight into complex genetic traits. Possessing a long history in research, the mouse represents the premier genetic model organism for the study of human diseases and development [51]. One reason favouring the mouse as model organism for studies of human disease is the developmental differences of mammalians compared to lower organisms such as *D.melanogaster* or *C.elegans*. The murine system is characterized by a short generation time (10 weeks) with large litter size and importantly, the mouse genome has been completely sequenced showing a high similarity with 95% homology to the human genome. The genome size is roughly equivalent to the human genome (3×10^9 bp) and nearly all human genes have an

orthologue in the mouse. Furthermore, large segments of synteny occur in the genome of both species, harboring hundreds of genes in the same order and with similar intergenic distances. In the mouse, forward and reverse genetic approaches are readily available and our knowledge regarding polymorphic markers (microsatellites, SNPs), exon-intron structure, restriction enzyme sites and other functional and structural features of the mouse genome increases daily. Therefore, the combination of genetics and genomics in the mouse provides access to molecular mechanisms of complex biological questions [36].

1.11. Mouse models for skeletal disorders

Bone disorders raise complex biological questions and as the skeleton was acquired late during evolution and lower model organisms such as *D.melanogaster* possesses unequal exoskeletal systems, it is necessary to develop disease models using vertebrate organisms such as the mouse. Therefore, beside its relatively unique applicability to genetic studies of immunology, cancer, behavior and mammalian development, the mouse is a valuable model organism for investigation of bone biology, allowing detailed molecular, functional and pathological studies as well as predicting candidate genes for human skeletal disorders [52]. As mutants represent one of the most effective ways to acquire information to a gene's function, various mutant lines with skeletal defects have been developed using either spontaneous or targeted mutagenesis and to date, nearly 3000 genotypes with over 10000 annotations have been listed in the Mouse Genome Informatics (MGI) database for skeletal phenotypes (www.informatics.jax.org). Large scale mouse mutagenesis screens have been conducted to further increase the number of mouse models for human diseases. Reverse genetic approaches have produced mice with gain of function (transgenic) and loss of function (knockout) alleles possessing abnormalities in patterning, bone remodeling and joints [35]. Among forward genetic approaches, ENU mutagenesis is the most powerful method creating mutants [53]. In the Munich ENU mutagenesis screen [54], various mouse mutants have been isolated as models for human diseases, including mice with different bone phenotypes. Among the mutants possessing skeletal abnormalities, phenotypes have been identified resembling Polydactylism, Syndactylism, *Osteogenesis imperfecta*, Achondroplasia, Osteoporosis and Rheumatoid Arthritis amongst others (unpuplished data).

1.12. *Aga2* - a mouse model for *Osteogenesis imperfecta*

A new mouse model for OI has recently been identified in the Munich ENU mutagenesis screen [55]. Due to the first observed phenotype it was referred to as *Aga2* (abnormal gait). A point mutation with a T to A transversion in the intron 50 of the *Col1a1* gene generated a novel cryptic 3' splice acceptor site. The alternative splice transcript possesses a 16 bp elongation with a frameshift of the endogenous stop, predicting 89 new amino acids beyond the original termination position and leading to structural alterations of the mutated type I collagen protein. Given the dominant negative mutation, homozygous animals are embryonic lethal. Heterozygous animals ($Col1a1^{Aga2}/Col1a1^+$) display hallmarks of OI symptoms including multiple fractures in long bone, pelvis and rib cage, scoliosis, reduced body size and an overall decrease in bone mass and density. Furthermore and comparable to clinical heterogeneity in man (see above), heterozygous *Aga2* mice varying in the severity of disease and two different phenotypes can be distinguished. Mildly affected $Col1a1^{Aga2}/Col1a1^+$ mice possess a moderate phenotype and survive to adulthood (herein after referred to as $Aga2^{mild}$). In contrast, severely affected $Col1a1^{Aga2}/Col1a1^+$ animals feature a strong disease pattern and succumb to postnatal lethality (herein after referred to as $Aga2^{severe}$) [55]. In depth analysis of this mouse line has proven *Aga2* to be a good murine model for OI and furthermore, a new pathological mechanism with the involvement of ER stress related apoptosis in the bone tissue was shown [55]. But according to the human situation, the reasons for lethality in the severely affected mice have not been identified so far and are still speculative.

1.13. The German Mouse Clinic

Once a mouse mutant has been established as model system for human diseases or for developmental studies, a comprehensive analysis of the phenotype is as important as the mutagenesis itself to unravel the molecular and pathological alterations that emerge from the genetic modification. The German Mouse Clinic (GMC) offers large scale phenotyping for standardized and comprehensive analysis of mouse mutant lines. Phenotypic investigation is performed in 14 different clinical screens covering allergy, clinical chemistry, cardiovascular analyses, dysmorphology,

immunology, lung function and molecular phenotyping amongst others [56]. The mice are non-invasively analyzed within the primary screen for more than 320 parameters in the various fields and if required, secondary and tertiary tests can be performed in addition for a more detailed characterization of the mutant mice.

The Dysmorphology screen comprises the phenotypic analysis of bone and cartilage [57]. Alterations in skeletal development, growth and mineralization, modeling and remodeling as well as aging and immune system effects can be detected. Anatomical observations together with X-ray analysis and DXA measurements are performed within the primary screen. In case of significant differences between mutant mice and wild type controls, more sophisticated investigations can be done in the secondary screen including µCT and pQCT analysis, three-point bending tests or determination of biochemical markers for bone formation and resorption like Osteocalcin (Bglap1 / OC), Alkaline Phosphatase (ALP), Tartrate-resistent acid phosphatase (TRAP) or deoxypyridinoline (DPD). Thus, the Dysmorphology screen of the GMC provides a comprehensive picture of morphological, structural and clinic chemical alterations of the skeletal system in mutant mice. However, as the deployed methods are of a more descriptive nature, they cannot unravel the cellular and molecular causes of the observed bone alterations as they can either be due to direct alterations of the bone cells (primary effect) or evoked by systemic influences on the bone in terms of hormonal / metabolic dysregulations (secondary effect). Therefore, *in vitro* cell culture studies with osteoblasts might provide a closer look to the cellular phenotype, thus assessing the nature of the bone alteration.

1.14. *In vitro* cell culture

To study the behavior, biochemical pathways and molecular mechanisms at the cellular level independently from systemic influences, the application of tissue culture is the method of choice. At the beginning of the last century, tissue culture came into being with the work of Harrison and Carrel [58, 59] and enabled the investigation of cellular parameters free of variations due to normal homeostasis and / or stress conditions in the animal. Since then, vast progress has been made in developing tissue culture methods and today they are widely distributed and closely related to basic and medical research as well as pharmaceutical drug development and production. Tissue culture is applied in virology, immunology, radiation biology,

cancer research and almost all fields in life science. It is of great importance in clinical diagnostics and biotechnological production of agents for prophylaxis and therapy as well as vaccines and drugs. Furthermore, with the latest developments in stem cell research and tissue engineering, tissue culture will become more and more relevant in regenerative medicine.

Tissue culture generally refers to the growth of eukaryotic cells separate from the organism *in vitro* [60]. It comprises (1) organ culture with *in vitro* cultivation of whole organs to maintain the architecture of the composing structures, (2) explant cultures with *in vitro* cultivation of tissue pieces to either investigate cells left in their surrounding matrix or to isolate them as they outgrow from the explant and (3) cell culture for *in vitro* cultivation of dispersed cells as permanent cell lines or primary cells. Permanent cell lines have originated from eukaryotic tissues and have spontaneously acquired or were treated to exhibit the capacity to perpetually re-divide and are therefore sometimes referred to as immortalized or established cell lines. In contrast, primary cells possess a delimited proliferation capacity and mitotic potential after isolation from the tissue and senescence occurs after few passages *in vitro*. For various research purposes, primary cells are more appropriate than permanent cell lines, as their phenotype matches the *in vivo* situation or is at least closer to that. Cell cultures can be used to assess intracellular activity, gene expression, protein synthesis, energy metabolism, ligand-receptor interactions and signal transduction processes, cell-cell / cell-matrix and cell-environment interactions, differentiation capacity and morphogenesis as well as various other parameters [60]. The uncoupling and disengagement from systemic effects of the whole organism and the possibility to define, control and influence the cultivation conditions are the major advantage of using tissue culture. Thus, biological samples can be kept under identical and well known conditions. Using primary cells from different animals (e.g. mutant and wild type control), their *in vitro* investigation can provide insights into possible cellular and molecular differences of the analyzed cells between both animal groups.

1.15. Goal

I. *In vitro* analysis of osteoblasts

To broaden the phentoyping options of the GMC Dysmorphology Screen and to extend the analysis to the cellular level, a primary cell culture system for osteoblasts should be established. The development and implementation of quantitative assays for various bone relevant parameter should allow for a comprehensive investigation of the cellular phenotype. Thus, the comparison of cells from bone diseased mice and wild type littermates should provide hints for possible cellular and molecular reasons of the bone alteration in the mutants. As the cells are thereby cultivated and investigated identical and uncoupled from systemic influences, one can determine whether cell autonomous (primary) or systemic (secondary) effects are responsible for the bone disease. An SOP for the "*In vitro* analysis of osteoblast" has been developed and is described in detail in Material and Method part 2.1.

II. Heart and lung investigation in the *Aga2* OI mouse model

Osteogenesis imperfecta (OI) is associated with an increased mortality and lung as well as heart alterations have been found to be the main causes of death. However, the cardiopulmonary defects are considered as asymptomatic and secondary due to an alteration of the skeletal phenotype. *Aga2* has recently been described as a new mouse model for OI. Comparable to human cases, mutant mice varying in the aetiopathology with a high mortality in severely affected mutants (*Aga2^{severe}*). To explain the postnatal lethality in *Aga2^{severe}* and to elucidate the pathological and molecular reasons for it, comprehensive and in depth analysis of *Aga2* should be conducted. Given the precognition of cardiac and pulmonary complications in human, heart and lung have been chosen as the most relevant and reasonable organs to be related with the lethality. Thus, investigations on the functional, morphological and molecular level should be performed with heart and lung of *Aga2^{severe}* mice *in vivo* and *in vitro*.

2. Material and methods

2.1. *In vitro* analysis of osteoblasts

2.1.1. General remarks

2.1.1.1. Workflow

The time frame for the complete analysis of the osteoblast phenotype from a mutant line comprises about 5 weeks after birth of the mice (figure 11). Since the characterization of the cellular phenotype is based upon the comparison of mutant cells with wild type controls, the offspring have to be grouped in mutant and wild type animals (e.g. by genotyping) prior to the cell preparation, which is performed after 3-6 days postnatally. The isolated cells are transferred into culture and incubated for 5 days (Pre-culture). Thereafter, the cells are stimulated (referred to as T0) and cultivated for another 21 days under stimulating conditions. The osteoblast phenotype is assessed throughout the whole culture period by taking samples for different cellular assays at 5 different time points (referred to as measurement days T0 / T3 / T9 / T15 / T21). After completing the culture period, the assays are evaluated by analyzing the collected samples (referred to as assay analysis) which takes another 5 days.
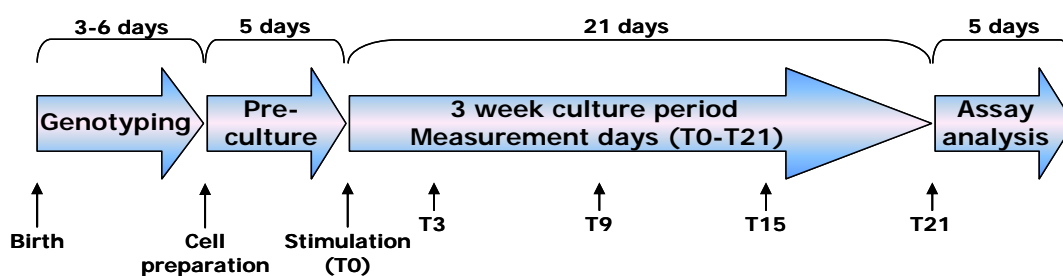
Figure 11. Workflow of the cell culture system.

2.1.1.2. Scheme of analysis, mating of mice and genotyping

Depending on the inheritance of the mutation, homozygous viability of the mice and the genotyping possibility, homozygous or heterozygous mutants can be applied in the cell culture analysis and the scheme of analysis and mating of mice for the cell culture system has to be set as depicted in table 2.

To obtain the wild type control mice for the osteoblast analysis, the mating has to be chosen carefully and different considerations have to be taken into account. To exclude biological variations between mutant and control mice, wild type littermates should always be used as control animals. If this is not feasible and wild type mice have to be mated separately, the strain of the wild type mice should correspond to the strain of the mutant line and animals should have the closest degree of relationship possible. Classification of offspring in mutant and wild type (not necessary in case of separate matings) can be done either by genotyping or, if the mutant phenotype is already visible prior to cell preparation between day 3 and 6, by phenotyping.

Inheritance of mutation	Homo-zygous viability	Geno-typing possibility[#]	Scheme of analysis	Mating	Alternatively[†]	
					Scheme of analysis	Mating
dominant	viable	yes	homo vs. wt	het x het	/	homo x homo wt x wt
		no	het vs. wt[2]	het x wt[1]	mut vs. wt[4]	mut x mut[3] wt x wt
	lethal	yes	het vs. wt	het x wt	/	/
		no	het vs. wt	het x wt	/	/
semi-dominant[*]	viable	yes	homo vs. wt	het x het	/	/
		no	homo vs. wt[6]	het x het[5]	/	/
	lethal	yes	het vs. wt	het x wt	/	/
		no	het vs. wt	het x wt	/	/
recessive	viable	yes	homo vs. wt	het x het	/	/
		no	homo vs. wt	homo x homo wt x wt	mut vs. wild[8]	het x het[7]
	lethal	phenotypic mutants do not exist				

Table 2. Analysis and mating scheme of the cell culture system. Genotype: wt – wild type / het – heterozygous / homo – homozygous. Phenotype: wild – wild type / mut – mutant

[*] semidominant correspond to an intermediate inheritance with both alleles contribute to the phenotype. Accordingly, heterozygous and homozygous mutants possess different phenotypes.
[#] if genotyping of a mutant line is not possible, mutants need to be distinguished from wild type mice prior to the cell isolation to enable analysis of the mutant line within the cell culture system.
[†] according to the conditions further alternative schemes for analysis and matings can be designed. Please note: the applied pattern of analysis and mating need to be considered for summary and interpretation of the results.
[1] if genotyping is not possible, heterozygous animals can be identified and mated with wild type mice based upon the previous breeding scheme. [2] heterozygous mutants can be compared with wild type littermates in the cell culture system if the phenotypic difference between wt and het animals is visible at the time point of preparation.
[3] if the previous breeding scheme is unknown, separate matings of phenotypic mutants (mut) and wild type mice (wt) are set. [4] the resulting phenotypic mutants (mut) can be compared with wild type animals (wt) in the cell culture system (please note: phenotypic mutants are genotypic heterogeneous composed of homo und het mice).
[5] if genotyping is not possible, heterozygous animals can be identified and mate among each other based upon the phenotype and previous breeding scheme. [6] based on the phenotype of the offspring, homozygous mutants

and wild type littermates are identified and applied for the cell culture system (possible if the phenotypic differences between wt, het and homo animals is visible at the time point of preparation).
[7] if genotyping is not possible, heterozygous animals can be identified and mated among each other based upon the previous breeding scheme. [8] the resulting phenotypic mutants (mut / genotypic = homo) can be compared with phenotypic wild type mice (wild) in the cell culture system (please note: phenotypic wild type mice are genotypic heterogeneous composed of het and wt mice).

2.1.1.3. Measurement days and assay analysis

For a comprehensive analysis and characterization of the osteoblasts on RNA-, protein- and functional level, 9 different assays have been developed. They are performed at 5 defined time points during the cultivation period referred to as measurement days (T0 / T3 / T9 / T15 / T21).

To avoid differences within a single assay due to variations in preparation and performance at the individual measurement days, the assays are not completely conducted at each day but samples are taken and stored until the cultivation period has ended. Thereafter, each assay is evaluated by analyzing the collected samples (referred to as assay analysis). Thus, a simultaneously and uniform analysis of all samples from the different measurement days is ensured, providing comparable and reliable results. A list of the developed assays and a schedule of the measurement days for sample taking is depicted in table 3. The left column (A1-A5) provides an overview if cultivated cells are applied for one or for multiple assays (e.g. in A1 the same cells are used for 4 different assays while in A3 the assay is performed with a single batch of cells).

	Assay	Measurement days				
		T0	T3	T9	T15	T21
A1	Proliferation	X	X	X	X	X
	Metabolic activity	X	X	X	X	X
	Protein content	X	X	X	X	X
	ALP activity	X	X	X	X	X
A2	Collagen secretion		X	X	X	X
	Collagen deposition		X	X	X	X
A3	Matrix mineralization		X	X	X	X
A4	Nodule quantification	differing measurement days*				
A5	Gene expression	X	X	X	X	X

Table 3. Assays and measurement scheme of the cell culture system. *starting with T3, this assay is performed 3x a week (Monday / Wednesday / Friday) until T21.

2.1.1.4. Cell preparation and cultivation

For the cell culture system, the cells are classified in two groups for cultivation, sample taking at the measurement days and the assay analysis and interpretation:

1) wild type cells (control / reference) = wt
2) mutant cells (to be assessed / investigated) = mut

Preparation of osteoblasts is performed with mice at the age of day 3 to 6 postnatal and cells are isolated enzymatically from the calvaria of the animals. Given the fact that 12.4×10^6 cells are needed for the culture system and that 7.5×10^5 cells are obtained on average out of a single calvaria, at least 16 mice (calvariae) have to be prepared for each group (mutant and wild type). However, it is recommended to prepare 20 mice to ensure the required number of 12.4×10^6 cells.

The isolated cells are cultivated under standard conditions with 37°C / 90% humidity / 5% CO_2 in a cell incubator using the following mediums:

Culture medium A (preparation / prior to stimulation / assay A1)
- α-MEM supplemented with 10% FCS / 2 mM glutamine / 100 U/ml penicillin / 100 µg/ml streptomycin

Culture medium B (stimulation from T0 - T21):
- α-MEM supplemented with 10% FCS / 2 mM glutamine / 100 U/ml penicillin / 100 µg/ml streptomycin / 10 mM β-glycerophosphate / 50 µg/ml ascorbic acid

Culture medium C (assay A2)
- α-MEM supplemented with 5% FCS / 2 mM glutamine / 100 U/ml penicillin / 100 µg/ml streptomycin / 10 mM β-glycerophosphate / 50 µg/ml ascorbic acid

At the beginning of the culture period (after preparation), the cells are kept in culture medium A for 5 days until they have reached confluence (Pre-culture). Thereafter, the cells are stimulated (referred to as T0) and cultivated for another 21 days under stimulating conditions using culture medium B. The medium is changed twice a week. Culture medium A and C are further needed for assay A1 and A2, respectively.

The cells are plated and incubated in the following culture vessels (brackets indicate the initial number of cells to be plate out after preparation per well or per flask):

- 24-well Lumox cell culture plates ($5x10^4$ cells / well)
- 24-well Primaria cell culture plates ($5x10^4$ cells / well)
- 6-well Primaria cell culture plate ($2x10^5$ cells / well)
- T12.5 cm^2 cell culture flask ($2.5x10^5$ cells / flask)

An overview about type and number of culture vessels for the different assays is given in table 4 below.

	Assay	Type of culture vessel	Number of culture vessel*
A1	Proliferation Metabolic activity Protein content ALP activity	24-well Lumox	6
A2	Collagen secretion Collagen deposition	6-well Primaria	5
A3	Matrix mineralization	6-well Primaria	5
A4	Nodule quantification	T12.5cm^2	8[#]
A5	Gene expression	24-well Primaria	6

Table 4. Overview about culture ware for the cell culture system. [*] number of culture vessels equates number of measurement days for sample taking including one plate as reserve. [#] number of flasks does not correspond to measurement days but equates the number of biological replicates used for nodule quantification (4 x wt / 4 x mut), since each flask is used throughout the whole culture period for every single measurement day.

The distribution of the cells in the culture vessels is outlined in the following illustration.

- 24-well cell culture plate (A1 / A5)
- 6-well cell culture plate (A2 / A3)
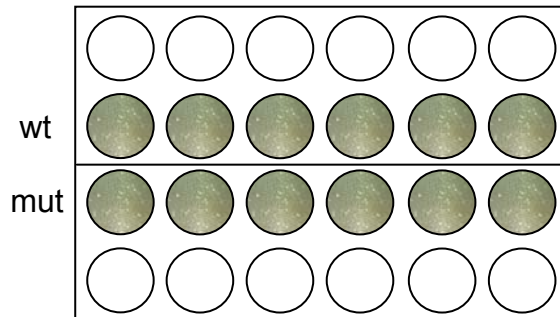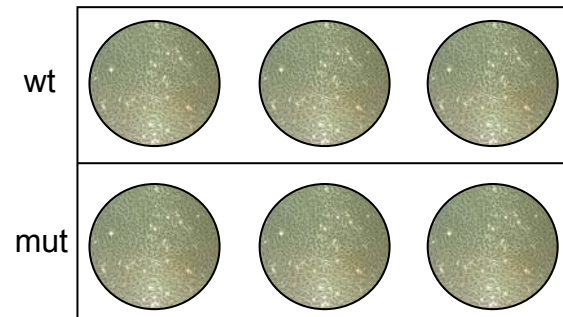
- T12.5 cm^2 cell culture flask (A4)
    - 4 x wt
    - 4 x mut

wt - cells of wild type control mice / mut - cells of mutant mice

2.1.1.5. Important considerations

For some of the reagents that are applied for the cell culture system, a strong variation of the quality between different batches of the product is observable. As the quality of a chemical can influence the preparation or cultivation of a cell culture, it is advisable to do a testing of different batches to find out the best batch for the cell culture system and arrange a reservation for a larger quantity of the product with the manufacturer. Thus, identical preparation and cultivation of the cells between different mutant lines can be ensured and variation in growth or differentiation is avoided.

In detail, the quality of the Collagenase IV which is used for the cell preparation is important for the yield and vitality of the isolated cells and the composition of the FCS as the most important supplement for the media critically influences growth and differentiation of the cells.

Quality feature for charge testing:

- Collagenase IV: yield of cells per calvaria
- FCS: ability of osteoblasts to differentiate during the culture period, determined (quantified) by means of nodule quantification

2.1.1.6. Statistical analysis

The mutant as well as the wild type control cultures each descends from a single pool of cells. Therefore, biological replicates of each group are not performed and thus, statistical analysis of the results can not be obtained. The multiple wells / flasks of each group that are used for the assays A1 / A2 / A3 / A4 (n = number of wells or flasks per group) only represent technical replicates and the error bars drawn in the diagrams represent the standard error of the mean (SEM) calculated from these technical replicates (from n). In assay A5 (Gene expression), the single wells of each group are pooled for the experiment and therefore no technical replicates are performed. Hence, SEM can not be calculated for the Gene expression assay.

Accordingly, the cell culture system only provide trends of the differences between mutant and wild type osteoblasts, but the development and course of each investigated parameter during the cultivation time should allow to assess possible disparities between mutant and wild type cells.

2.1.2. Material and methods

2.1.2.1. Cell preparation and cultivation

<u>I. Material</u>

- EDTA
- 1x PBS (Lonza / BE17-516F)
- Collagenase IV (Sigma-Aldrich / C5138-500MG / charge of importance)
- α-MEM (Lonza / BE12-169F)
- FCS (Gibco / 10500-064 / charge of importance)
- Glutamine (Lonza / BE17-605E)
- Penicillin / streptomycin (Lonza / DE17-602E)
- Ascorbic acid (Sigma-Aldrich / A4544-25G)
- β-glycerol phosphate (AppliChem / A2253,0100)
- Ethanol 70%
- Trypan blue 0.4%

- 15 ml / 50 ml tubes
- Petri dishes
- 0.22 μm syringe filter (Millipore / SLGP033RS)
- 40 μm cell strainer (BD / 3523409)
- 0.2 μm bottle-top-filter (NeoLab / 431097)
- 24-well Lumox cell culture plates (Greiner bio one / 96110024)
- 24-well Primaria cell culture plates (BD / 353847)
- 6-well Primaria cell culture plates (BD / 353846)
- T12.5 cm^2 cell culture flasks (BD / 353107)
- Dissecting set
- Neubauer cell counting chamber
- 37°C water bath
- Laminar flow
- Cell culture incubator

- 0.1% Collagenase IV in 1x PBS (filter steril 0.22 μm syringe filter / make fresh)
- 4 mM EDTA in 1x PBS (ph7) (superposable)
- Culture medium A:
  - α-MEM supplemented with 10% FCS / 2mM glutamine / 100 U/ml penicillin / 100 μg/ml streptomycin
- Culture medium B:
  - α-MEM supplemented with 10% FCS / 2mM glutamine / 100 U/ml penicillin / 100 μg/ml streptomycin / 10 mM β-glycerol phosphate / 50 μg/ml ascorbic acid

II. Method

- Preparation of mutant and wild type control mice is performed in parallel but in two separate groups (mut / wt)
- After decapitation of mice the skull is briefly immerged in 70% ethanol and afterwards kept on ice in 1x PBS
- The following steps are performed under a laminar flow
- Calvariae are dissected by cutting the skin from posterior (foramen magnum) to anterior (nose), the skin is removed and the calvaria is carefully taken off from the brain
- Calvariae are placed in a petri dish with 1x PBS and superfluous contaminating tissues are removed
- For each group (mut / wt): 4-5 calvariae are placed in a 15 ml tube - it is advisable to split the total number of calvariae from each group in 4 x 15 ml tubes (correspond to 4 tubes with 5 calvaria each if preparing 20 calvaria per group)
- Each tube is incubated twice with 4-5 ml (1 ml per calvaria) 4 mM EDTA in 1x PBS for 7 min at 37°C (water bath), the supernatant is discarded
- Each tube is washed three times with 4-5 ml (1 ml per calvaria) 1x PBS
- Predigestion: each tube is incubated once with 2 ml 0.1% Collagenase IV for 7 min at 37°C (water bath) and the supernatant is discarded
- Digestion step 1: each tube is incubated with 5 ml 0.1% Collagenase IV for 30 min at 37°C (water bath) under occasionally agitation, the supernatant from the digestion of each group (4 x 15 ml tubes a 5 ml) is filtered through a 44 µm cell strainer in one 50 ml tube and 20 ml culture medium A is added (yield in 40 ml cell suspension per group) - attention should be paid to retain the undigested remains of the calvariae in the 15 ml tubes for the second digestion step
- Digestion step 2: equal to digestion 1
- During the second digestion both 50 ml tubes with the cell suspension of the first digestion (1 x wt / 1x mut) are kept at 37°C in the incubator
- The resulting 4 x 50 ml tubes of both digestion steps (2 x wt / 2 x mut) are centrifuged for 10 min / 1200 rpm / RT
- For each group: the supernatant is discarded and the cell pellets of both 50 ml tubes are resuspended and put together in 10 ml culture medium A, the quantity of cells is estimated using the Neubauer counting chamber and cells are plated according to the scheme in 2.1.1.4.
- The medium is changed 24 h after plating using culture medium A and thereafter, the medium is regularly changed twice a week (monday / thursday or tuesday / friday), starting with the first stimulation at T0 using culture medium B

2.1.2.2. Proliferation / Metabolic activity / Protein content / ALP activity (A1)

<u>I. Material</u>

- CellQuanti-Blue (BioAssay Systems; Biotrend Chemikalien GmbH / CQBL-05K)
- CellyticM (Sigma-Aldrich / C2978-50ML)
- Complete Mini Protease Inhibitor (Roche / 11836153001)
- Quant-iT dsDNA Assay Kit Broad Range (Invitrogen / Q33130)
- BCA-Protein Assay Kit (Thermo Scientific / 23225)
- 4-Nitrophenylphosphate (PNPP) (Sigma-Aldrich / N4645-1G)
- Proteinase K (20 mg/ml)
- EDTA
- Glycine
- $MgCl_2$
- NaCl
- NaOH
- SDS
- Tris
- $ZnCl_2$

- 96-well plate black (Nunc / 237107)
- 96-well plate transparent (Nunc / 260860)
- Bench top centrifuge with refrigeration to 4°C
- Fluorescence micro plate reader (Tecan Safire^2)
- Spectrophotometer for 96-well plates (Molecular Devices / SpectraMax 190) including software (SOFTmaxPRO 3.1.2)

- SDS-buffer (for 200ml / superposable):
    - 2% SDS
    - 10 mM Tris
    - 5 mM EDTA
    - 200 mM NaCl
- ALP-buffer (for 100ml / superposable):
    - 0,1 M glycine (pH 9,6)
    - 1 mM $MgCl_2$
    - 1 mM $ZnCl_2$
- PNPP-buffer (for 500ml / superposable):
    - 3,75 g glycine
    - 1 mM $MgCl_2$
    - 1 mM $ZnCl_2$
    - dissolve in in 400 mL H_2O
    - adjust pH to 10,4 using NaOH
    - fill up to 500 ml with H_2O
- PNPP in PNPP-buffer (make fresh):
    - 1 ml PNPP-buffer + 20 mg PNPP

II. Measurement day

- 24-well lumox cell culture plate
- The samples (n wells) of both biological groups are prepared separately (technical replicates)
  - 6 x wt
  - 6 x mut

- CellQuanti-Blue reagent is diluted 1:10 with culture medium A (CQBM-solution)
- Aspiration of old media from the wells
- 1 ml CQBM solution is added per well and incubated for 1 h at 37°C
  (the lower row of wells without cells is used as blank by adding 1 ml CQBM solution per well)
- Fluorescence spectroscopy with the cell culture plate (Tecan – Safire[2])
  - extinction: 530 nm
  - emission: 590 nm
  - band width: 10 nm
  - z-value: 11200 µm
  - gain: 65 nm (manual)
  - range of temperature: 36.5 – 37.5°C
  - measurement is saved → Metabolic activity

- Preparation of cell lysis reagent: 10 ml CellyticM + 1 tablet Complete Mini Protease Inhibitor (CMCM solution)
- CQBM solution is aspirated and cells are washed once with 1x PBS
- 500 µl CMCM solution is added per well and incubated for 15 min at 4°C under continuous shaking (orbital shaker)
- 4°C room: supernatant of each well is transfered under multiple up and down pipetting (complete lysis of cells) in 1.5 ml Eppendorf tubes and centrifuged for 10 min / 4°C / 12000 rpm
- 350 µl supernatant is carefully transfered in new 1.5 ml tube and stored at -20°C (tube 1) → Protein content / ALP activity
- Pellet (contains nuclei) including remaining 150 µl supernatant is stored at -20°C (tube 2) → Proliferation (DNA-contant)

III. Assay analysis

→ Metabolic activity

- The metabolic activity of the cells is directly obtained and saved as fluorescent value per sample (well) at every measurement day [fluorescence/well]
- A standard curve is not applied, metabolic activity is described as raw fluorescence value (RFU)

→ Protein content

- An existing standard curve is applied for the analysis
    o the standard curve is generated according to the protocol of the BCA Protein Assay Kit with µg/ml protein (x-axis) again OD (y-axis), saved and reused for every analysis
- For each group (wt = 30 samples / mut = 30 samples) one 96-well plate (transparent) is used, samples can be measured in duplicate
- Two plates are needed, each plate is prepared according to the following scheme
    o 30 samples in duplicate (60 wells)
    o blank (CMCM solution) in duplicate (2 wells)

- Tube 1 (350 µl supernatant) is thawed at 4°C
- Analysis of protein is performed using the BCA Protein Assay Kit in the 96-well plates
    o working solution (WS) is prepared: 50 units BCA reagent A + 1 unit BCA reagent B
    o samples: 25 µl of lysate (tube 1) per well
    o blank: 25 µl CMCM solution per well
    o 200 µl WS is added to each well and both plates are incubated for 30 min at 37°C
    o photometric absorption reading (photometer Spectramax)
        o endpoint reading
        o wave length: 562 nm

- The protein content of each sample is calculated according to the following scheme
    o both plates (wt / mut) are analysed separately
    o standard curve with [µg/ml] of protein
    o automatically via SOFT maxPRO: blank value is subtracted from the absorption values of the samples, thereafter the protein content of each sample is calculated on the basis of the standard curve in [µg/well]
    o please note: the applied volume of 500 µl CMCM solution per well (for cell lysis at the measurement days) has to be taken into account for the calculation

→ ALP activity

- A standard curve is not applied, ALP activity is described as absorption value (arbitrary units)
- For each group (wt = 30 samples / mut = 30 samples) one 96-well plate (transparent) is used, samples can be measured in duplicate
- Two plates are needed, each plate is prepared according to the following scheme
    - 30 samples in duplicate (60 wells)
    - blank (CMCM solution) in duplicate (2 wells)

- Tube 1 (350 µl supernatant) is thawed at 4°C
- Analysis of ALP activity is performed in the 96-well plates according to the following procedure
    - working solution (WS) is prepared: 9 units ALP-buffer + 1 unit PNPP in PNPP-buffer
    - samples T0: 100 µl lysat (tube 1) per well (undiluted)
    - samples T3-T21: 5 µl lysat (tube 1) + 95 µl H_2O per well (1:20)
    - blank: 5 µl CMCM solution + 95 µl H_2O per well (1:20)
    - 100 µl WS is added to each well and both plates are incubated for 30 min at 37°C
    - 50 µl 1 M NaOH is added to each well
    - photometric absorption reading (photometer Spectramax)
        - endpoint reading
        - wave lenght: 405 nm

- The ALP activity of each sample is calculated according to the following scheme
    - both plates (wt / mut) are analysed separately
    - without standard curve
    - automatically via SOFT maxPRO: blank value is subtracted from the absorption values of the samples, thereafter the ALP-activity of each sample is described as absolute absorption value in [absorption/well]
    - please note: from the 500 µl CMCM solution per well (for cell lysis at the measurement days) only 100 µl were used for the analysis either undiluted (T0) or 1:20 diluted (T3-T21)

→ Proliferation (DNA content)

- A standard curve is used for the analysis and prepared for each measurement (each plate)
    - the standard curve is described as µg DNA (x-axis) again fluorescence (y-axis)
- Both groups (wt = 30 samples / mut = 30 samples) are analysed on one 96-well plate (black), the samples can not be measured in duplicate
- To still analyze each sample in duplicate, two plates are used and identically prepared according to the following scheme
    - 60 samples (60 wells)
    - 8 standard concentrations (0 – 1 µg) in duplicate (16 wells)
    - blank (1:1 mixture of CMCM solution and SDS-buffer with Proteinase K) in triplicate (3 wells)

- Tube 2 (pellet including 150 µl supernatant) is thawed at 4°C
- 150 µl SDS-buffer and 1.5 µl Proteinase K is added to each well (yield in 300 µl lysat), vortexed, spinned down and incubated for 3 h at 56°C using a thermo shaker (750 rpm)
- Analysis of DNA content is performed using the Quant-iT DNA Assay Kit Broad Range in the 96-well plates
  - working solution (WS) is prepared: Quant-iT reagent is diluted 1:200 with Quant-iT buffer
  - samples: 10µl lysat (tube 2) + 10 µl H_2O per well
  - standard: 10µl blank (1:1 mixture of CMCM solution and SDS-buffer with Proteinase K) + 10 µl of each DNA standard concentration from the kit per well
  - blank: 10 µl blank (1:1 mixture of CMCM solution and SDS-buffer with Proteinase K) + 10 µl H_2O per well
  - 200 µl WS is added to each well and both plates are incubated for 5 min at RT
  - fluorescence spectroscopy (Tecan – Safire[2])
    - extinction: 490nm
    - emission: 527nm
    - band width: 10 nm
    - gain: optimal

- DNA content of each sample is calculated according to the following scheme
  - both plates (wt / mut) are analysed separately
  - standard curve with [µg] of DNA (based on the fluorescence values of the standards of each plate)
  - blank value is subtracted from the fluorescence values of the samples, thereafter the DNA content of each sample is calculated on the basis of the standard curve in [µg/well]
  - please note: from the 300 µl overall lysate per sample (150 µl pellet + 150 µl SDS-buffer) only 10 µl were used for the analysis
  - the mean value from both measurements (plate 1 / plate 2) result in the DNA content of each sample

<u>VI. Results and presentation</u>

→ Proliferation (DNA content)

- For each sample (well) the DNA content is determined in [µg DNA/well]
- For each measurement day the mean value of each group (wt / mut) is calculated by averaging the 6 single values of each group (6 x wt / 6 x mut)
- For graphic presentation of the proliferation during the culture period, a combined diagram for both groups is drawn with the obtained values on the y-axis [µg DNA/well] against the measurement days on the x-axis

→ Metabolic activity

- For each sample (well) the metabolic activity is determined in [fluorescence (RFU)/well]
- To normalize the metabolic activity to the cell number, the value is divided by the DNA content of the sample to obtain the metabolic activity per DNA amount in [fluorescence (RFU)/µg DNA] for each sample
- For each measurement day the mean value of each group (wt / mut) is calculated by averaging the 6 single values of each group (6 x wt / 6 x mut)
- For graphic presentation of the metabolic activity during the culture period, a combined diagram for both groups is drawn with the obtained values on the y-axis [fluorescence (RFU)/µg DNA] against the measurement days on the x-axis

→ Protein content

- For each sample (well) the protein content is determined in [µg protein/well]
- To normalize the protein content to the cell number, the value is divided by the DNA content of the sample to obtain the protein content per DNA amount in [µg protein/µg DNA] for each sample
- For each measurement day the mean value of each group (wt / mut) is calculated by averaging the 6 single values of each group (6 x wt / 6 x mut)
- For graphic presentation of the protein content during the culture period, a combined diagram for both groups is drawn with the obtained values on the y-axis [µg protein/µg DNA] against the measurement days on the x-axis

→ ALP activity

- For each sample (well) the ALP activity is determined in [absorption (arbitrary units)/well]
- To normalize the ALP activity to the cell number, the value is divided by the DNA content of the sample to obtain the ALP activity per DNA amount in [absorption (arbitrary units)/µg DNA] for each sample
- For each measurement day the mean value of each group (wt / mut) is calculated by averaging the 6 single values of each group (6 x wt / 6 x mut)
- For graphic presentation of the ALP activity during the culture period, a combined diagram for both groups is drawn with the obtained values on the y-axis [absorption (arbitrary units)/µg DNA] against the measurement days on the x-axis

2.1.2.3. Collagen secretion / Collagen deposition (A2)

I. Material

- Bouin's solution (Sigma-Aldrich / HT10132-1L)
- Sircol Dye reagent (from Sircol Collagen Assay Kit) (Biocolor; Tebu-bio / S1005)
- Sirius Red FB3 (Fluka; Sigma-Aldrich / 43665)
- Saturated picric acid solution (Fluka; Sigma-Aldrich / 80456)
- Picric acid (Sigma-Aldrich / 239801-50G)
- Collagen solution
- HCl / NaOH

- 96-well plate transparent (Nunc / 260860)
- Spectrophotometer for 96-well plates (Molecular Devices / SpectraMax 190) including software (SOFTmaxPRO 3.1.2)

- Culture medium C:
    - α-MEM supplemented with 5% FCS / 2 mM glutamine / 100 U/ml penicillin / 100 µg/ml streptomycin / 10 mM β-glycerol phosphate / 50 µg/ml ascorbic acid
- Sirius Red solution:
    - 0.25 g Sirius Red FB3
    - 250 ml saturated picric acid solution
    - 1 ml picric acid (to ensure saturation of the solution)

- Please note: the medium has to be changed in the cells to be analyzed 24 h before the measurement day
    - 6-well Primaria cell culture plate
    - aspiration of old media from the wells
    - 2 ml culture medium C is added per well and incubated for 24 h at 37°C

II. Measurement day

- 6-well Primaria cell culture plate with culture medium C for 24 h
- The samples (n wells) of both biological groups are prepared separately (technical replicates)
    - 3 x wt
    - 3 x mut

- 1ml of the cell culture supernatant (culture medium C) is transferred in a 1.5 ml tube and stored at -20°C → Collagen secretion
- Aspiration of the remaining media from the wells
- Cells are washed once with 1x PBS
- 2ml Bouin's solution is added to each well and incubated for 60 min at RT
- Bouin's solution is aspirated and cells are washed twice with H_2O for 5 min at RT each
- 5 ml of H_2O and 200 µl Penicillin / Streptomycin solution is added to each well, the plates are sealed with parafilm and stored in a closed box (e.g. styrofoam-box) at RT → Collagen deposition

III. Assay analysis

→ Collagen secretion

- An existing standard curve is applied for the analysis
    - the standard curve is generated according to the protocol explained below with µg/ml collagen (x-axis) again OD (y-axis), saved and reused for every analysis
- The Sircol Dye reagent (from Sircol Collagen Assay Kit) is used for the analysis
- Both groups (wt = 12 samples / mut = 12 samples) are analyzed on one 96-well plate (transparent), the samples can be measured in duplicate, the plate is prepared according to the following scheme
    - 24 samples in duplicate (48 wells)
    - blank (culture medium C) in duplicate (2 wells)

- Supernatant is thawed at 4°C
- 200 µl of the supernatant of each sample is transferred to a new 1.5 ml tube
- Preparation of blank: 200 µl of fresh culture medium C is transferred to a new 1.5 ml tube
- 1 ml Sircol Dye reagent is added, tubes are briefly vortexed, spinned down and incubated for 30 min at RT under continuing shaking (750 rpm on shaker)
- Tubes are centrifuged for 10 min / RT / 13000 rpm
- Supernatant is discarded and tubes are centrifuged for another 5 min / RT / 13000 rpm
- Remaining supernatant is carefully removed via pipette tip (contact of pipette tip with pellet has to be avoided)
- 1 ml 0.5 M NaOH is added, the tubes are briefly vortexed, spinned down and incubated for 10 min at RT under continuing shaking (750 rpm on shaker) → pellet has to be completely dissolved (tubes have to be vortexed again if necessary)
- The Sircol Dye reagent that was bounded to the collagen of the cell culture supernatant (pellet) is unhinged by the NaOH and the concentration of the dye in each sample is determined by photometric absorption reading in a 96-well plate according to the following scheme:
    - samples and blank: 40 µl NaOH-Sircol Dye solution and 160 µl H_2O is added per well (1:5)
    - photometric absorption reading (photometer Spectramax)
        - endpoint reading
        - wave length: 550 nm

- The absorption values correlate with the amount of bounded Sircol Dye reagent, that is proportional to the concentration of collagen in the respective sample (200 µl cell culture supernatant); therefore, the amount of collagen in each sample can be calculated by the absorption values according to the following scheme
    - standard curve with [µg/ml] collagen
    - automatically via SOFT maxPRO: blank value is subtracted from the absorption values of the samples, thereafter the amount of collagen in each sample is calculated on the basis of the standard curve in [µg/well]

- o please note: given that 1 ml NaOH was applied for unhinge the Sircol Dye reagent from the pellet and that the standard curve is depicted in µg/ml, the amount of collagen can directly be obtained from the standard curve, but it has to be taken into account, that only 200 µl from the 2 ml cell culture supernatant of each well were used for the analysis and that the NaOH-Sircol Dye solution was 1:5 diluted for the absorption reading

→ Collagen deposition

- An existing standard curve is applied for the analysis
    - o the standard curve is generated according to the protocol explained below with µg/ml collagen (x-axis) again OD (y-axis), saved and reused for every analysis
- The Sirus Red solution (self-made) is used for the analysis
- Both groups (wt = 12 samples / mut = 12 samples) are analyzed on one 96-well plate (transparent), the samples can be measured in duplicate, the plate is prepared according to the following scheme
    - o 24 samples in duplicate (48 wells)
    - o blank (NaOH) in duplicate (2 wells)

- Aspiration of the water in the wells
- 2 ml Sirius Red solution is added to each well and incubated for 1 h at RT
- Sirius Red is aspirated and cells are washed twice with H_2O for 5 min at RT
- Cells are washed once with 0.01 M HCl for 2 min at RT
- 1 ml 0.5 M NaOH is added per well and incubated for 60 min at RT
- The Sirius Red solution that was bounded to the collagen of the cell matrix (well) is unhinged by the NaOH and the concentration of the dye in each sample is determined by photometric absorption reading in a 96-well plate according to the following scheme:
    - o samples: 20 µl NaOH-Sirius Red solution and 180 µl H_2O are added per well (1:10)
    - o blank: 20 µl fresh NaOH solution and 180 µl H_2O are added per well (1:10)
    - o photometric absorption reading (photometer Spectramax)
        - o endpoint reading
        - o wave length: 550 nm

- The absorption values correlate with the amount of bounded Sirius Red solution, that is proportional to the concentration of collagen in the respective sample (well), therefore, the amount of collagen in each sample can be calculated by the absorption values according to the following scheme
    - o standard curve with [µg/ml] collagen
    - o automatically via SOFT maxPRO: blank value is subtracted from the absorption values of the samples, thereafter the amount of collagen in each sample is calculated on the basis of the standard curve in [µg/well]
    - o please note: given that 1 ml NaOH was applied for unhinge the Sirius Red solution from the well and that the standard curve is depicted in µg/ml, the amount of collagen can directly be obtained from the

standard curve, but it has to be taken into account, that the NaOH-Sirius Red solution was 1:10 diluted for the absorption reading

Generation of the standard curve for Collagen secretion / Collagen deposition

- Material: 96-well plate (transparent) / collagen solution [1mg/ml] / 0.1 M NaOH / Sircol Dye reagent (from Sircol Collagen Assay Kit)

- Using the collagen solution [1mg/ml] 6 standard samples are prepared in 1.5 ml tubes with an amount of 0 / 20 / 40 / 60 / 80 / 100 µg collagen
- 1 ml Sircol Dye reagent is added to each standard sample, the tubes are briefly vortexed, spinned down and incubated for 30 min at RT under continuing shaking (750 rpm on shaker)
- Centrifugation for 10 min / RT / 13000 rpm
- Supernatant is discarded and the tubes are centrifuged for another 5 min / RT / 13000 rpm
- Remaining supernatant is carefully removed via pipette tip (contact of pipette tip with pellet has to be avoided)
- 1 ml 0.5 M NaOH is added, the tubes are briefly vortexed, spinned down and incubated for 10 min at RT under continuing shaking (750 rpm on shaker) → pellet has to be completely dissolved (tubes have to be vortexed again if necessary)
- The Sircol Dye reagent that was bounded to the collagen in the standard samples (pellet) is unhinged by the NaOH and the concentration of the dye in each standard sample is determined by photometric absorption reading in a 96-well plate according to the following scheme:
  - o standards (in duplicate): 200 µl NaOH-Sircol Dye solution are added per well
  - o blank (in duplicate): 200 µl fresh NaOH is added per well
  - o photometric absorption reading (photometer Spectramax)
    - o endpoint reading
    - o wave length: 550 nm

- The absorption values correlate with the amount of bounded Sircol Dye reagent, that is proportional to the concentration of collagen in the respective standard samples (0 / 20 / 40 / 60 / 80 / 100 µg), therefore, a standard curve can be generated with µg/ml collagen (x-axis) again OD (y-axis), saved and reused for every analysis

IV. Results and presentation

→ Collagen secretion

- For each sample (well) the amount of secreted collagen is determined in [µg collagen/well]
- The value correspond to the overall amount of secreted collagen from the cells of one sample (well) inbetween 24h of incubation [µg collagen/well/24h]
- For each measurement day the mean value of each group (wt / mut) is calculated by averaging the 3 single values of each group (3 x wt / 3 x mut)
- For graphic presentation of the collagen secretion during the culture period a combined diagram for both groups is drawn with the obtained values on the y-axis [µg collagen/well/24h] against the measurement days on the x-axis

→ Collagen deposition

- For each sample (well) the amount of deposited collagen is determined in [µg collagen/well]
- For each measurement day the mean value of each group (wt / mut) is calculated by averaging the 3 single values of each group (3 x wt / 3 x mut)
- For graphic presentation of the collagen deposition during the culture period a combined diagram for both groups is drawn with the obtained values on the y-axis [µg collagen/well] against the measurement days on the x-axis

2.1.2.4. Matrix mineralization (A3)

I. Material

- 4% paraformaldehyde
- Alizarin Red S (Sigma-Aldrich / A5533-25G)
- Cetylpyridinium chloride (Sigma-Aldrich / C5460-100G)

- 96-well plate transparent (Nunc / 260860)
- Spectrophotometer for 96-well plates (Molecular Devices / SpectraMax 190) including software (SOFTmaxPRO 3.1.2)

- 5% Alizarin Red S stock solution in H_2O (ph 4.0 / filter sterile 0.22 µm / superposable)
- 0.5% Alizarin Red S working solution in H_2O (make fresh)
- 10% cetylpyridinium chloride solution in H_2O (make fresh)

II. Measurement day

- 6-well Primaria cell culture plate
- The samples (n wells) of both biological groups are prepared separately (technical replicates)
    - 3 x wt
    - 3 x mut

- Aspiration of old media from the wells
- Cells are washed once with 1x PBS
- 2 ml 4% PFA is added per well and incubated for 15 min at 4°C
- PFA is aspirated and cells are washed twice for 5 min at RT with H_2O
- Plates are air-dried and afterwards stored in a closed box (e.g. styrofoam-box) at RT

III. Assay analysis

- An existing standard curve is applied for the analysis
    - the standard curve is generated according to the protocol explained below with µM Alizarin (x-axis) again OD (y-axis), saved and reused for every analysis

- Both groups (wt = 12 samples / mut = 12 samples) are analyzed on one 96-well plate (transparent), the samples can be measured in duplicate, the plate is prepared according to the following scheme
    - 24 samples in duplicate (48 wells)
    - blank (10% cetylpyridinium chloride) in duplicate (2 wells)

- 2 ml 0.5% Alizarin Red S is added per well and incubated for 60 min at RT
- Alizarin is aspirated and cells are washed 4 times with H_2O for 5 min at RT each
- 1 ml 10% cetylpyridinium chloride is added per well and incubated for 60 min at RT

- Bounded Alizarin is unhinged by the cetylpyridinium chloride and the concentration of the dye in each sample is determined by photometric absorption reading in a 96-well plate according to the following scheme:
    - samples T3: 200 µl of the cetylpyridinium chloride-Alizarin solution is added per well (undiluted)
    - samples T9-T21: 40 µl of the cetylpyridinium chloride-Alizarin solution and 160 µl H_2O are added per well (1:5)
    - blank: 40 µl fresh cetylpyridinium chloride and 160 µl H_2O are added per well (1:5)
    - photometric absorption reading (photometer Spectramax)
        - endpoint Reading
        - wave length: 562 nm

- The absorption values correlate with the concentration of Alizarin Red S in the respective sample and therefore, the amount of bounded Alizarin in each well (sample) can be calculated according to the following scheme
    - standard curve with [µM] Alizarin
    - automatically via SOFT maxPRO: blank value is subtracted from the absorption values of the samples, thereafter the amount of bounded Alizarin of each sample is calculated on the basis of the standard curve in [µmol/well]
    - please note: the applied volume of 1ml cetylpyridinium chloride per well and the 1:5 dilution for absorption reading in the samples T9-T21 (T3 undiluted) has to be taken into account for the calculation

Generation of the standard curve for Matrix mineralization

- Material: 96-well plate (transparent) / 0.5% Alizarin Red S (=14.6 mM) / 10% cetylpyridinium chlorid

- Preparation of 10 standard solutions according to table 5

Standard	µl Alizarin Red S	µl cetylpyridinium chloride	Final concentration in µM[*]
1	0	1000	0
2	0.68	999.32	2
3	3.4	996.6	10
4	6.84	993.16	20
5	17.1	982.9	50
6	34.2	965.8	100
7	68.4	931.6	200
8	136.8	863.2	400
9	205.2	794.8	600
10	273.6	726.4	800

Table 5. Preparation of a standard curve for the Matrix mineralization assay. [*] final concentration already including a 1:5 dilution of the standard solutions for the absorption reading

- Concentration of all 10 standards is determined according to the following scheme
    - standards (in duplicate): 40 µl standard solution + 160 µl H_2O is added per well (1:5)
    - blank (in duplicate): 200 µl H_2O is added per well
    - photometric absorption reading (photometer Spectramax)
        - endpoint reading
        - wave length: 562 nm

- The absorption values correlate with the concentration of Alizarin Red S in the respective standards and thus, a standard curve can be generated with µM Alizarin (x-axis) again OD (y-axis), saved and reused for every analysis
- Please note: the final concentration [µM] of the standards depicted in table 5 already include the 1:5 dilution of the standard solutions for the absorption reading

IV. Resultats and presentation

- For each sample (well) the amount of bounded Alizarin is determined in [µmol Alizarin/well]
- For each measurement day the mean value of each group (wt / mut) is calculated by averaging the 3 single values of each group (3 x wt / 3 x mut)
- For graphic presentation of the matrix mineralization during the culture period a combined diagram for both groups is drawn with the obtained values on the y-axis [µmol Alizarin/well] against the measurement days on the x-axis

2.1.2.5. Nodule quantification (A4)

I. Material

- Stereo microscope equipped with camera and software for image acquisition (Leica MZ16F / DFC320 / Firecam)
- Holding frame for T12.5 cm^2 cell culture flasks (enables identical positioning of the culture flask under the stereo microscope at every measurement day)
- Pixel counting software (Image J 1.38x)

II. Measurement day

- T12.5 cm^2 cell culture flasks
- The samples (n cell culture flasks) of both biological groups are used for the whole culture period and are analyzed separately at each measurement day (technical replicates)
    - 4 x wt
    - 4 x mut

- Transmitted light images are taken from all cell culture flasks using a stereo microscope with the following settings (Leica MZ16F / DFC320 / Firecam)
    - Source of light: Leica KL1500LCD / 3200K (5/E)
    - Bright field
    - Objective: 0.63x
    - Magnification: 1.0x
    - Exposure: 10msec
    - Gain: 1.0x
    - Live Video: Progressive VGA
    - Color: Auto
    - Levels: Auto
    - Output: Full Frame HQ 2088 / JPEG
    - to arrange and arrest the flasks in the same position on the microscope stage at each measurement day, they are placed in a special custom-built holding frame for T12.5 cm^2 cell culture flasks
    - the raw images are stored until the Assay analysis

III. Assay analysis

- The JPEG images are analyzed using the pixel counting software ImageJ (Version 1.38x) according to the following procedure (all images from both groups are analyzed in parallel in terms of a stack analysis):
    - File → Import → Image Sequence…
    - Process → Substract Background… → Rolling Ball Radius: 50 / Light Background √ → Process all slices yes √
    - Process → Binary → Make Binary → Calculated Threshold for Each Image √
    - Analyze → Set Scale → Distance in Pixel: 97 / Unit of Length: mm / Global √
    - Analyze → Analyze Particle → Display Results √ / Summarize √ → Process all slices √

- o for each image the parameter Count / Total Area / Average Size / Area Fraction are obtained and summarized in the Summary Table (according to the parameter, the numerical values correspond to mm or mm^2)
- o the results of the Summary Table are transferred into an Excel Table
- o the different parameter of an image correspond to the following feature in the respective sample (cell culture flask):
    - o Count → number of nodules
    - o Total Area → total area of nodules
    - o Average Size → average size of a nodule
    - o Area Fraction → fraction of nodule area from total area in the flask (%)

IV. Results and presentation

- For each sample (cell culture flask) the total area of nodules is determined in [mm^2]
- For each measurement day the mean value of each group (wt / mut) is calculated by averaging the 4 single values of each group (4 x wt / 4 x mut)
- For graphic presentation of the nodule development during the culture period a combined diagram for both groups is drawn with the obtained values on the y-axis [mm^2] against the measurement days on the x-axis

2.1.2.6. Gene expression (A5)

<u>I. Material</u>

- RNeasy Mini Kit (Qiagen / 74106)
- QIAshredder (Qiagen / 79654)
- β-mercaptoethanol
- SuperScript II Reverse Transcriptase (Invitrogen / 18064-014)
- RNAse OUT Recombinant Ribonuclease Inhibitor (Invitrogen / 10777-019)
- Primer OligodT (15er) (Promega / C110A)
- dNTP's (10mM each)
- *Power* SYBR Green PCR Master Mix (Applied Biosystems / 4367659)
- Primers according to table 6

Gene	forward primer 5' → 3'	reverse primer 5' → 3'
ALP	TTGTGCCAGAGAAAGAGAGAGAC	TTGGTGTTATATGTCTTGGAGAGG
Bglap1	GACCTCACAGATGCCAAGC	GACTGAGGCTCCAAGGTAGC
Col1a1	CCAAGAAGACATCCCTGAAGTC	TTGGGTCCCTCGACTCCT
Cst3	CGTAAGCAGCTCGTGGCT	CAGAGTGCCTTCCTCATCAGA
E11	CAGATAAGAAAGATGGCTTGCC	CTCTTTAGGGCGAGAACCTTC
Fos	CAACACACAGGACTTTTGCG	TCAGGAGATAGCTGCTCTACTTTG
Fosl2	AGATGAGCAGCTGTCTCCTGA	TCCTCGGTCTCCGCCT
Ibsp	AGGAAGAGGAGACTTCAAACGA	TGCATCTCCAGCCTTCTTG
Mmp13	GCAGTTCCAAAGGCTACAACTT	TCATCGCCTGGACCATAAAG
Osterix	TCTCTGCTTGAGGAAGAAGCTC	TTGAGAAGGGAGCTGGGTAG
Runx2	AGTCAGATTACAGATCCCAGGC	GCAGTGTCATCATCTGAAATACG
Spp1	AGCAAGAAACTCTTCCAAGCA	TGGCATCAGGATACTGTTCATC
Twist1	GCTCAGCTACGCCTTCTCC	ACAATGACATCTAGGTCTCCGG
Actin beta	GCCACCAGTTCGCCAT	CATCACACCCTGGTGCCTA
Pgk1	GAGCCCATAGCTCCATGGT	ACTTTAGCGCCTCCCAAGA

Table 6. qRT-PCR primer for the cell culture system.

- 384-well plates (ABgene / TF-0384)
- Optical PCR protective film – Optical Adhesive Covers (Applied Biosystems / 4311971)
- Taq-Man 7900HT Fast Real-Time PCR System (Applied Biosystems) including software (Applied Biosystems ABIprism SDS 2.1)

<u>II. Measurement day</u>

- 24-well Primaria cell culture plate
- The samples (n wells) of both biological groups are pooled for the preparation (no technical replicates)
    - 6 x wt → 4 wells are pooled for wt sample
    - 6 x mut → 4 wells are pooled for mut sample

- RNA isolation is performed using the RNeasy Mini Kit according to the protocol "Purification of Total RNA from Animal Cells Using Spin Technology"
    - 10 µl β-mercaptoethanol is added to 1ml of buffer RLT

- o aspiration of old media from the wells
- o cells are washed once with 1x PBS
- o for each group (6 wells) the RNA of 4 wells is pooled: 350 µl buffer RLT is added to well 1 and afterwards transferred to well 2, well 3 and well 4 for cell lysis (repeated up and down pipetting of the buffer should be performed to ensure complete lysis of the cells)
- o the lysate of each pooled sample (350 µl) is loaded onto a QIAshredder column and centrifuged for 2 min / RT / 13000 rpm to homogenize the lysate
- o both homogenized lysates (1 x wt / 1 x mut) are stored at -80°C

III. Assay analysis

- • RNA isolation
    - o RNA isolation is completed with all frozen samples (lysates) according to the protocol (5 x wt / 5 x mut)
    - o RNA is eluted in 50 µl RNAse free H_2O and stored at -80°C

- • cDNA synthesis
    - o for each sample the RNA is reverse transcribed into cDNA according to the following scheme

RNA	15 µl
Primer OligodT	2 µl
→ **Pre-annealing**	**10 min / 65°C**
5x buffer	10 µl
dNTP-Mix	2.5 µl
RNAse Out	2 µl
Super Script II	2 µl
H_2O	16.5 µl
→ **Incubation**	**60 min / 42°C**
→ 50µl cDNA	(stored at -80°C)

- • qPCR reaction / master mix
    - o for each sample a qPCR reaction is performed as described below
    - o the cDNA is applied in a 1:10 dilution with H_2O
    - o each sample is analyzed with 4 technical replicates for the expression of 15 genes (overall 60 qPCR reactions for each sample) – therefore a master mix of 65x is recommended for each sample
    - o please note: the forward and reverse primer for each gene are combined in one mixture with 5 µM each, the primers are not included in the master mix but pipetted separately

Reagents	qPCR reaction 1x	qPCR master mix (65x)
2x Power Sybr Green	10 µl	650 µl
cDNA (1:10)	2 µl	130 µl
H_2O	6 µl	390 µl
Primer fw + rv (5µM each)	2 µl	/
	→ 20 µl	→ 1170 µl

- Expression analysis with Taq-Man 7900HT
  - the 15 genes that are analyzed in the expression analysis are classified in 2 groups:

    1) target genes (target) (13) - bone relevant marker genes, expression is compared between the different samples
    2) reference genes (reference) (2) - internal reference for the target genes in each probe (housekeeping genes)

  - the qPCR reactions are pipetted in 384well plates and the expression analysis is performed using the Taq-Man 7900HT
  - given the huge number of samples, genes to be analyzed and technical replicates (10 samples x 15 genes x 4 replicates = 600 reactions overall), two plates have to be applied with the following distribution of the samples

Plate 1	Plate 2
wt T0	wt T15
mut T0	mut T15
wt T3	wt T21
mut T3	mut T21
wt T9	/
mut T9	/

  - the samples (master mix) and primers are pipetted in a 384well plate according to the following scheme (red - target genes / green - reference genes)

Primers are described by the name of the respective genes and the samples are labeled with S1 - S6. As depicted, each sample is analyzed with 4 technical replicates for the expression of each gene (S1 = 1/2/3/4, S2 = 5/6/7/8 …).

- o the qPCR reactions (master mix and primer) are pipetted in the 384well plate using an adjustable Matrix 8-channel pipette
- o primers are added first with 2 µl per well according to the scheme and afterwards the master mixes are added with 18 µl per well
- o the plate is sealed with the Optical Adhesive Covers and centrifuged for 2 min / RT / 2000 rpm
- o the qPCR is performed in the Taq-Man 7900HT according to the following scheme and the results are saved as SDS file

Temperature	Time	Cycles
95°C	10 min	1
95°C	15 sec	40
60°C	1 min	
Melting curve (55°C – 95°C)		1

- Evaluation of the qPCR and determination of the crossing point (C_t)
  - o the saved SDS files are analyzed using the software ABIPrism SDS 2.1
    - o File → Open
    - o Analysis → Analysis Settings… → Automatic C_t √
    - o Analysis → Analyze
    - 1) melting curve of each qPCR has to be checked
    - 2) C_t-values are exported: File → Export → save as Text file

- Determination of target gene expression
  - o C_t-values are transferred from the Text file into Excel file
  - o <u>for each sample</u> the determination of the expression values of the 13 target genes is performed according to the following procedure:

    1) the C_t values of the 4 technical replicates ($C_{t1/2/3/4}$) from each gene (13 x target and 2 x reference) are averaged to obtain the arithmetic mean C_t for each gene (please note: $C_{t1/2/3/4}$ values with a difference of ± 0.5 from the mean value are not considered for the calculation)

    $$C_t = \frac{(C_{t_1} + C_{t_2} + C_{t_3} + C_{t_4})}{4}$$

    2) the C_t value of both housekeeping genes *Actin beta* ($C_{tActin\ beta}$) and *Pgk1* (C_{tPgk1}) is averaged to obtain the reference C_t value (C_t reference) for the determination of the target gene expression

    $$C_{t\ reference} = \frac{(C_{t\ Actin\ beta} + C_{t\ Pgk1})}{2}$$

3) the following equation is used to calculate the expression for each of the 13 target genes (E_{target})

$$E_{target} = \frac{2^{C_t \text{ reference}}}{2^{C_t \text{ target}}} \times 100$$

4) E_{target} corresponds to the expression level of the respective target gene in percentage to the reference value (expression of *Actin beta* and *Pgk1* = as 100%) in the analyzed sample

e.g.: expression of *ALP* in a sample xy (for instance T3 wt)

$$C_t \text{ reference} = \frac{C_{t \text{ (Actin beta + Pgk1)}}}{2} = 18.2$$

$$C_t \text{ target} = C_{t \text{ ALP}} = 19.7$$

$$E_{target} = \frac{2^{C_t \text{ reference}}}{2^{C_t \text{ target}}} \times 100 = E_{ALP} = \frac{2^{18.2}}{2^{19.7}} \times 100 = \underline{\underline{35.36}}$$

→ in the sample T3 wt, the expression of the *ALP* gene equates 35.36% compared with the expression of the reference value (*Actin beta* and *Pgk1* = 100%)

5) for each of the 10 samples the expression values for all 13 target genes is determined and saved (Exel file)

VI. Results and presentation

- For each sample (biological group at certain measurement day) the expression level of the 13 target genes is determined in [%] to the expression of the reference
- For graphic presentation of the gene expression during the culture period a single diagram for each of the 13 target genes is drawn with the expression level of the respective gene on the y-axis against the measurement days on the x-axis for both groups (wt and mut)

2.2. Heart and lung investigation in the *Aga2* OI mouse model

2.2.1. Animal keeping and handling

As the *Aga2* mutant line was generated on the C3HeB/FeJ background in the Munich ENU mutagenesis screen [54, 55], breeding for animal maintenance and experimental needs were performed by continuing mating of heterozygous *Aga2* males with wild type C3HeB/FeJ female mice.

Mouse husbandry was conducted under a continuously controlled specific-pathogen-free (SPF) hygiene standard in compliance with the Federation of European Laboratory Animal Science Associations (FELASA) protocols. Mice received standard rodent nutrition and water *ad libitum* and all animal experiments were performed under the approval of the responsible animal welfare authority.

2.2.2. Genotyping

The offspring were tail-clipped and the DNA was isolated using QIAamp DNA Mini Kit (Qiagen, Germany). Afterwards, forward primer 5'-ggcaacagtcgcttcaccta-3' and reverse primer 5'-ggaggtcttggtggttttgt-3' were used to amplify the entire intron 50 of *Col1a1* in a standard PCR. The product was cleaved using MspAII yielding 156 bp and 75 bp fragments in wild type mice and 231 bp / 156 bp and 75 bp fragments in heterozygous *Aga2* as detected on a 2% agarose gel [55].

2.2.3. Cardiovascular phenotyping

Heart function and performance was investigated in living mice using the cardiovascular screen of the German Mouse Clinic (GMC). The GMC is a unique mouse phenotypic center consisting of 14 different screens covering various fields of mouse biology, thus allowing for comprehensive phenotyping [61].

Within the primary cardiovascular screen 20 *Aga2^{mild}* and 19 wild type control mice at the age of 14 weeks underwent ECG analysis.

ECG was performed on isoflurane anesthetized mice (Baxter, Germany). Three metal bracelets were bonded to the feet joints together with electrode gel. The

complete setup was located in a faraday cage. The electrodes were positioned on the front-paws and the left hind-paw, resulting in the bipolar standard limb leads I, II and III and the augmented unipolar leads AVF, AVR, AVL. ECG was recorded for approximately seven minutes and a shape analysis of the ECG traces was performed with the ECG-auto software (EMKA technologies, France). For each animal, intervals and amplitudes were evaluated from five different sets of averaged beats (usually lead II). The parameter Q-T interval was also corrected for the RR interval. In addition, the recordings were screened for arrhythmias including supraventricular and ventricular extrasystoles and conduction blockages. In the quantitative ECG analysis, sets of five analyzed beats were averaged for one animal.

The data were statistically analyzed using the Statistica program. Analysis of variance (ANOVA) tests were used for multi-factorial analysis of sex and genotype. Post hoc analysis for multiple comparisons included a Duncan's Multiple Range Test and Critical Ranges.

The secondary screen comprised echocardiography followed by an ECG analysis and was performed with 6 $Aga2^{severe}$ and 6 wild type control mice at the age of 10 and 11 days.

Left ventricular function was determined by transthoracic echocardiography using high-frequency ultrasound biomicroscopy with a Vevo 660 30-MHz transducer and 30 Hz frame rate (VisualSonics, Canada). The shaved and isoflurane (1%) anesthetized mice (Baxter, Germany) were fixed in supine position on a heated platform. Thus, the body temperature was maintained at 36°C - 38°C and monitored via a rectal thermometer (Indus Instruments, USA). Left ventricular parasternal short-axis views were obtained in M-mode imaging at the papillary muscle level. We performed four recordings and averaged the measurements from four cardiac cycles of each record for the left ventricular end-diastolic internal diameter (LVEDD) and the left ventricular end-systolic internal diameter (LVESD) using the leading-edge convention, as suggested by the American Society of Echocardiography [62]. Fractional shortening was calculated as FS (%) = [(LVEDD – LVESD) / LVEDD] × 100 and ejection fraction as EF (%) = $[7/(2.4+LVEDD) \times LVEDD^{3}] – [7/(2.4+LVESD) \times LVESD^{3}]$ as described elsewhere [63, 64].

2.2.4. pO$_2$ measurement

We collected blood samples from 4 *Aga2^{severe}* as well as 6 *Aga2^{mild}* and 15 wild type control mice at the age of 8 to 11 day to measure blood gas parameters. Animals were decapitated and blood leaking from the arteria carotis was directly soaked into an 85 µl blood gas capillary (Kabe, Germany). Blood pH, pO$_2$ and pCO$_2$ was immediately determined by direct measurement using an ABL5 blood gas analyzer (Radiometer, Germany) and the corresponding parameters O$_2$ saturation, carbon dioxide concentration (HCO$_3^-$) and actual base excess (ABE) were automatically calculated.

2.2.5. Histology and SEM

Animals at the age of 11 and 10 days were used for histological studies and SEM analyses, respectively.

For histological evaluation of the heart, *Aga2^{severe}* were compared to wild type littermates and lung tissues were investigated by comparing *Aga2^{severe}* and *Aga2^{mild}* with wild type controls. After decapitation of the animals, organs were removed and fixed in 4% paraformaldehyde at 4°C over night. To overcome the drawbacks of examining collapsed lungs, we additionally applied the technique of lung perfusion prior to histological procedures. Under deep anesthesia by intraperitonal injection of a mixture of xylazin and ketamine, the animals were exsanguinated through chopping of the abdominal aorta. After dissection of the thorax, the lungs were uncovered and surrounding tissues removed. A blunted 22-gauge needle was used for intratracheal injection of the fixative (4% paraformaldehyde) to perfuse the lungs. Finally the trachea was ligated with a surgical thread to avoid leakage of the fixative and the lungs were immersed in 4% paraformaldehyd and incubated at 4°C over night.

After fixation, heart and lung tissues were either paraffin embedded or cryosectioned. Paraffin embedding was performed by dehydrating tissues through a graded ethanol series, clearing in xylene and embedding them in paraffin. Afterwards, samples were cut to 7 µm sections for staining procedures. For cryosectioning, tissues were infiltraded in graded series of 5%, 10% and 20% sucrose and finally embedded in O.C.T. medium. Thereafter, they were cut to 10 µm or 50 µm thickness according to the staining requirements.

For histological examination, sections were stained by haematoxylin and eosin (H&E) or for more detailed analysis subjected to immunohistochemistry (IHC).

Primary antibodies used for IHC include polyclonal rabbit-anti type I collagen and polyclonal rabbit-anti CD31 (Abcam, UK) as well as polyclonal rabbit-anti activated caspase-3 (R&D Systems, Germany). They were applied according to manufacturer's recommendations and detected with fluorescent labelled Alexa Fluor 594 donkey-anti-rabbit IgG (Molecular Probes) or by using Vectastain ABC kits for DAB staining (Linaris, Germany).

Samples were analysed under a Zeiss Axioplan2 fluorescent microscope equipped with AxioVision 4.6.3.0 software and under a Zeiss LSM510 confocal microscope with the corresponding program 3.2 SP2 (Zeiss, Germany).

For scanning electron microscopy (SEM) of the hearts, tissues were additionally subjected to a maceration protocol to remove cellular components and ECM elements, thereby preserving and exposing the remaining collagen structure and network [65, 66].

Briefly, bisected hearts were fixed in 2.5% glutaraldehyde for 6 days and immersed in 2 M NaOH for additional 6 days with replacing the NaOH maceration solution every second day.

Subsequently, hearts were washed in several changes of distilled water to remove the cellular debris. Tissue was further immersed in 1% Tannic acid for 3 hours, rinsed in distilled water for several hours and postfixed in 1% OsO_4 for 1 hour. Samples were dehydrated in a graded series of 25%, 50%, 70%, 95% and 100% ethanol. Finally, the specimens were critical-point-dried, coated with platin and observed under a JEOL JSM 6300F scanning electron microscope (JEOL, Japan).

2.2.6. *In vitro* cell culture and TEM

For in vitro analysis of the heart and lung phenotype, we include cell culture experiments for primary heart and lung fibroblasts comparing *Aga2severe* with *Aga2mild* and wild type littermate controls at the age of 12 days.

To isolate the cells, we used an enzymatic collagenase digestion method previously described for both cell types [67-72]. We optimized the protocol according to our requirements and isolation of heart and lung fibroblasts was performed in a similar manner.

Animals were killed by decapitation, tissues were excised, immediately placed in 4°C HBSS and brought under a sterile working bench for subsequent preparation steps. Tissues were minced with scissors to pieces of approximately 1-2 mm and washed 3 times with HBSS buffer. To remove debris and loosely attached contaminating cells, the pieces were subjected to a 5 minute predigesting step with 0.1% collagenase IV (Sigma) at 37°C. The supernatant was discarded and to obtain the required fibroblasts, two successively digestion steps were performed. Briefly, the tissues were treated with fresh collagenase mixture for 30 minutes at 37°C. The supernatant containing dispersed cells was collected by filtration through sterile gauze, leaving behind the undigested tissue. Equal amounts of DMEM supplemented with 10% FCS, 2 mM Glutamine and antibiotics (Penicillin / Streptomycin 100U/ml each) were added and the cell suspension was stored at 4°C. The remaining tissue underwent a second digestion step with fresh collagenase solution for a further 30 minutes. After gauze filtration of the second digestion mixture, the supernatants of both digestion steps were pooled and the containing cells were pelleted by centrifugation for 10 minutes at 1200 rpm. The pellet was resuspended in DMEM media and the cells were plated in T25 cm^2 cell culture flask for 1 hour. Thereafter, non-adherent cells were removed by rinsing with PBS and fresh media was added to the attached cells. The fibroblasts were incubated in a humidified incubator at 37°C and 5% CO_2 with media changes twice a week. After reaching confluence, the cells were passaged by detaching with 0.25% trypsin-EDTA solution and splitting 1:2 or 1:3 in new flasks. Cells from single mice were cultivated individually, or they were pooled between phenotype-alike animals (WT, *Aga2mild, Aga2severe*).

Cultures were used for the experiments between the first and third passage and therefore seeded on Lumox™ 24-well plates (Greiner, Germany) for ICC studies, on Thermanox™ coverslips (Nunc, Germany) for TEM analysis and on standard 24-well plates for RNA isolation, with an initial density of 1×10^5 cells per well. After 48 hours of incubation, ascorbic acid (50 µg/ml) was added and the cells were grown for another 24 hours before being deployed in our studies.

For immunocytochemistry (ICC), fibroblasts were washed with PBS, fixed in 4% paraformaldehyde for 15 min and permeabilized in 0.1% Trition-X100 for 5 minutes. After incubation with 5% bovine serum albumin over night, the ICC was performed with polyclonal rabbit-anti type I collagen, polyclonal rabbit-anti activated caspase 3 and monoclonal mouse-anti alpha-Tubulin as primary antibodies according to the manufacturer's recommendations (Abcam, UK). According to the primary antibodies, we used fluorescent labelled Alexa Fluor 488 goat-anti-rabbit IgG or Alexa Fluor 594 goat-anti-mouse IgG (Abcam, UK) as secondary antibodies. Finally, specimens were coated with Vectashield mounting medium (Linaris, Germany) containing DAPI for concomitant counterstaining of the nuclei. Samples were observed under a Zeiss Axioplan2 fluorescent microscope equipped with AxioVision 4.6.3.0 software (Zeiss, Germany).

Transmission electron microscopy (TEM) was conducted by Microscopy Services Dähnhardt GmbH (Flintbek, Germany) according to the following procedure. Cells were washed with PBS and fixed in a mixture of 2% paraformaldehyde and 2.5% glutaraldehyde for at least 24 hours at 4°C. After rinsing twice with 0.133 M Na-cacodylatbuffer for 5 minutes each, they were postfixed in 1% osmium tetroxide for 10 minutes and again rinsed twice with 0.133M Na-cacodylatbuffer for another 5 minutes each. Specimens were dehydrated in a graded series of 50%, 70%, 90% and 100% ethanol 10 minutes each and embedded in graded series of 30%, 50%, 70% and 100% Agar 100 epoxy resin (Plano, Germany) for 20min each. Ultra-thin sections were cut, stained with uranyl acetate and lead citrate and examined with a Tecnai Spirit G2 transmission electron microscope (FEI, the Netherlands).

RNA isolation of the primary cultures was done as described below.

2.2.7. RNA Isolation

For isolation of RNA from heart and lung tissue, animals were killed at the indicated ages by decapitation for postnatal stages or by CO_2 for pregnant mice with subsequent embryo withdrawal for prenatal stages. The organs were immediately removed and frozen in liquid N_2. In some cases, animals were used for pO_2 measurement or cardiovascular examination and afterwards killed as described.

Before the RNA extraction was performed, hearts and lungs were treated with Trizol (Invitrogen, Germany). Afterwards the tissues were homogenized using a Polytron homogeniser (Heidolph, Germany) and total RNA from each sample was obtained using the RNeasy Mini or Micro Kit – depending on the tissue weight – according to manufacturer's protocol (Qiagen, Germany). The RNA was eluted with RNase free water and the concentrations were determined by $OD_{260/280}$ readings with NanoDrop ND-1000 Spectrophotometer (peqlab, Germany). The samples were stored at -80°C until used for expression profiling or qPCR study.

For RNA extraction of *in vitro* cultivated primary heart and lung fibroblasts, the cells were seeded in 24 well-plates and 24 hours before extraction additionally treated with 50 µg/ml ascorbic acid (see below). Cultures were washed in PBS one time and RNA was isolated by use of RNeasy Mini Kit pursuant to manufacturer's recommendations with addition of β-mercaptoethanol to buffer RLT (10 µl/ml) for cell lysis. After elution in RNase free water, the specimens were stored at -80°C until qRT-PCR analysis was conducted.

2.2.8. Expression profiling

We performed a cDNA-chip based expression profiling study of heart and lung tissue. Therefore we include three *Aga2severe* female mice and four wild type female littermate controls at the age of 11 days.

Glass cDNA-chips were made encompassing the fully sequenced 20K cDNA mouse array TAG library (Lion Bioscience, Germany) as well as several hundred cDNA clones not included in the commercial clone set as previously described [73]. A full description of the probes on our microarray is available in the GEO database under GPL4937 [74].

PCR products with 5' amino modification were amplified from these clone set and purified by use of multiscreen PCR filter plates (Macherey & Nagel, Germany) in a liquid handling robot (Tecan, Switzerland). Amplified probes were dissolved in three-fold SSC buffer and spotted on aldehyde-coated microarray slides (CEL Associates, USA) using a Micorgrid TAS II spotter (Genomic Solutions, UK) with Stealth™ SMP3 pins (CEL Associates, USA). Spotted slides were rehydrated overnight, blocked in sodium borohydride solution, heat denatured by boiling in water for two minutes, immersed in 100% ethanol and air-dried. Slides were treated with prehybridisation buffer (6x SSC, 1% BSA, 0.5% SDS), rinsed in water, dried and hybridised the same day as described below.

The RNA was isolated from heart and lungs as described above, the concentration measured by $OD_{260/280}$ readings and the integrity checked by running 2 µg of each sample on a formaldehyde agarose gel.

For RNA labeling and hybridisation to cDNA microarrays, the RNA samples of the three *Aga2severe* mice were treated as single probes and from the four RNA samples of the wild type littermate controls, one pool was made to obtain a reference, each with heart and lung.

Per chip experiment, 20 µg of each RNA sample was reverse transcribed and indirectly labelled with Cy3 or Cy5 fluorescent dye (Amersham, Germany) in accordance with a modified TIGR protocol [75].

Labelled cDNA was dissolved in 50 µl hybridisation buffer (6x SSC, 0.5% SDS, 5x Denhardt's solution and 50% formamide) and mixed with equal volume of reference

cDNA solution labelled with the second dye. The hybridisation mixture was placed on a prehybridised microarray and incubated for 16-18 h in a thermostatic water bath at 42°C. Afterwards, slides were consecutively washed with 3x SSC, 1x SSC, 0.5x SSC and 0.1x SSC at room temperature and dried by centrifugation. Prehybridisation, hybridisation, washing and drying (nitrogen) steps were automated by application of a HS400 Hybstation (Tecan, Switzerland).

Slides were scanned with a GenePix 4000A microarray scanner and the images were analyzed using the GenePix Pro6.1 image processing software (Molecular Devices, USA). Two independent dual colour hybridisations (technical replicates) including a dye swap experiment were performed for each of the individual $Aga2^{severe}$ RNA samples (biological replicates) using the wild type RNA pool as reference. Expression data of the analysed $Aga2$ samples from heart and lung have been submitted to the GEO database (GSE12847).

Statistical analyses were performed using TM4 Microarray software suite including MIDAS (Microarray Data Analysis System) for normalization [76] and SAM (Significant Analysis of Microarrays) for determination of genes showing significant differential regulation [77]. Expression data were processed applying a total intensity normalization to transform the mean $\log_2$ ration to zero. To identify significantly regulated genes, a one class analysis was performed for each probe of the $Aga2^{severe}$ mice. The false discovery rate (FDR) - which is the percentage of genes identified by change - was estimated by calculating 1000 permutations of the measurements and the cut-off for discrimination of the top differentially expressed genes with reproducible up- or down regulation was set below 10% false positives (FDR).

In silico analysis of differentially expressed genes was performed using EASE, a module of the DAVID database [78], assigning genes to Gene Ontology (GO) functional categories. EASE analysis includes a Bonferroni multiplicity correlation and evaluates the set of differentially expressed genes for over-representation of biological processes. In depth analysis and description of the denoted genes for molecular function and pathological involvements was additionally done using BiblioSphere Pathway Edition including a comprehensive manual interpretation of the gene functions by intensive literature study with EndNote program.

2.2.9. qRT-PCR

Quantitative RT-PCR studies (qRT-PCR) were carried out with RNA extracted from heart and lung tissue or primary cell cultures as specified and RNA was isolated as described above.

cDNA was synthesized by using Superscript II ReverseTranscriptase Kit (Invitrogen, Germany) and Oligo(dT)$_{15}$ primer (Promega, Germany). Briefly, 15 µl of RNA was incubated with 2 µl of Oligo(dT) primer for 10 minutes at 65°C. Thereafter the preincubation mixture was supplemented with 10 µl 5x first strand buffer, 2.5 µl dNTP mixture, 2 µl Superscript II, 2 µl RNaseOUT ribonuclease inhibitor and 16.5 µl RNase free water and incubated for 1 hour at 42°C. The cDNA was stored at -80°C or directly implemented for qPCR.

For conducting the qPCR we prepared an amplification mixture consisting of 2 µl 1:10 diluted cDNA, 10 µl Power Sybr Green (Applied Biosystems, Germany), 6 µl water and 1 µl of forward and reverse primer (10 µM each). Reactions were pipette on Thermo-Fast 384-well PCR plates (Thermo Scientific, Germany) and run on an ABI Prism 7900HT Sequence Detection System (Applied Biosystems, Germany). Cycling conditions comprised of 10 min at 95°C for initial denaturation and activation of Hotstart Polymerase followed by 40 cycles of 15 sec at 95°C for denaturation and 1 min at 60°C for annealing as well as elongation. Finally all PCR reactions were validated by presence of a single peak in a melting curve analysis starting at 55°C reaching 95°C under continuous fluorescence measurement. Each PCR was done in 3 technical replicates.

C_t values were obtained by automatic C_t analysis of the ABI Prism SDS 2.1 software (Applied Biosystems, Germany) and the mean C_t value from the 3 replicates of each PCR was determined.

Table 7 compile the Primers used for the qPCR analysis. To avoid contaminating amplification of genomic DNA, each single primer was designed to prime in contiguous sequences of two adjacent exons, allowing binding of primers exclusively after introns are spliced out. Thereby, the product automatically span at least one intron to additional impede the amplification of genomic DNA.

Determination of the gene expression was performed as relative quantification with calibrator normalization, whereby the wild type samples were used as calibrator with target gene expression set as 100%. Expression data were calculated using the equation of Pfaffl [79] with assuming an identical amplification efficiency of the target and reference genes according to the $2^{-\Delta\Delta Ct}$ method [80]. Efficiency testing of all amplicons confirmed their equal amplification efficiency.

For normalization of the target gene expression, the C_t values from two or three housekeeping genes were averaged to obtain a mean internal reference value in each sample.

Gene / Allele	forward primer 5' → 3'	reverse primer 5' → 3'
Actin beta	GCCACCAGTTCGCCAT	CATCACACCCTGGTGCCTA
GAPDH	TGGAGAAACCTGCCAAGTATG	CATTGTCATACCAGGAAATGAGC
Pgk1	GAGCCCATAGCTCCATGGT	ACTTTAGCGCCTCCCAAGA
Hprt1	CTGATTATGGACAGGACTGAAAGA	CCGTTGACTGATCATTACAGTAGC
Col1a1	CCAAGAAGACATCCCTGAAGTC	TTGGGTCCCTCGACTCCT
Col1a1^{WT}	GATGGATTCCCGTTCGAGTA	AGTTCCGGTGTGACTCGTG
Col1a1^{Aga2}	GATGGATTCCCGTTCGAGTA	GACTCTGGTGTGAATGAAGACG

Table 7. qRT-PCR primer for heart and lung investigation in *Aga2*.

2.2.10. Statistical analysis

Mean values and corresponding SEM of the obtained results were determined from the indicated number (n) of biological replicates of each group (WT, *Aga2^{mild}*, *Aga2^{severe}*) used for the indicated experiment. In case sample size was n ≥ 3, statistical significance of the observed differences between the groups was tested by applying non-parametric Mann-Whitney U test using the Stat View software package (SAS cooperation). A p-value of 0.05 was chosen as the critical factor for significance and [*] indicate the significance-ranking according to the following classification: [*] = p ≤ 0.05, [**] = p ≤ 0.01, [***] = p ≤ 0.001.

3. Results

3.1. *In vitro* analysis of osteoblasts

3.1.1. Establishment of the cell culture system

3.1.1.1. Growth and differentiation of the osteoblasts

Cells were isolated from the calvaria of newborn mice using enzymatic digestion of the tissue with Collagenase VI to dissolve the cell matrix, thereby releasing the cells. The age of the mice used for the isolation protocol was important for the quantity of cells that were obtained from the calvariae. Between day 3 and 6 postnatal, 7.5×10^5 cells could be isolated in average out of a single calvaria. Thereafter, with advancing age of the animals, the amount of cells that were released from the calvaria was markedly decreased. Furthermore, the quality of the applied Collagenase VI was as well important for the isolation efficiency and the yield of cells depended on the batch of the enzyme.

The isolated cells appeared morphological polygonal / cuboidal and were cultivated under proliferating conditions for 5 days to reach confluence (figure 12).
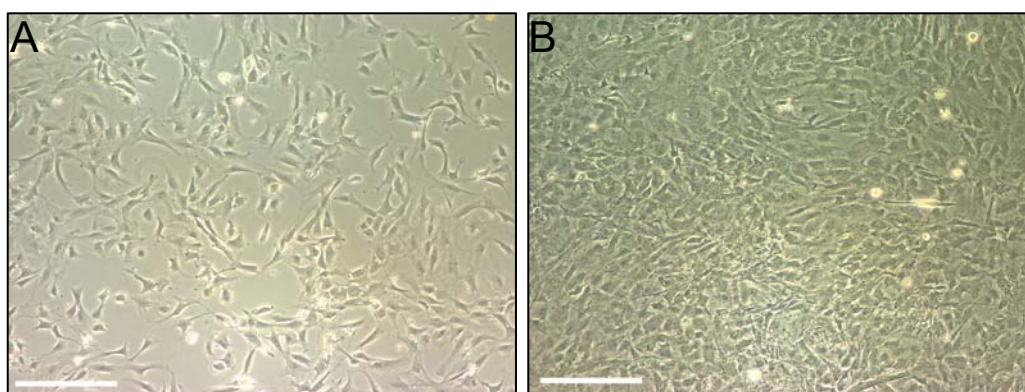
Figure 12. Primary calvarial cells after isolation. Two days after preparation single cells are visible (A) that form a monolayer after 5 days (B). Scale bar in A,B = 250 µm.

After confluence has reached, differentiation of the cells towards a more mature osteoblast phenotype was initiated by adding β-glycerophosphate and ascorbic acid to the culture (culture medium B). That time point was referred to as T0 and thereafter, the cells were cultivated for another 21 days (T0-T21) under stimulating conditions.

The differentiation of the cells was morphological discernable by the development of nodule-like structures (nodules), that first appeared between T7-T10 and grew in size throughout the cultivation period. The nodules possessed a 3D-structure and immunocytochemical analysis for E11 (Gp38) revealed exclusive staining of the nodules in the stimulated cell culture (figure 13).
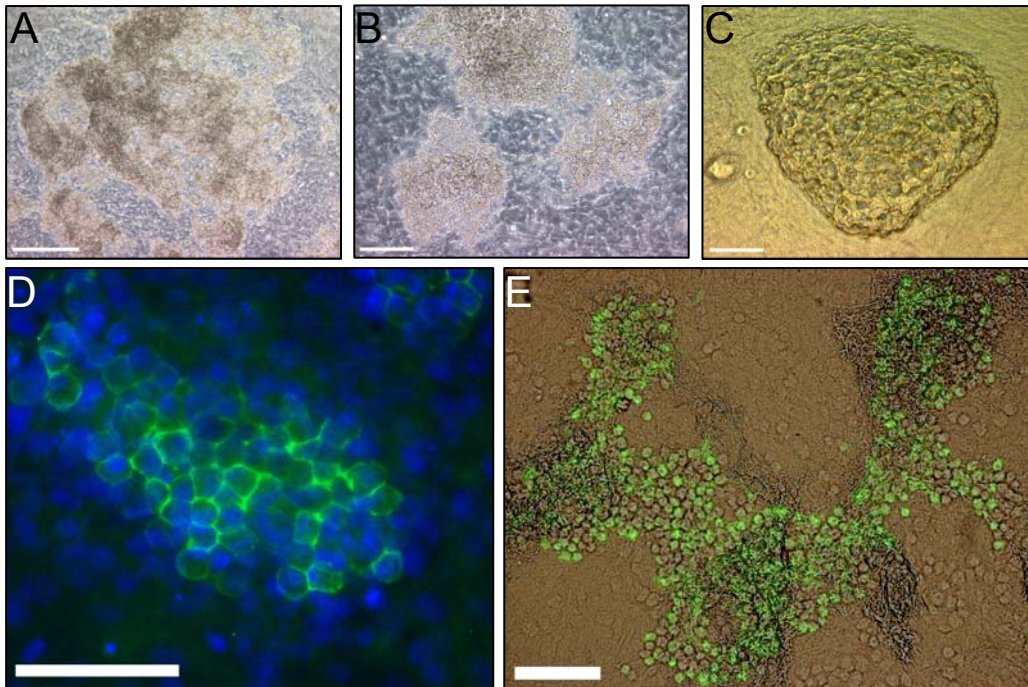
Figure 13. Nodule formation in primary calvarial cell cultures. **A,B,C** Transmitted light images of primary calvarial cultures. After stimulation with ascorbic acid and β-glycerophosphate, nodule-like structures are formed (A,B = T8; C = T11). **D,E** ICC for E11 on primary calvarial cultures (green - E11; blue - DAPI counterstain). After stimulation, E11 is expressed only within the nodules (D = T7; E = T10 / overlapping picture of fluorescent image and transmitted light image). Scale bar in A = 250 µm; B,E = 100 µm; C,D = 50 µm.

Initial experiments have shown that the ability and degree of differentiation / nodule formation depend on three important conditions. (1) Nodule formation only occurred in cells directly descending from the calvaria (passage P0) and completely disappeared when the cells were trypsinized and subcultivated (figure 14 A,B). (2) The cell density at the time point of stimulation (T0) considerably influenced the degree of differentiation with increasing nodule formation at higher cell densities (figure 14 C,D). (3) Finally, the quality of the FCS used as media supply was also found to be crucial for the differentiation of the culture and the number as well as the size of the nodules varied between different batches of the FCS as depicted in figure 14 E,F.
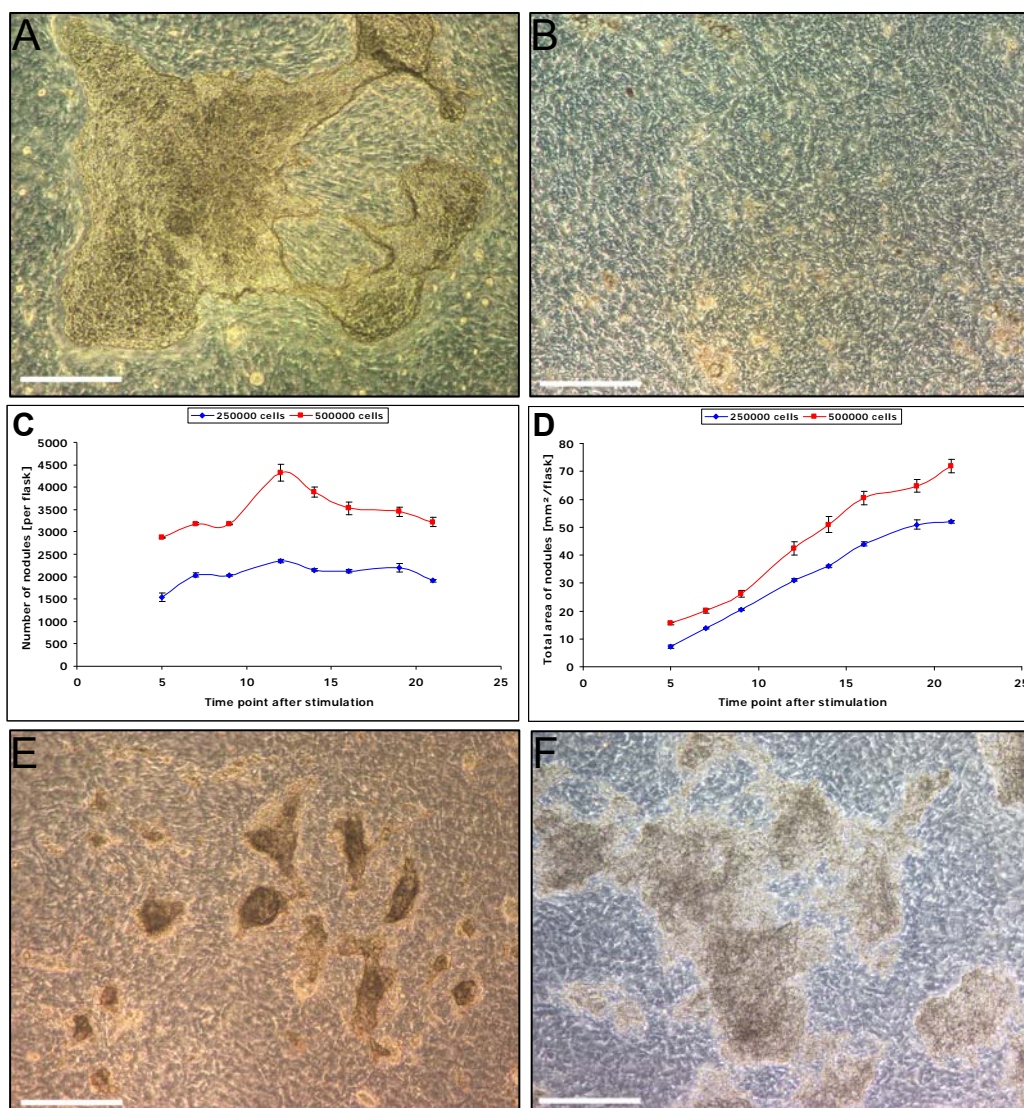
Figure 14. Influence of culture condition on nodule formation. **A,B** Influence of cell passage. Primary cells directly descending from the calvaria develop nodules (A = P0/T16), whereas subcultivation prevent nodule formation (B = P1/T33). **C,D** Influence of cell density. In cultures with $5x10^5$ initially plated cells (n = 3) the number (C) as well as the total area (D) of nodules is higher throughout the culture period compared to cultures with initially $2.5x10^5$ plated cells (n = 3). The observed decrease in the number of nodules towards the end of the culture period in cultures with $5x10^5$ plated cells results from the fusion of small single nodules when they increase in size. **E,F** Influence of FCS. Depending on the quality of FCS, nodule formation is poor (E = T7) or highly pronounced (F = T8). Scale bar in A,B,E,F = 250 µm.

3.1.1.2. Proliferation / Metabolic activity / Protein content / ALP activity (A1)

The proliferation was determined by quantification of the DNA content in the cultivated cells at each measurement day to receive a growth curve for the culture. Furthermore, the DNA amount was used as a reference value to normalize the Metabolic activity, Protein content as well as ALP activity in each sample.

The DNA was quantified using a fluorescence dye (Quant-iT dsDNA Assay Kit) that intercalates into dsDNA with the emitted fluorescence being proportional to the amount of dsDNA in the sample.

To validate the established method, the DNA was measured in samples with different cell numbers. As depicted in figure 15, the applied method provides a strong correlation between cell number and DNA concentration.
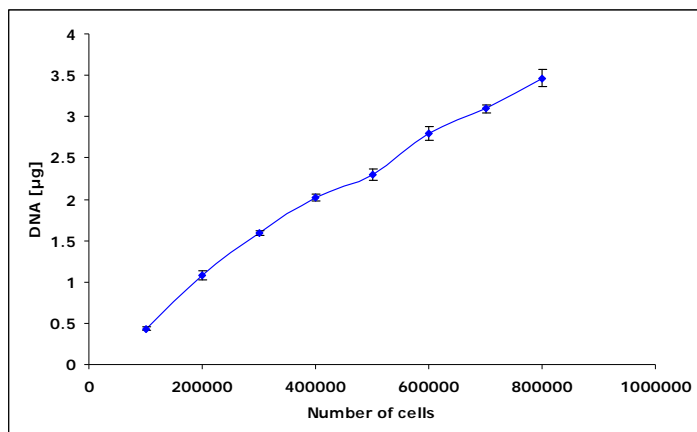
Figure 15. Validation of the Proliferation assay. The DNA amount in the cell culture is directly correlated with the cell number (n = 5).

The metabolic activity of the cells was assessed by using Resazurin (CellQuanti-Blue Reagent) for the Metabolic activity assay. The non-fluorescent redox dye can penetrate the cells and becomes reduced to the fluorescent product Resorufin inside living cells using the coenzyme NADH as reducing agent to donate electrons as shown below. Thus, the fluorescence intensity is proportional to the metabolic activity of the cells present in the culture [81, 82].
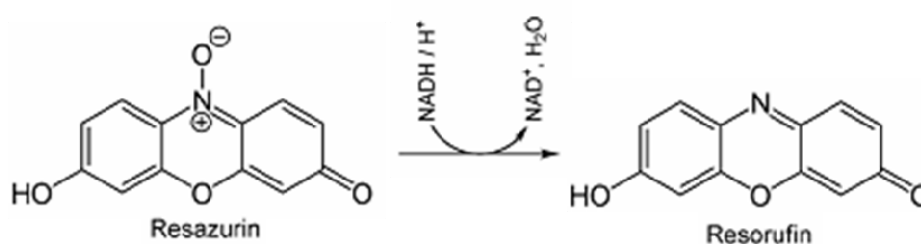
To validate the assay, the fluorescence was determined against the metabolic activity in samples with different cell numbers and furthermore related to the DNA amount of each sample, to prove if DNA can be included as reference value to normalize the metabolic activity. The fluorescence values (RFU) were directly correlated with the metabolic activity (figure 16 A) and after normalization, each sample possessed the same metabolic activity per µg DNA (figure 16 B).
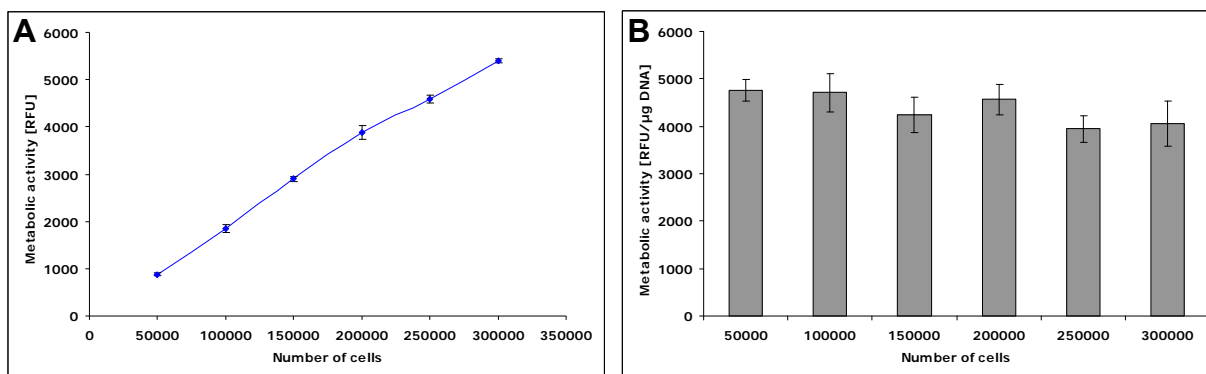
Figure 16. Validation of the Metabolic activity assay. The metabolic activity in a cell culture is directly correlated with the cell number (A) (n = 3). After normalization to the DNA amount, the metabolic activity is similar in all cultures independent from the cell numbers (B).

The cellular protein content was quantified based on the Cu^{+2} to Cu^{+1} reduction by proteins in an alkaline medium (biuret reaction). The amount of reduced Cu^{+2} is proportional to the amount of proteins present in the sample and the resulting cuprous cation (Cu^{+1}) can be colorimetric detected using bicinchoninic acid (BCA Protein Assay Kit) that chelate Cu^{+1} yielding in a purple water-soluble complex [83, 84].
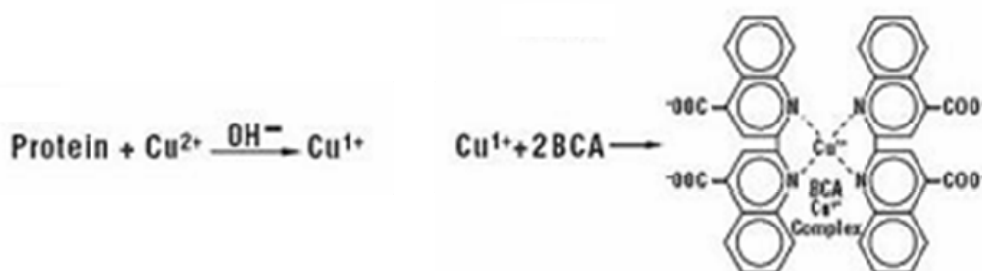
To validate the Protein quantification assay, the protein content was measured in samples with different cell numbers and furthermore related to the DNA amount of each sample, to prove if DNA can be included as reference value to normalize the protein content. There was a strong correlation between the protein concentration and the amount of cells (figure 17 A) and after normalization, each sample possessed the same protein content per µg DNA (figure 17 B).
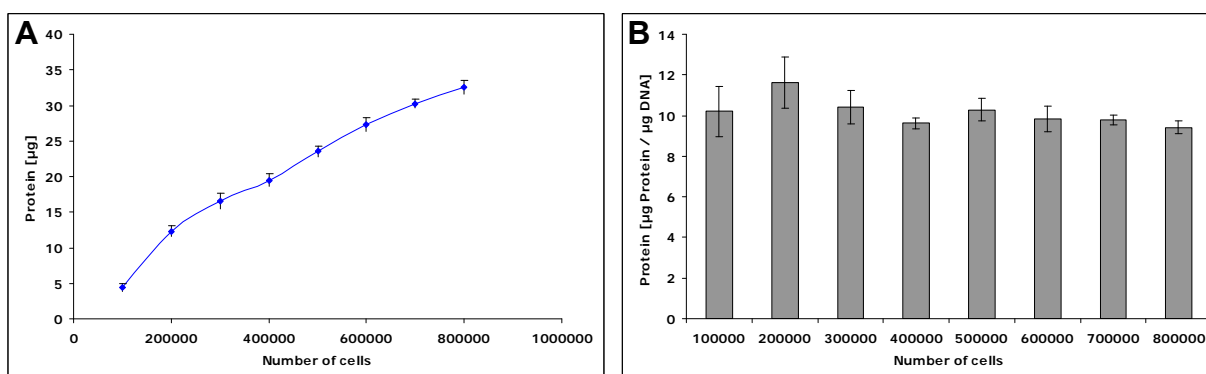
Figure 17. Validation of the Protein quantification assay. The protein content in a cell culture is directly correlated with the cell number (A) (n = 5). After normalization to the DNA amount, the protein content is similar in all cultures independent from the cell numbers (B).

The ALP activity of the cells was quantified using 4-Nitrophenylphosphate (PNPP). ALP catalyzes the hydrolysis of PNPP to p-nitrophenol, a chromogenic yellow product that can be determined colorimetrically. As the hydrolysis of the substrate is proportional to the activity of the enzyme, the absorption of the product is a quantitative measure for the ALP activity [85, 86].
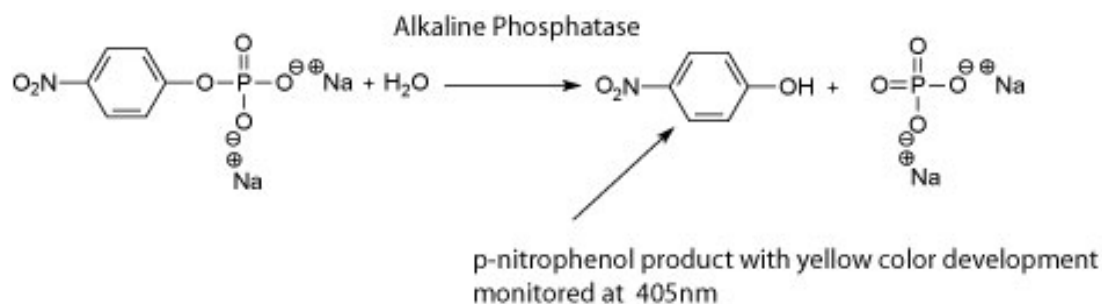
As the expression of ALP is related to the differentiation level of the cell culture, the enzyme activity was compared in unstimulated and stimulated cells against the cultivation time to validate the assay (figure 18). Indeed, there was a strong increase of the absorption values (arbitrary units) corresponding to the ALP activity in stimulated cells while no alteration of the enzyme activity could be observed in the unstimulated cells throughout the culture period.
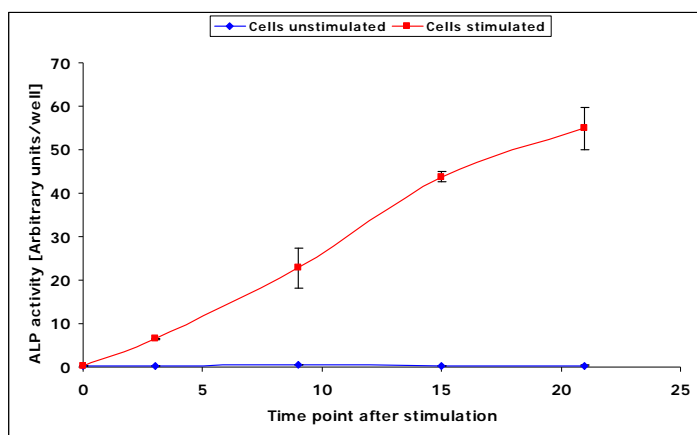
Figure 18. Validation of the ALP activity assay. ALP activity is only detectable in stimulated cultures (n = 3) and increased with cultivation time. In unstimulated cultures (n = 3), ALP activity is not detected.

3.1.1.3. Collagen secretion / Collagen deposition (A2)

The extracellular secretion as well as the matrix incorporation of collagen from the cultured osteoblasts was assessed based on the precipitation of collagen by Sirius Red (Sircol Dye reagent / Sirius Red FB3) [87, 88]. The anionic dye binds to the side chain groups of the basic amino acids with the [Gly-x-y] helical structure typical for all collagens in a parallel fashion to the triple helical collagen molecules. Therefore, it exclusively binds to native collagen and not to denatured or degraded collagens or other proteins without the typical collagenous triple helical structure. The amount of bounded dye is proportional to the amount of collagen in the sample.

Secreted collagen in the culture supernatant was precipitated by the Sircol Dye reagent and quantified by dissolving and colorimetric detection of the previously bounded dye. Collagen that became incorporated in the extracellular matrix was first stained with Sirius Red FB3 and thereafter colorimetric quantified by releasing the dye from the matrix.

As the secretion and matrix deposition of collagen is related to the differentiation level of the cell culture, both parameter were assessed in stimulated cells against the cultivation time to validate both assays (figure 19). The amount of secreted collagen into the media decreased throughout the cultivation time while the incorporation of collagen into the extracellular matrix increased. The addition of secreted and deposited collagen in µg per well revealed a permanent increase in the overall collagen produced by the stimulated cells during the culture period (T3 - 1120 µg / T9 - 1240 µg / T15 - 1310 µg / T21 - 1430 µg). In unstimulated cells, secretion and deposition of collagen was not detected.
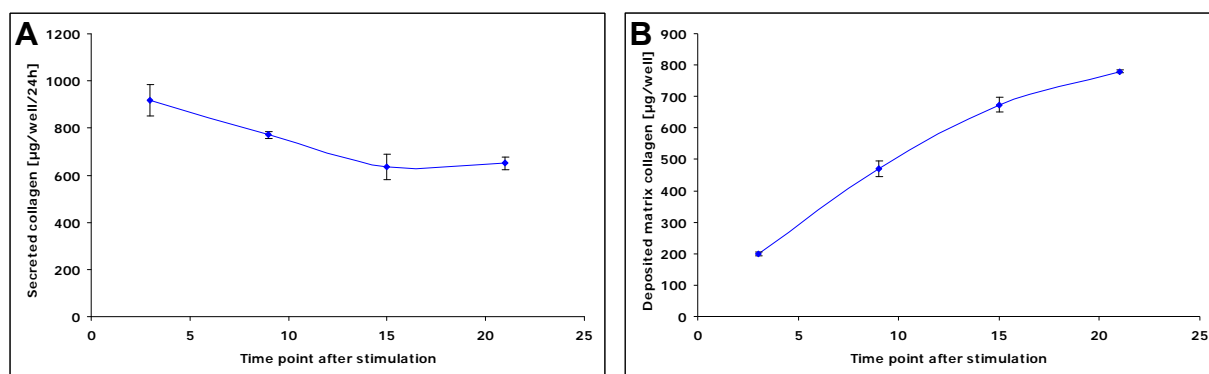
Figure 19. Validation of the Collagen secretion and deposition assay. There is an inverse correlation between collagen secretion and deposition in stimulated cultures. While the amount of secreted collagen decreases with cultivation time (A), deposited collagen increases (B) as well as the overall collagen amount (secreted + deposited / not shown) (n = 3).

3.1.1.4. Matrix mineralization (A3)

The mineralization of the extracellular matrix in the osteoblast culture was determined using Alizarin Red [89]. The dye chelates Ca^{2+} yielding in a red-colored Alizarin Red S-calcium complex. As the amount of bounded Alizarin is proportional to the amount of calcified matrix, the colorimetric detection of Alizarin (after unhinging the dye with cetylpyridinium chloride) can be used to quantify the degree of matrix mineralization. As the calcification of the matrix is related to the differentiation level of the cell culture, the mineralization was assessed in stimulated cells against the cultivation time to validate the assay (figure 20). There was a strong increase in culture mineralization in stimulated cells throughout the culture period with a slight decline of the rise at the end of the cultivation time. In unstimulated cells, mineralization was not observed.
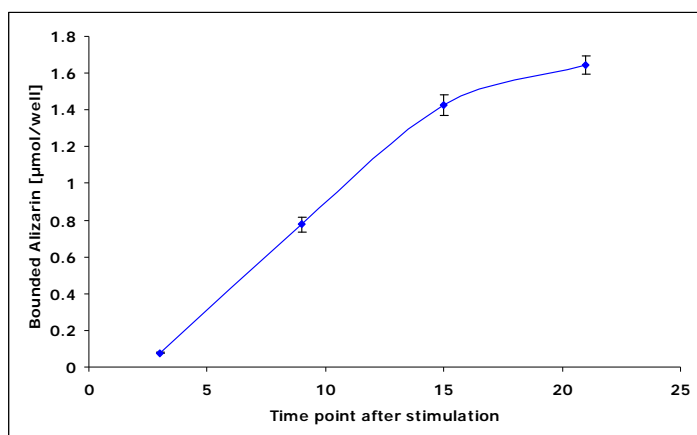
Figure 20. Validation of the Matrix mineralization assay. Calcium incorporation in the ECM only occurs in stimulated cultures and increases with cultivation time (n = 3).

3.1.1.5. Nodule quantification (A4)

To assess the osteoblast differentiation at the morphological level, the development of nodule-like structures in the culture was quantified by analyzing images of the culture using a pixel counting software (Image J). The software localizes and distinguishes the nodules in the picture and after conversion into a binary file, the size of the nodule area can be calculated (figure 21 A,B).

As the development of the nodules is related to the differentiation level of the cell culture, the nodule size was compared in unstimulated and stimulated cells against the cultivation time to validate the assay (figure 21 C). There was a strong increase of the nodule area (in mm²) in stimulated cells throughout the culture period while in

unstimulated cells nodules were not observed and therefore pictures of these group could not be analyzed by the pixel counting software (no values for the diagram).

Figure 21. Nodule quantification assay. **A,B** Principle of the assay using pixel counting software Image J. A transmitted light picture (A) is converted into a binary picture with the nodules displayed in black (B), enabling the counting and quantification of the nodules in the picture. **C** Validation of the assay. Nodule formation only occurs in stimulated cultures and increases with cultivation time (5×10^5 cells were plated / n = 3).

3.1.1.6. Gene expression (A5)

For the gene expression analysis, 13 genes have been chosen that are key factors in bone biology important for development and maturation of bone cells, matrix synthesis and cell-cell interaction. The expression of these marker genes was assessed using qRT-PCR including two housekeeping genes as internal reference.

As a basic requirement for the mathematical equation that was applied to determine the gene expression (see 2.1.2.6.), similar amplification efficiencies of the target and the reference genes were needed [79, 80]. To assure a reliable quantification, efficiency testing was performed for all primers and confirmed equal amplification efficiencies in the range between 1.92 and 1.96 for all amplicons (table 8).

To validate the assay, cells from individual calvariae were cultivated separately (biological replicates) and the expression of the target genes was quantified in each culture at T9 to assess expression differences between multiple biological replicates. Table 8 depicts the expression of all genes in percent to the internal housekeeping

control (mean of *Actin beta* and *Pgk1*) for each single replicate (1-5). Furthermore, the mean value of the five replicates with SEM and % SEM related to the mean value were calculated for each gene. For all genes, the expression difference between independent biological replicates was very low ranging between 2% and 7% SEM. Only *Ibsp* and *Mmp13* possessed a higher variation of the expression level with 10 - 11.5 % SEM between the different samples.

Gene	Efficiency	Biological replicates*[#]					Mean value	SEM	% SEM of mean value
		1	2	3	4	5			
ALP	1.92	68.8	83.0	64.8	91.4	88.4	79.3	5.32	6.7
Bglap1	1.96	843.3	842.2	890.6	764.7	859.1	840.0	20.76	2.5
Col1a1	1.96	10754.7	12963.3	9581.8	11010.2	12270.9	11316.2	593.35	5.2
Cst3	1.94	161.1	145.7	146.9	113.8	123.6	138.2	8.55	6.2
E11	1.94	14.8	13.8	13.9	12.8	9.8	13.0	0.87	6.7
Fos	1.93	0.9	0.9	0.8	1.0	0.9	0.9	0.03	3.3
Fosl2	1.94	3.0	2.9	2.3	2.4	2.5	2.6	0.14	5.4
Ibsp	1.95	575.2	850.0	490.2	799.8	688.2	680.6	67.20	9.9
Mmp13	1.96	59.4	75.1	53.2	93.3	95.6	75.3	8.60	11.4
Osterix	1.93	12.8	13.6	12.9	14.6	14.1	13.6	0.33	2.4
Runx2	1.94	2.7	2.9	2.1	2.2	2.9	2.5	0.18	7.1
Spp1	1.92	1109.9	1214.2	1110.8	1590.3	1149.3	1234.9	90.85	7.4
Twist1	1.96	0.8	0.9	0.9	0.8	0.6	0.8	0.06	7.0
Actin beta	1.93	371.6	405.8	392.3	380.6	398.1	389.7	6.12	1.6
Pgk1	1.94	26.9	24.6	25.5	26.3	25.1	25.7	0.41	1.6

Table 8. Efficiency of the qRT-PCR primers for the cell culture system and expression differences between biological replicates. *each investigated cell culture (1 - 5) was obtained from a single calvaria. [#] expression of each gene in percent to the housekeeping control (mean of *Actin beta* and *Pgk1* set as 100%).

3.1.2. Validation of the cell culture system

3.1.2.1. Selection of suitable mouse mutants with bone phenotype

Two mutant lines with alterations of their bone phenotype and known mutations have been chosen to be investigated in the entire cell culture system.

Aga2 has recently been described as a new mouse model for *Osteogenesis imperfecta* with a dominant negative mutation in the *Col1a1* gene causing structural alterations of the mutated type I collagen protein (see also 1.12.) [55]. The primary screen in the Dysmorphology, Bone and Cartilage module of the GMC revealed abnormal gait, significantly reduced body weight and size as well as shortened and bended limbs, toes and a kinky tail in the mutants. X-ray analysis detected abnormalities in shape and size of many bones and joints (tibia, fibula, humerus,

ulna, radius, pelvis) and bone densitometry using DXA analysis showed significantly reduced BMD, pBMD, BMC and bone content values in the *Aga2* mice (table 9). pQCT analysis within the secondary screen revealed a strong decrease of total, trabecular and cortical BMD in the femoral metaphysis and diaphysis as well as a pronounced reduction of total and cortical/subcortical BMC in mutants. Furthermore, the total and cortical area was decreased and the trabecular area increased in *Aga2* mice (figure 22). Taken together, *Aga2* mutants possessed a clear bone phenotype and displayed hallmarks of OI symptoms with multiple fractures, scoliosis and an overall decrease in bone mass and density.

Bone- and weight-related quantitative parameters					
	Wild type (A)		*Aga2* (B)		A~B	
Parameter	Male	Female	Male	Female	Male	Female
	n=10	n=10	n=10	n=10	*p–value*	*p–value*
BMD [mg/cm^2]	67 ± 1	69 ± 2	53 ± 1	53 ± 1	< 0.0001	< 0.0001
pBMD [mg/cm^2]	57 ± 1	60 ± 2	42 ± 1	42 ± 1	< 0.0001	< 0.0001
BMC [mg]	928 ± 17	945 ± 46	307 ± 20	310 ± 13	< 0.0001	< 0.0001
Bone Content [%]	2.89 ± 0.04	2.89 ± 0.11	1.44 ± 0.07	1.56 ± 0.05	< 0.0001	< 0.0001
Body Length [cm]	9.95 ± 0.05	10.15 ± 0.08	8.95 ± 0.09	8.90 ± 0.07	< 0.0001	< 0.0001
Body Weight [g]	32.14 ± 0.33	32.73 ± 0.96	21.28 ± 0.65	19.89 ± 0.54	< 0.0001	< 0.0001

Table 9. DXA analysis of *Aga2*. Data presented as mean ± standard error of mean and were obtained from 16 week old mice.
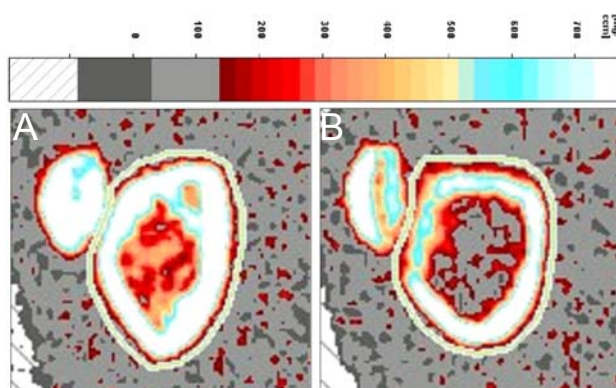
Figure 22. pQCT scan of *Aga2* femur. pQCT scan of transversal sections of the femoral metaphysis in 17 week old mice (resolution 70µm). Compared to wild type control (A), there is a decrease of total, trabecular and cortical BMD as well as total and cortical area in *Aga2* (B).

The *ABE2* line was also identified in the Munich ENU mutagenesis screen based on a behavioral phenotype with abnormal head shaking symptom (**A**bnormal **Be**havior). Mutant mice possess a G → A missense mutation in the *Jag1* gene that causes a nonconservative amino acid substitution of a glycine by an aspartic acid residue.

The mutation resides in the second epidermal growth factor (EGF)-like repeat of the extracellular domain of Jag1, a region that is important for Notch binding [90]. Bone densitometry in the primary screen of the GMC Dysmorphology, Bone and Cartilage module disclosed significantly increased sBMD (BMD related to the body weight) values in both sexes of the *ABE2* line. But with DXA analysis, no differences were found in BMD and bone content (BMC related to the body weight) between mutants and wild type control (table 10). Body length, body weight, fat mass, fat content and subcutaneous fat were significantly decreased in mutants, while lean mass (only female mutants) and lean content were significantly increased in *ABE2* compared to controls. pQCT analysis was conducted in the secondary screen indicating an increase of total and trabecular BMD, total and cortical BMC as well as total and cortical area of bone metaphysis and diaphysis in the mutants. The trabecular BMC was decreased in the metaphysis and the trabecular area was as well reduced in mutant mice. Taken together, *ABE2* depicted a clear bone phenotype with more cortical bone and a higher trabecular bone mineral density (figure 23).

Bone- and weight-related quantitative parameters					
	Wild type (A)		*ABE2* (B)		A~B	
Parameter	Male	Female	Male	Female	Male	Female
	n=10	n=10	n=10	n=10	*p–value*	*p–value*
BMD [mg/cm^2]	72 ± 1	74 ± 1	72 ± 1	72 ± 1	n.s.	n.s.
sBMD [10^{-3} x cm^{-2}]	1.99 ± 0.06	2.03 ± 0.05	2.29 ± 0.03	2.61 ± 0.07	< 0.001	< 0.0001
Bone Content [%]	3.46 ± 0.14	3.36 ± 0.11	3.36 ± 0.12	3.27 ± 0.11	n.s.	n.s.
Body Length [cm]	10.40 ± 0.07	10.40 ± 0.10	10.10 ± 0.07	9.80 ± 0.08	< 0.01	< 0.001
Body Weight [g]	36.63 ± 1.35	36.74 ± 1.30	31.45 ± 0.85	27.66 ± 1.13	< 0.01	< 0.0001

Table 10. DXA analysis of *ABE2*. Data presented as mean ± standard error of mean and were obtained from 16 week old mice.
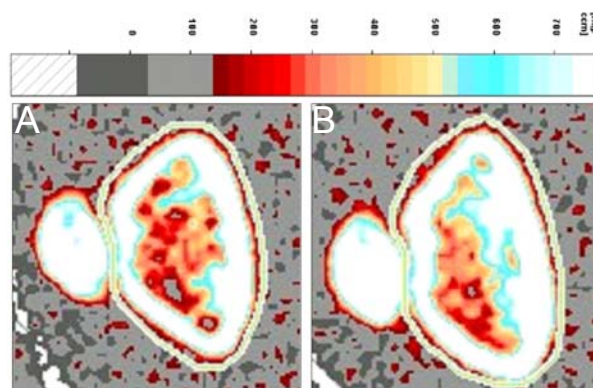

Figure 23. pQCT scan of *ABE2* femur. pQCT scan of transversal sections of the femoral metaphysis in 19 week old mice (resolution 70µm). Compared to wild type control (A), there is an increase in total and trabecular BMD as well as total and cortical area in *ABE2* (B).

3.1.2.2. Analysis of *Aga2* and *ABE2* within the cell culture system

Given the distinct alterations in their bone parameters, *Aga2* and *ABE2* were considered to be good candidates for the validation of the whole cell culture system. Primary calvarial osteoblasts of both mutant lines were investigated according to the developed SOP. The results of both studies are displayed on the following pages with diagrams / tables for each assay. The findings in *Aga2* are illustrated on the left site and the findings in *ABE2* on the right site. The error bars represent the SEM values calculated from the technical replicates (number of wells per assay, see SOP).

Proliferation (A1)
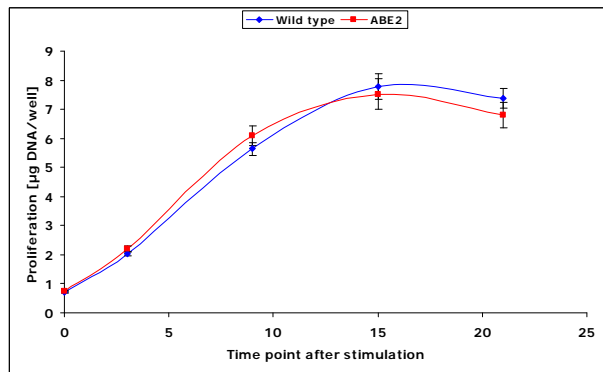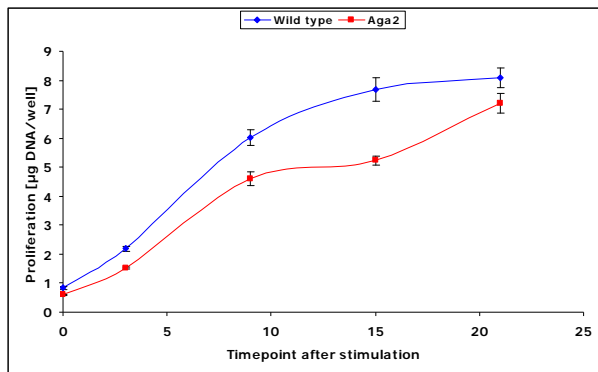
Metabolic activity (A1)
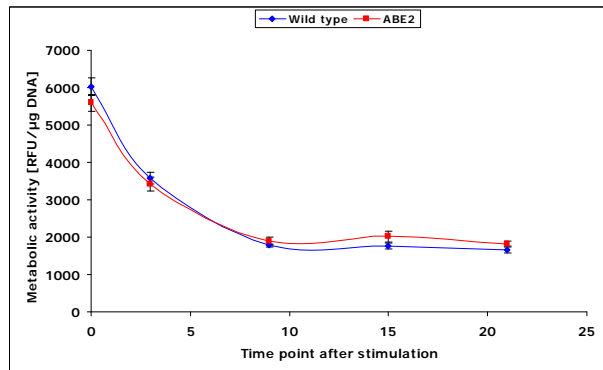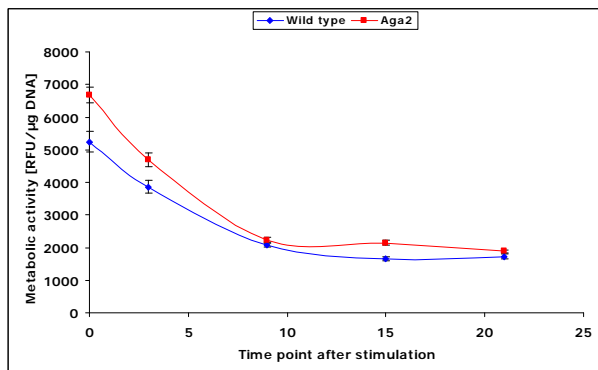
Protein content (A1)
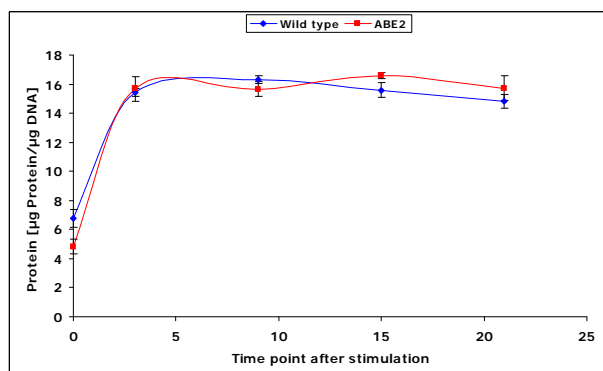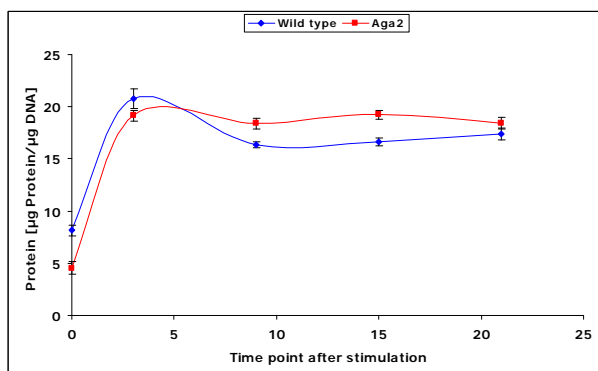
ALP activity (A1)
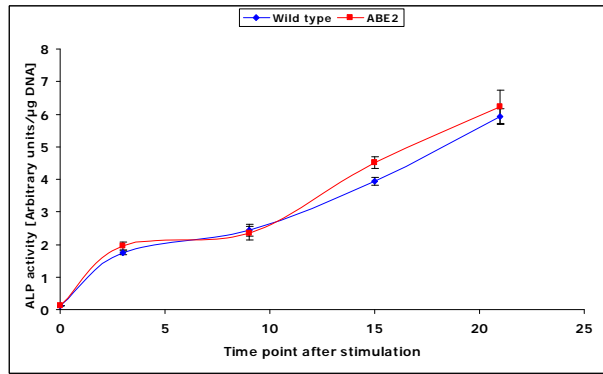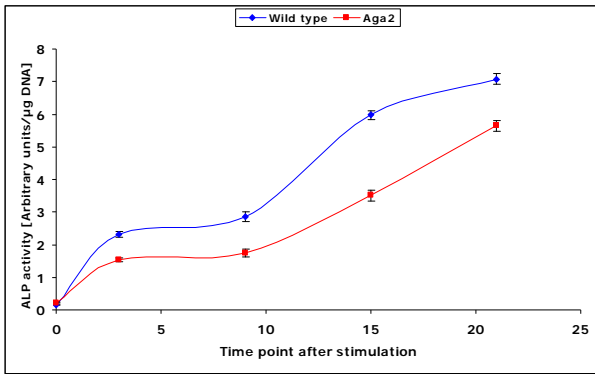
Collagen secretion (A2)
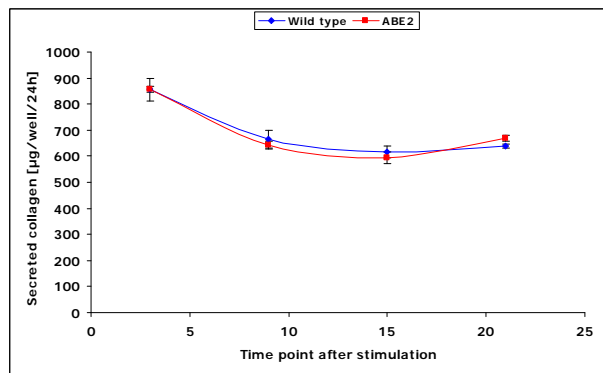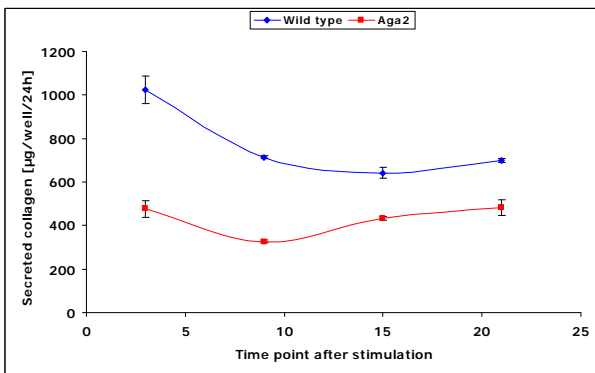
Collagen deposition (A2)
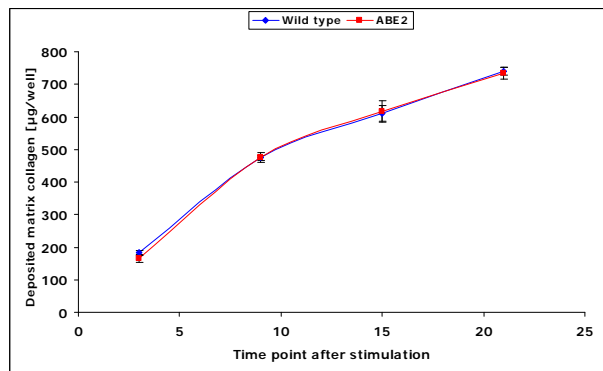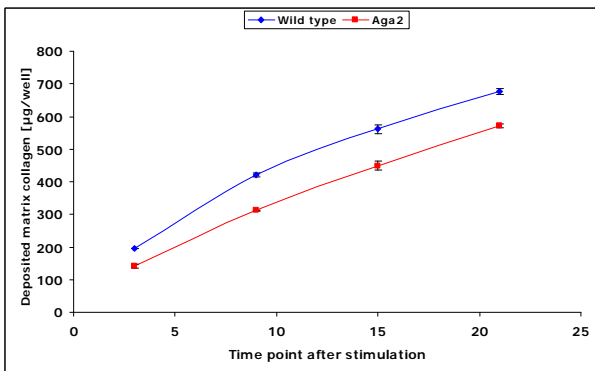
Matrix mineralization (A3)
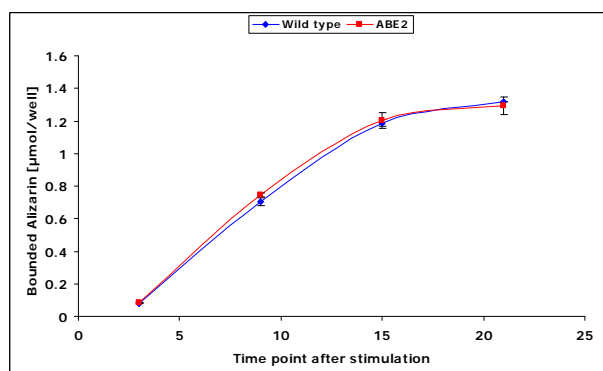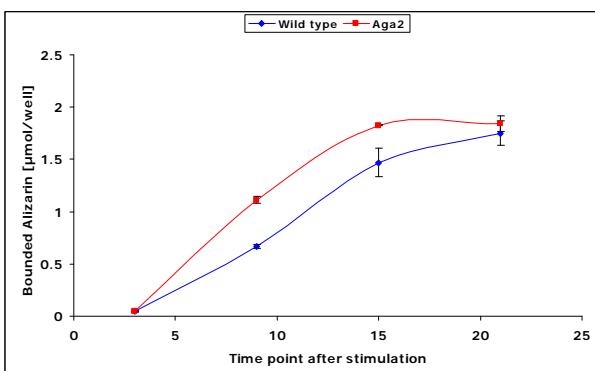
Nodule quantification (A4)
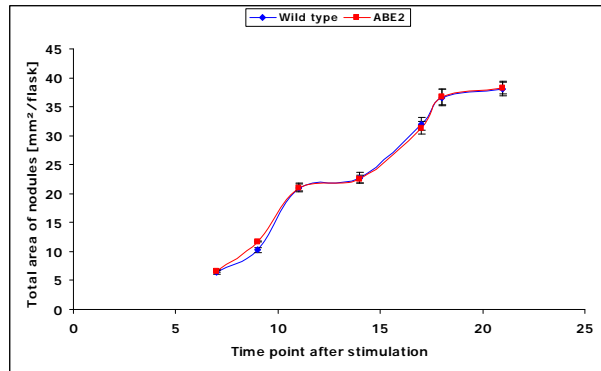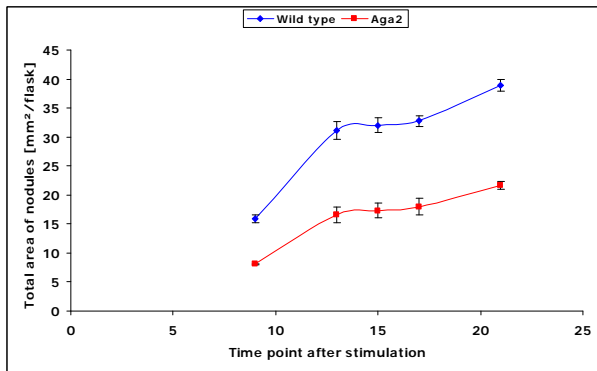
Gene expression (A5)

The expression of *ALP*, *Col1a1* and *Spp1* is exemplarily shown by diagrams and the overall result of the gene expression analysis is summarized in table 11 for *Aga2* and table 12 for *ABE2*. The level of expression difference between wild type mice and mutants for a certain gene at a distinct measurement day is indicated by colored boxes (yellow box > 25% and red box > 50% difference).
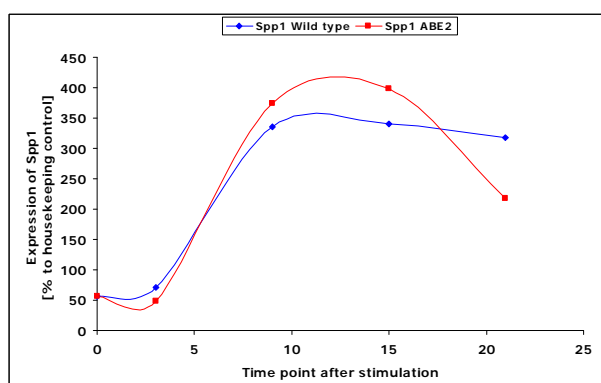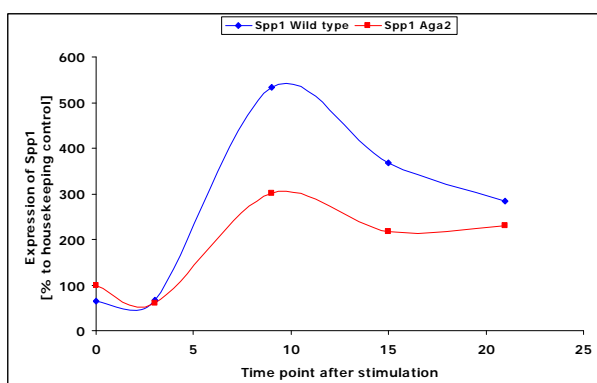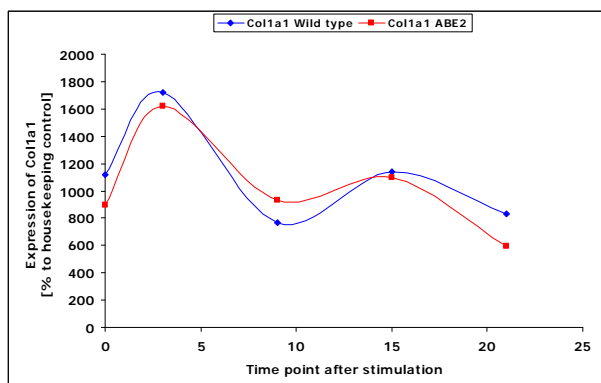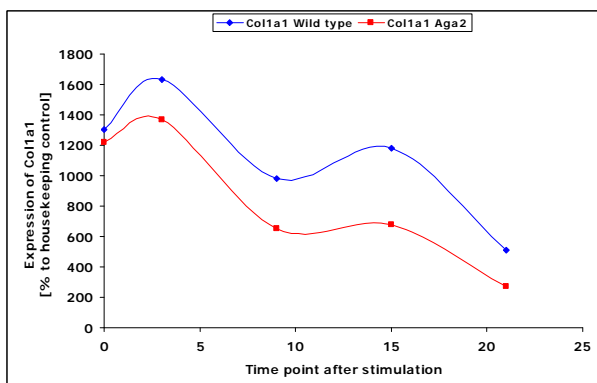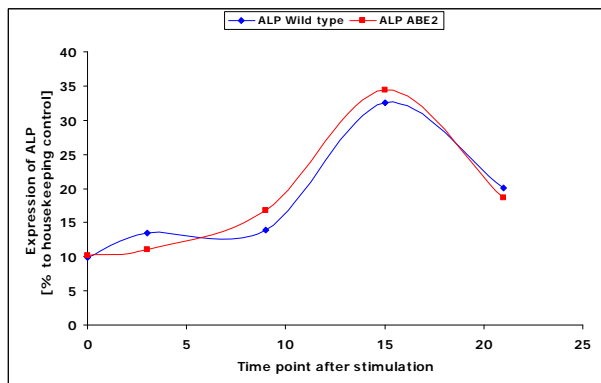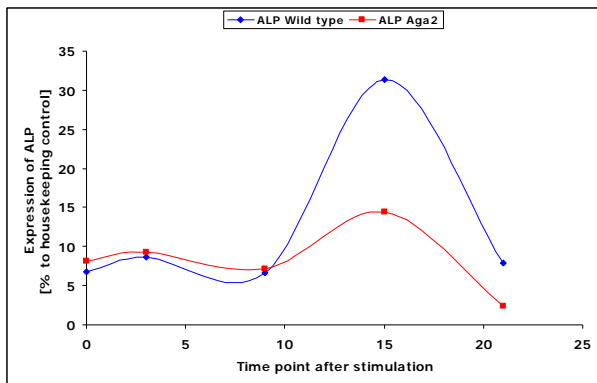
Gene	Pheno-type	Measurement day (Expression in % to housekeeping control *Actin beta* + *Pgk1*)				
		0	**3**	**9**	**15**	**21**
ALP	WT	6.8	8.6	6.6	31.4	8.0
	Aga2	8.1	9.2	7.1	14.4	2.4
Bglap1	WT	1.3	7.4	15.4	32.5	16.3
	Aga2	1.4	5.3	16.2	15.8	4.5
Col1a1	WT	1302.6	1633.4	980.3	1182.8	507.7
	Aga2	1221.7	1370.0	650.4	676.3	271.4
Cst3	WT	51.0	45.3	45.2	91.0	75.4
	Aga2	45.1	47.9	49.5	91.9	68.4
E11	WT	4.8	3.4	10.4	5.4	4.3
	Aga2	8.2	5.7	8.8	5.7	5.6
Fos	WT	0.8	0.5	0.5	0.5	0.4
	Aga2	0.7	0.6	0.5	0.6	0.5
Fosl2	WT	5.6	3.4	3.3	2.4	2.1
	Aga2	4.6	3.0	2.5	2.2	2.5
Ibsp	WT	0.6	30.7	15.2	103.7	39.6
	Aga2	0.6	17.4	12.6	46.0	9.0
Mmp13	WT	37.4	42.7	145.1	74.7	64.4
	Aga2	79.1	62.0	69.7	54.3	46.5
Osterix	WT	5.2	2.1	4.6	5.9	1.5
	Aga2	4.8	2.5	2.4	2.5	0.4
Runx	WT	2.3	0.9	1.9	1.5	0.9
	Aga2	1.9	1.2	1.1	1.0	0.6
Spp1	WT	64.4	66.0	533.1	368.1	283.9
	Aga2	98.8	61.2	302.1	218.1	230.7
Twist1	WT	3.5	2.1	3.6	3.9	2.5
	Aga2	4.2	2.8	2.8	3.6	2.2

Table 11. Expression analysis of *Aga2* osteoblasts within the cell culture system.

Gene	Pheno-type	Measurement day (Expression in % to housekeeping control *Actin beta* + *Pgk1*)				
		0	**3**	**9**	**15**	**21**
ALP	WT	9.9	13.5	13.9	32.5	20.0
	ABE2	10.2	11.1	16.8	34.4	18.6
Bglap1	WT	0.7	18.5	22.1	31.0	29.9
	ABE2	1.0	27.2	37.3	43.2	36.3
Col1a1	WT	1119.0	1717.4	766.9	1139.8	830.1
	ABE2	898.7	1617.9	928.7	1093.9	594.9
Cst3	WT	39.6	40.8	36.1	60.0	73.5
	ABE2	40.7	37.2	35.8	56.6	76.9
E11	WT	3.8	3.9	4.6	5.0	4.6
	ABE2	3.9	3.0	4.5	4.6	3.7
Fos	WT	1.7	1.5	1.0	0.3	0.4
	ABE2	1.5	1.6	1.4	0.3	0.3
Fosl2	WT	6.5	2.6	2.4	1.8	1.9
	ABE2	5.4	2.9	3.3	2.1	1.6
Ibsp	WT	0.7	78.1	56.7	191.7	99.9
	ABE2	1.6	92.3	102.2	218.7	111.6
Mmp13	WT	51.2	58.2	65.4	40.9	67.3
	ABE2	54.2	43.6	79.2	67.4	39.8
Osterix	WT	4.7	4.4	2.4	2.5	2.1
	ABE2	4.3	3.8	2.9	2.7	1.9
Runx	WT	1.5	0.9	0.7	1.0	0.9
	ABE2	1.3	0.8	0.8	1.0	0.9
Spp1	WT	56.7	71.5	334.8	340.6	318.0
	ABE2	56.8	48.9	374.9	398.4	218.3
Twist1	WT	1.5	1.7	1.1	1.3	1.9
	ABE2	1.8	1.1	1.2	1.5	1.5

Table 12. Expression analysis of *ABE2* osteoblasts within the cell culture system.

3.2. Heart and lung investigation in the *Aga2* OI mouse model

3.2.1. Phenotypic classification of heterozygous *Aga2*

Among the heterozygous *Aga2* offspring, two different phenotypes could be distinguished according to the clinical features they possessed [55].

The first group was characterized by a gentle occurrence of symptoms. Animals displayed typical hallmarks of OI like diastrophic limbs, long bone and rib cage fractures, generalized decreases in DXA-based bone parameters and slight changes in body composition with about 80% of body weight compared to wild type littermates (figure 24). These mice survive to adulthood and were classified as mild affected *Aga2* (*Aga2^{mild}*). Within the second group, heterozygous animals were much more heavily affected and suffered from serious clinical symptoms. They developed thin calvaria, precocious hemorrhaging at joint cavities and intracranial sites, severe bone deformities with pronounced scoliosis as well as provisional rib and long bone calluses accompanied by comminuted fractures. Pectus excavatum, gasping and cyanosis were further hallmarks just as platyspondyly, endema of eyes and eczema. As the most typical criteria for the phenotypic classification, mice had a strong physique deficit with a body weight reduction to about 50% compared to wild type littermates and appeared weak and asthenic (figure 24). Mutants belonging to the second group were severely affected and entirely succumbed to postnatal lethality (*Aga2^{severe}*).

This morphological diversity was discernable starting between days 6 - 11 postnatal. Classification of progeny was done prior to experiments and depended on body weight and severity of symptoms.

Figure 24. Appearance of heterozygous *Aga2* mutants. *Aga2^{mild}* (middle) possess slight changes in body parameters with marginal changes in body weight and size compared to wild type littermates (left). In contrast, *Aga2^{severe}* (right) feature vigorous alterations in body composition with strong reduction of body weight and size compared to wild type control.

3.2.2. Cardiovascular phenotyping

Knowing that heart alterations can be observed in human OI, we assessed heart function in heterozygous *Aga2* animals by applying the GMC cardiovascular screen. The first round of evaluation was performed with $Aga2^{mild}$ mice surviving to adulthood using ECG analysis (table 13). We observed an extension of the J-T interval and increased QRS amplitude in $Aga2^{mild}$ at the age of 14 weeks. This was caused mainly by differences in the amplitudes of the Q and S wave with higher values in the mutants (table 13). The increased J-T interval could indicate alterations in the repolarization of the ventricle and the higher amplitudes of the QRS complex argues for a changed QRS axis.

ECG analysis						
	Wild type (A)		*Aga2* (B)		A~B	
	male	female	male	female	male	female
Parameter	n = 10	n = 9	n = 10	n = 10	p–value	p–value
Heart rate (bpm)	471.9 +/- 17	529.4 +/- 15	572.4 +/- 9.6	573.9 +/- 7.9	< 0.001	< 0.05
JT interval (ms)	3.6 +/- 0.3	3.6 +/- 0.1	4.4 +/- 0.1	4.6 +/- 0.3	< 0.05	< 0.05
Q amplitude (mV)	0.01 +/- 0	0.02 +/- 0.01	0.05 +/- 0.01	0.05 +/- 0	< 0.01	< 0.01
R amplitude (mV)	2.15 +/- 0.11	2.06 +/- 0.17	1.86 +/- 0.08	2.04 +/- 0.13	n.s.	n.s.
S amplitude (mV)	-0.28 +/- 0.12	-0.83 +/- 0.18	-1.37 +/- 0.15	-1.3 +/- 0.19	< 0.001	< 0.05
QRS amplitude (mV)	2.48 +/- 0.09	2.88 +/- 0.23	3.24 +/- 0.14	3.34 +/- 0.16	< 0.01	= 0.058

Table 13. ECG analysis of $Aga2^{mild}$ within the primary cardiovascular screen of the GMC.

As the result of the primary screen indicated potential pathological alterations in morphological or conductional properties of the heart, a more comprehensive analysis was performed investigating $Aga2^{severe}$ within the secondary screen at the age of 10 days to further define possible heart alterations in the case of lethal OI affection. Ultrasound analysis revealed significant functional and anatomical alterations in the moribund OI mice. The hearts of $Aga2^{severe}$ reached the same maximum extension during the diastole as wild type controls, seen with equal LVEDD. In contrast, the left ventricular end-systolic internal diameter (LVESD) was significant higher in $Aga2^{severe}$ (figure 25). Accordingly, the derived fractional shortening (FS) and ejection fraction (EF), which relate the diastolic and systolic diameter and indicate the blood volume which can be ejected by the heart,

respectively, were significant lower in *Aga2^severe* (figure 25). In addition, the B-mode picture revealed a deformation of the septum with a convex bulge into the left ventricle during contraction in severely affected animals (figure S1).

Given the strong differences in body constitution with half weights in severe mutants, the equal LVEDD as well as the perceptible morphological abnormality of the septum suggest cardiac hypertrophy and the increased LVESD indicate a restricted ability to contract the heart muscle in *Aga2^severe*. The kind of septal deformation hints to right ventricular hypertrophy. Taken together, the ultrasound analysis revealed a dysfunction of the heart in severely affected mutants.
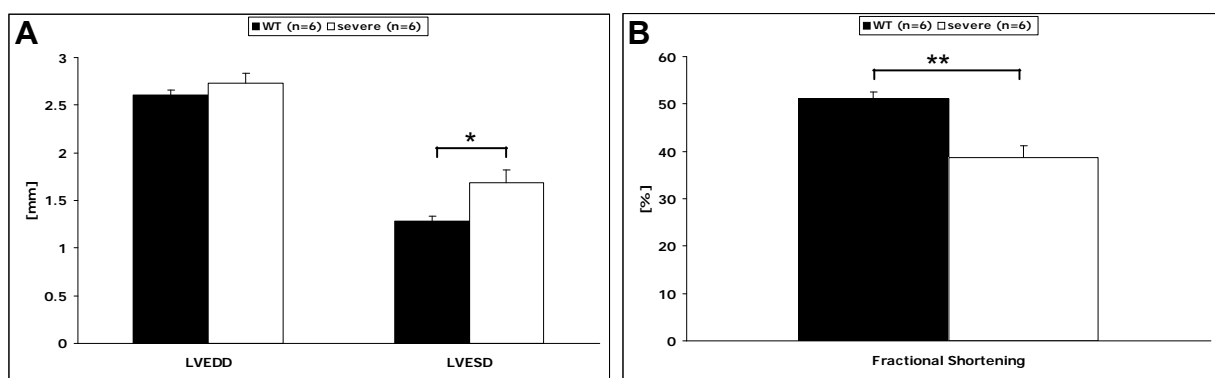
Figure 25. Quantitative analysis of heart function via ultrasound imaging. No alterations were detected in the left ventricular end-diastolic internal diameter (LVEDD) between *Aga2^severe* and wild type littermates (A). In contrast, a significant difference in the left ventricular end-systolic internal diameter (LVESD) (A) as well as the corresponding fractional shortening (B) can be observed between the mutants and wild type control animals. * = p ≤ 0.05, ** = p ≤ 0.01, *** = p ≤ 0.001.

3.2.3. Histology

Subsequently to the cardiovascular screen we tried to confirm the observed functional impairments and relate them to alterations on the morphological and structural level. Therefore we applied standard histological staining and immunohistochemistry beside SEM analysis on hearts from *Aga2^severe* and their wild type littermates at the age of 10-11 days. (The histological studies were perfomed by Christian Cohrs and will be described in more detail in his PhD thesis).

Although there is a vast difference in their body constitution, the heart size of the *Aga2^severe* was similar compared to wild type control. As the basic cause for this we discovered that *Aga2^severe* possess an enlarged septum and muscle tissue with right ventricular hypertrophy as depicted with H&E staining in figure 26. The heart hypertophy was also evident at the macroscopical level (figure 28).
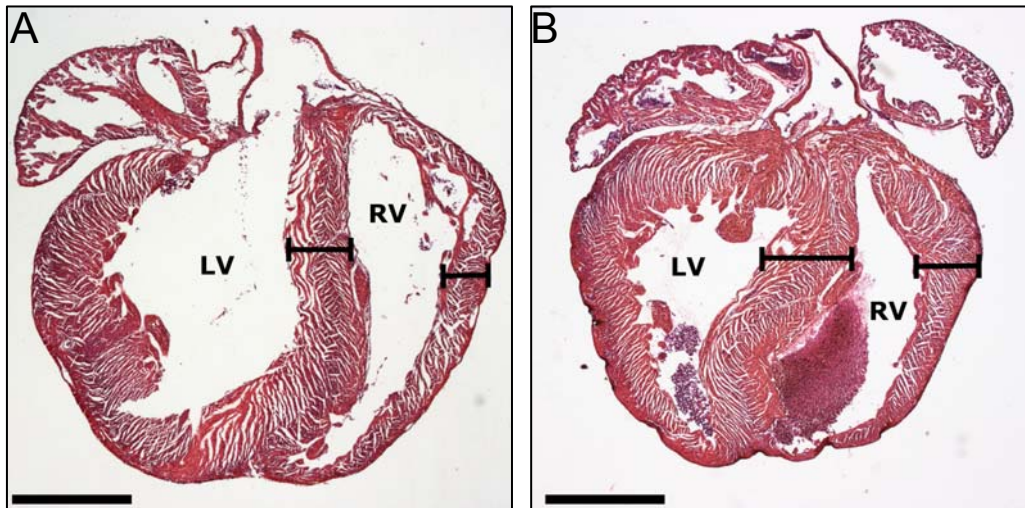
Figure 26. Morphological appearance of heart tissue. H&E staining of longitudinal heart sections reveals enlarged septum and right ventricular hypertrophy (black bars) in *Aga2[severe]* (B) compared to wild type control (A). LV - left ventricle; RV - right ventricle. Scale bar in A,B = 1 mm.

To further ascertain the morphological changes in *Aga2[severe]*, we performed IHC on heart sections for type I collagen. Diseased mice exhibited a reduced collagen expression and a dispersed staining pattern without continuous collagen distribution in the ECM (figure 27 A,B). This was accompanied by a disordered cellular organization and the collagen seemed to accumulate closer to the nuclei. Additionally, the vascular structure in the *Aga2[severe]* hearts differed from the wild type situation as shown with a reduced PECAM staining in the heart vessels (figure 27 C,D). DAPI counterstain revealed an unsorted cell arrangement along with thinner blood vessel walls. This might be due to a reduction in the vessel collagen content (figure 27 A,B). IHC studies for activated caspase 3 revealed no signs for increased apoptosis (data not shown).

To broaden the aspects of the supposed collagen alterations, we applied SEM analysis along with tissue maceration to solely visualize the overall collagen network in the hearts. This ultrastructural analysis confirmed a reduced collagen amount in the *Aga2[severe]* cardiac tissue (figure 27 E,F). Furthermore, there was a significant difference in the structure, organization and spatial arrangement of the cardiac collagen fibrils between *Aga2[severe]* and controls. An altered ratio between the different collagen types which normally appear in the hearts is clearly distinguishable and mutants exhibited an increased amount of smaller fibrils with stronger bending and reduced thickness.
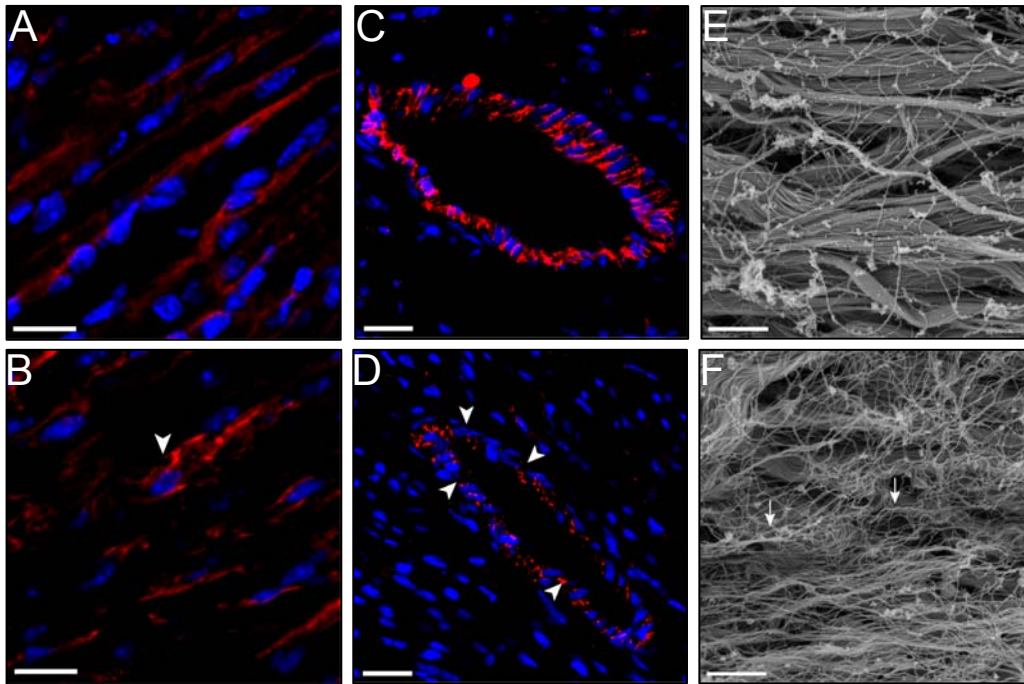
Figure 27. Histological investigation of heart tissue. **A,B** Immunhistological analysis of type I collagen (red - type I collagen; blue - DAPI counterstain). An irregular staining pattern in *Aga2^severe* hearts is evident (B) compared to wild type control (A). Additionally, a more frequent type I collagen accumulation close to the nuclei is visible in mutant specimens (arrowhead in B). **C,D** PECAM staining for morphological analysis of blood vessels in the myocard (red - PECAM; blue - DAPI counterstain). Wild type (C) sample show a staggered formation of endothelial cells with continuous PECAM staining between the cells. In *Aga2^severe* (D), the regulated cell arrangement is lost and PECAM staining is markedly reduced (white arrowheads). **E,F** Scanning electron microscopical analysis of the myocard. Orientation of type I collagen fibres in wild type hearts (E) is predominantly parallel. In contrast, collagen fibres in mutant hearts (F) display irregularly distributed main fibres and an increased content of smaller collagen fibres in the ECM is obvious (white arrows in F). red in A,B – type I collagen; red in C,D – PECAM; blue – DAPI counterstain. Scale bar in A,B = 10 µm; C,D = 20 µm; E,F = 3 µm.

Corresponding to the fact that pulmonary disorders are the most prominent accessory symptoms in human OI, we secondarily examined lung tissues of *Aga2^severe* and *Aga2^mild* at the age of 10-11 days and compared them with their wild type littermates.

Haematoxylin and eosin staining showed no differences between the lungs of *Aga2^mild* and the wild type control mice. Pulmonary tissues of both groups seemed morphological healthy with similar appearances. In contrast, about 90% of *Aga2^severe* possessed strong hemorrhagic lungs and pneumonia with infiltration of polymorphonuclear neutrophils (PMN) and alveolar macrophages (figure 28 A,B,C). In most cases pleurisy can also be diagnosed. Importantly, the alveolar bleedings were equally distributed in the whole lung tissue.

Following the H&E observations we tried to figure out if the hemorrhagic lungs in severe *Aga2* are due to fractures, as it is assumed to be in human cases, or if other reasons account for the bleedings. Therefore we simply correlated the lung morphology to the ribcage aspect in all three groups (figure 28 D,E,F). In *Aga2^mild* and *Aga2^severe*, rib fractures associated with callus formation were numerous and equally distributed all over the rib cage. However, although the frequency and distribution of fractures were the same in both mutant groups, only *Aga2^severe* exhibited strong heamorrhagic lungs while *Aga2^mild* possessed healthy lungs comparable to wild type littermates.
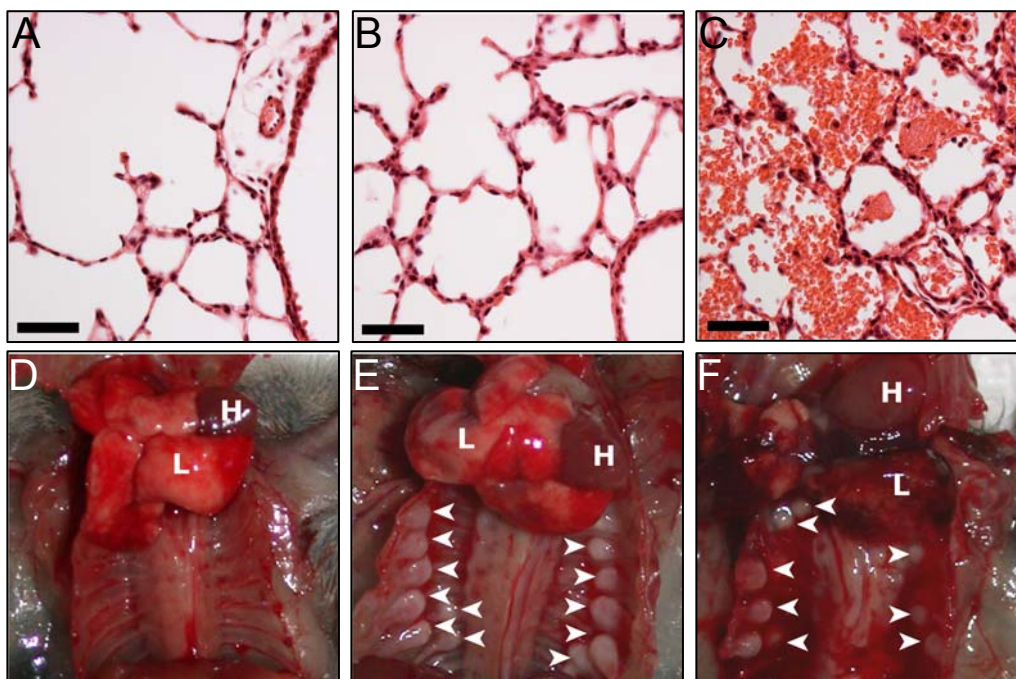
Figure 28. Morphological appearance of lung tissue. **A,B,C** H&E staining of transversal sections. No obvious differences are visible between wild type (A) and *Aga2^mild* (B) tissue. However, *Aga2^severe* animals (C) display excessive bleedings and pneumonia-associated cell types such as granulocytes are evident. **D,E,F** Macroscopical aspects of the thorax. Wild type situation without callus formation in the rib cage and normal appearance of lung and heart (D). In contrast, *Aga2^mild* (E) as well as *Aga2^severe* (F) exhibit strong callus formation in the rib cage (white arrows). Intriguing, while *Aga2^mild* display wild type like lung morphology, *Aga2^severe* possess hemorrhagic lungs. Additionally, heart hypertrophy in *Aga2^severe* is also evident (F). H - heart; L - lung. Scale bars in A-C = 100 µm.

As with heart tissue, the vascular structure of the lungs was examined by PECAM staining (figure 29). Again, there was no difference between wild type mice and *Aga2^mild*. Both groups showed a positive and uniform staining in large blood vessels and capillaries. A positive staining in the large blood vessels was also observed in *Aga2^severe* with only slightly decreased staining intensity. But in contrast, the capillary staining showed an enormous reduction in these moribund mutants, especially at the

areas where the bleedings occurred. Remaining capillary staining was only visible at sites where the alveoli were not affected by the bleedings.

Finally, IHC analysis for collagen I and activated caspase 3 revealed no hints for an aberration of the collagen composition or an increased apoptosis rate in the lung tissue of *Aga2^mild^* and *Aga2^severe^* compared to wild type control (data not shown).
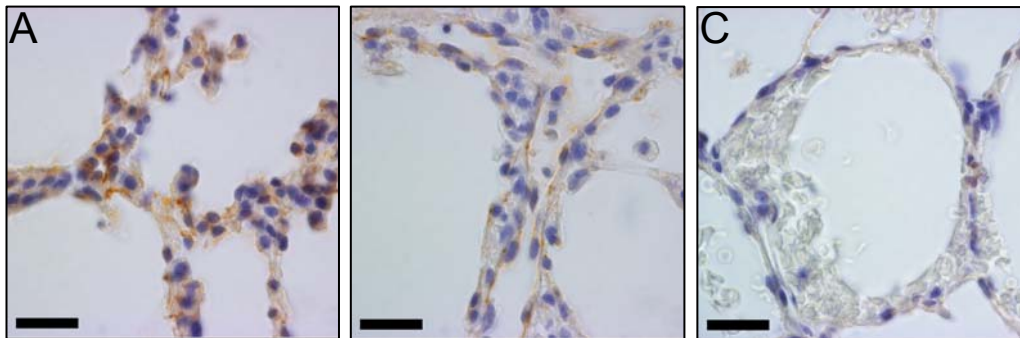
Figure 29. Vasculature in lung tissue. PECAM staining on lung tissue reveals intact capillary network in wild type (A) and *Aga2^mild^* lung sections (B). In *Aga2^severe^* specimens (C), capillary staining is markedly reduced. Scale bars in A-C = 50 µm.

3.2.4. *In vitro* cell culture analysis of heart and lung fibroblasts

To substantiate our results from the previous studies and to extend our understanding of the pathophysiological alterations in heart and lung of OI affected mice to the cellular level, we performed *in vitro* cell culture experiments. Being the major collagen producing cells, we chose primary heart and lung fibroblasts as the cells to be investigated and compared *Aga2^severe^* and *Aga2^mild^* with wild type littermates. Thus, we obtained insights into the cellular events uncoupled of any systemic influences like hormonal and intercellular regulation.

Immunocytochemistry on primary heart fibroblasts revealed an immense reduction of the type I collagen protein in *Aga2^severe^* compared to their wild type littermates, which possessed a strong and uniform staining pattern (figure 30 A,B,C). This result supported our findings from the histology of a tremendous downregulation of the type I collagen protein in hearts of *Aga2^severe^*. Furthermore, also heart cells from *Aga2^mild^* showed a modified collagen I staining with a slight alleviated intensity compared to wild type. qRT-PCR for *Col1a1* on cellular RNA probes verified the observed changes in the type I collagen staining pattern showing a reduction of the *Col1a1* transcript to about 25% in *Aga2^severe^* and to about 65% in *Aga2^mild^* compared to wiltype cells set as 100% (figure 31). ICC for activated caspase 3 showed no signs for an elevated apoptosis in heart cells from mutant mice (data not shown).
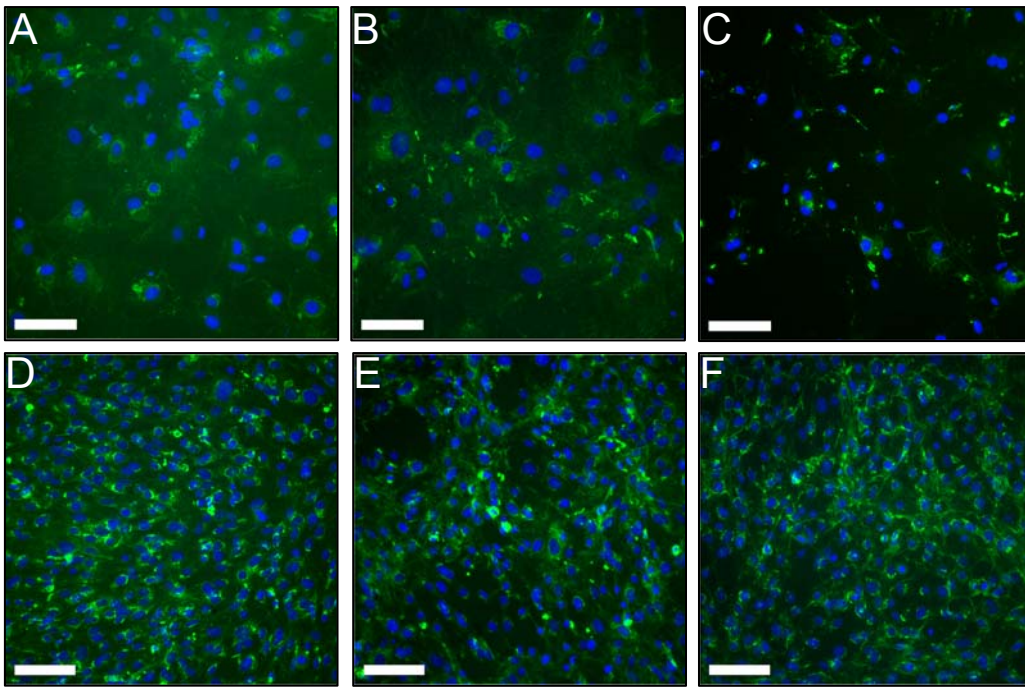
Figure 30. ICC for type I collagen of *in vitro* cultivated heart and lung fibroblasts. **A,B,C** Heart fibroblasts (green - type I collgen; blue - DAPI counterstain). Unlike the wild type situation (A), there is a decrease of the type I collagen staining in *Aga2^mild^* samples (B) and a further strong reduction in *Aga2^severe^* heart fibroblasts (C). **D,E,F** Lung fibroblasts (green - type I collgen; blue - DAPI counterstain). Compared to the wild type sample (D), lung fibroblasts of *Aga2^mild^* (E) and *Aga2^severe^* (F) show a slight reduction of the type I collagen protein and no obvious difference is visible between the both mutant groups. Scale bars in A-C = 100 μm; D-F = 200 μm.

TEM analysis was used to further unravel the cellular alterations in the heart fibroblasts. In wild type culture, cells grew in up to three layers and showed a normal development of the Golgi, mitochondria, rER and ECM. In contrast, fibroblasts from *Aga2^severe^* exhibited disordered cytoplasm, many bullous structures, empty vacuoles, changes in ER and Golgi with membrane leftovers and protuberances at the cell membrane with enlarged surface area. There was no evidence showing the formation of extracellular matrix, but heart fibroblasts of *Aga2^severe^* accumulated huge amounts of additional intracellular filamentous structures as depicted in figure S2 A, B, C. Heart cells of *Aga2^mild^* possessed only few of the changes seen in the severe mutants like disordered cytoplasm, vesicular structures and dilated Golgi, but the burden was not that vigorous as in *Aga2^severe^*.

Primary lung fibroblasts of *Aga2*^{severe} stained for type I collagen showed only a slight decrease of the staining intensity and no obvious differences in the staining pattern in cells of *Aga2*^{mild} was observed compared to wild type control (figure 30 D,E,F). This confirmed our observations of unchanged type I collagen expression in lungs of *Aga2*^{mild} and *Aga2*^{severe}, seen with histological methods. Corresponding to the ICC result, qRT-PCR yield only a marginal decrease of the *Col1a1* transcript level in severely affected *Aga2* to about 75% compared to wild type and no significant alterations in mild affected *Aga2* with about 90% expression, respectively (figure 31). Staining for activated caspase 3 revealed no alterations concerning the apoptotic rate in lung fibroblasts of mutant mice (data not shown).

As with heart cells, TEM analysis was performed for in-depth morphological investigation of lung fibroblasts. Wild type cells grew in up to a three layers and possessed a normal Golgi apparatus, mitochondria, rER and ECM. Within the lung fibroblasts of *Aga2*^{mild} and *Aga2*^{severe}, the ECM was nearly unabatedly distinguishable in both cultures compared to the wild type control. Merely the rER was more distinctive and the Golgi was changed in both groups with a somewhat more pronounced phenotype in lung fibroblasts of severe mutants (figure S2 D,E,F).
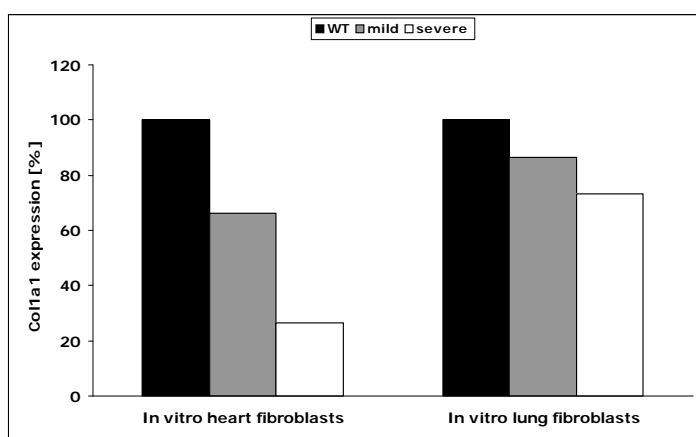
Figure 31. *Col1a1* expression in cultivated heart and lung fibroblasts (qRT-PCR). In heart fibroblasts, the *Col1a1* transcript is decreased to 65% in *Aga2*^{mild} and highly reduced to 25% in *Aga2*^{severe} compared with wild type control. Within lung fibroblasts, the *Col1a1* expression is only slightly reduced to 90% in *Aga2*^{mild} and to 75% in *Aga2*^{severe}. Statistical analysis was not performed since the cells were pooled for the experiment (n=1).

3.2.5. Expression profiling

To further understand the observed structural alterations from the histological examination and to explain them on the molecular and genetic level, we applied chip based expression profiling. RNA samples of three *Aga2/+severe* at the age of 11 days were used as individual probes and compared against one wild type reference RNA pool made from four littermate control mice - each with heart and lung.

In heart tissue of *Aga2severe* we identified 56 significantly regulated genes, whereas 35 of which were upregulated and 21 downregulated (figure S3). As indicated in the figure, the regulation of the listed genes ranged between 1.5 and 3.1 fold compared to wild type control and the strong correlation of the denoted genes between all three single mutants argues for a high reproducibility of the selected genes. The estimated number of falsely significant genes was calculated for 1000 permutations, yielding a FDR of 0.5% for this data set including six chip experiments.

In silico analysis of the differentially expressed genes revealed multiple over-represented biological processes in the heart, summarized in table S1.

Several of the differentially regulated genes were associated with the constitution and remodeling of the extracellular matrix (ECM). Striking, the *Col1a1* was the most prominent dysregulated gene of these ECM associated factors showing a 2.5 fold downregulation in *Aga2severe*. To strengthen the observed decrease of the *Col1a1* transcript, we additional applied qRT-PCR for the *Col1a1* using aliquots of the same RNA probes as for the expression analysis. Thus, we confirmed the assumed downregulation of *Col1a1* to about 25% in *Aga2severe* hearts compared to the littermate controls (figure 32). Noticeable, the estimated reduction of the *Col1a1* transcript on tissue level in severe *Aga2* hearts correspond to the calculated decrease seen on cellular level in severe *Aga2* heart fibroblasts obtained in the cell culture experiments described above. Intriguing, *Col1a2* was also downregulated and the alteration of the both collagen I transcripts was confirmed by the fact, that three independent probes for *Col1a1* and four independent probes for *Col1a2* on the array showed the similar decrease on the expression level. Moreover, we found a downregulation of the genes for *Col2* and *Col3*. In accordance with the decline of the different collagen types there was a downregulation of *Dpt* and *Mfap4*, important factors for the collagen fibrillogenese and matrix assembly. Upregulation of *Col8*, *Tgm2* and *Ctgf* further indicate pronounced ECM remodeling.

A group of significantly expressed genes account for changes on the metabolic pathway and alteration of the oxygen supply like *Egln3*, *Ldha*, *Aldoa*, *Eno1*, *Cox6a1*, *Gapdh* and *Pgm2*. Since all of them were upregulated, this argues for a pathological situation of the heart tissue with low oxygen tension (hypoxia). Consistent with our findings in the cardiovascular and histology examinations, we found an upregulation of *Nppa* and *Slc25a4* as marker for hypertrophy. Finally, expression profiling revealed no signs for dysregulation of genes associated with apoptosis.
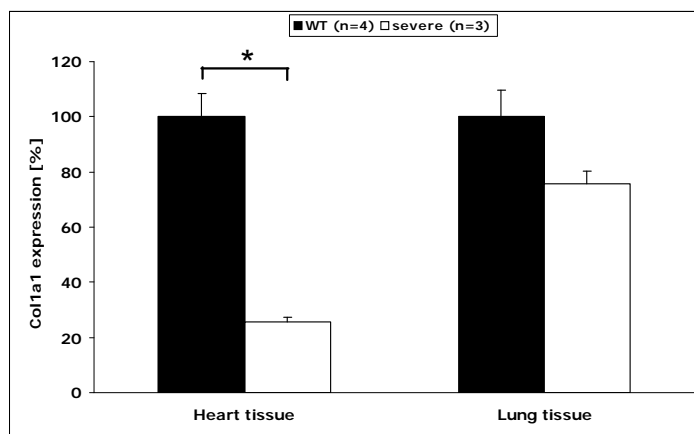
Figure 32. *Col1a1* expression in heart and lung tissue (qRT-PCR). Within the heart, a significant downregulation of the Col1a1 transcript to 25% in *Aga2^severe^* was detected compared with wild type control. In lung tissue, there is only a slight reduction of the Col1a1 expression to 75% in *Aga2^severe^*. * = p ≤ 0.05, ** = p ≤ 0.01, *** = p ≤ 0.001.

Expression profiling in lung tissue revealed 156 regulated genes, allocated in 65 upregulated and 91 downregulated markers with 1.5 to 6.8 fold expression differences compared to wild type littermates (figures S4 / S5). The selected genes were highly reproducible, as given by a strong correlation of these genes between all three investigated *Aga2^severe^* samples. Furthermore, all of the denoted genes were significantly regulated, since the number of falsely significant genes (FDR) was 0%, determined for 1000 permutations including six chip experiments.

Over-represented biological processes ascertained by EASE analysis of the differentially expressed genes are indicated in table S2.

In contrast to the heart, *Col1a1* was not regulated in pulmonary tissue. This was confirmed by an additional qRT-PCR showing only a slight decrease of the *Col1a1* transcript to about 75% as compared to the wild type situation (figure 32). That negligible tendency of downregulation was not detectable by the cDNA-Chip experiment. The small decrease of the *Col1a1* expression on tissue level in *Aga2^severe^* lungs correspond to the observed weak reduction on the cellular level obtained within the cell culture experiments described above.

Other ECM related markers showed a significant alteration on the expression level. For example, *Col3* and *Col5* were upregulated in pulmonary tissue of *Aga2^{severe}* as well as *Mfap2* and *Tnc*. Contrary to the heart, *Ctgf* was downregulated and *Dpt* was increased.

Signs for inflammation and wound healing were obtained by elevation of certain markers like *Tnc*, *Wnt11*, *Tgfbi* and *Ltbp3*. Molecular markers inducible by hypoxia were also increased, like *Pltp*, *Cd248*, *AR*, *Gdf10* and *Prkce*. Upregulation of *Agt* arguing for hypertension and the downregulation of some pro-angiogenesis markers like *Ang*, *Cxcl12* or *Ctgf* suggest a diminished angiogenesis in lungs of *Aga2^{severe}*. Finally and according to our histological observation of unchanged apoptotic rates in lung tissue of mutants, no signs for increased apoptosis were obtained. Instead, proapoptotic factors *Bnip3*, *Hey1* and *Dusp6* were even downregulated and anti-apoptotic marker *Prkce* was elevated.

3.2.6. pO$_2$ measurement

To substantiate the upregulation of hypoxia associated marker in heart and lung tissue, we measured blood gas parameter in both mutant groups and wild type littermates at the age of 8 to 11 days.

Indeed, we obtained a tremendous reduction in the pO$_2$ arterial pressure of *Aga2^{severe}* to 56% compared with wild type littermates, concurrently with a significant increased pCO$_2$ to about 140% (Fig.10). The derived oxygen saturation was accordingly decreased to 61% in the severely affected mutants. In contrast, *Aga2^{mild}* showed no alterations in their blood gas parameter versus wild type mice (figure 33).
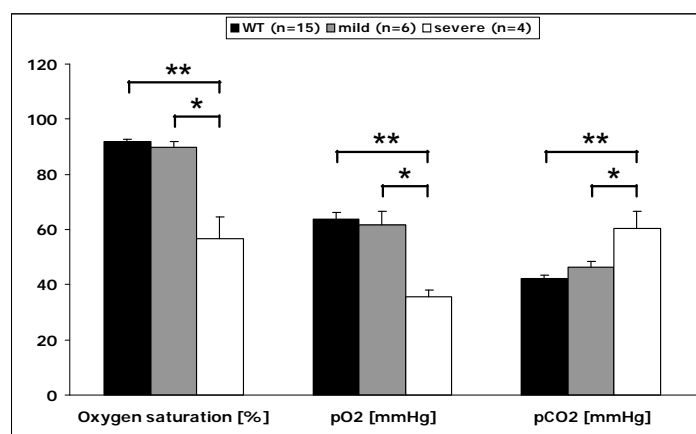
Figure 33. Quantitative analysis of blood gas parameters. No differences were obtained for all parameter tested between *Aga2^{mild}* and wild type mice. In contrast, oxygen saturation and pO$_2$ is significantly decreased and pCO$_2$ is significantly increased in *Aga2^{severe}* compared to control. * = $p \le 0.05$, ** = $p \le 0.01$, *** = $p \le 0.001$.

3.2.7. Onset of *Col1a1* down regulation and analysis of allele specific *Col1a1* expression in heart

Given the strong collagen I reduction on protein and transcript level in hearts of *Aga2^severe^*, seen with histology, cell culture and expression profiling, we tried to ascertain the onset of the *Col1a1* downregulation during the development of heterozygous *Aga2* mice. Therefore we performed qRT-PCR for *Col1a1* with RNA extracts from hearts of heterozygous animals and wild type controls at 14dpc, 20dpc as well as days 1, 3 and 6 postnatal (figure 34).

Remarkably, the *Col1a1* expression was decreased in the hearts of all heterozygous animals throughout all developmental stages to about 55%-70% compared to wild type littermates, starting already at 14dpc. These values coincide with the later observed *Col1a1* downregulation to about 65% in *Aga2^mild^* seen with heart fibroblasts from 12 day old mice. The first heterozygous animals showing the severe phenotype corresponding downregulation of the *Col1a1* transcript to about 25% arise at day 6, according to the time point when mild and severely affected *Aga2* can be distinguished for the first time.
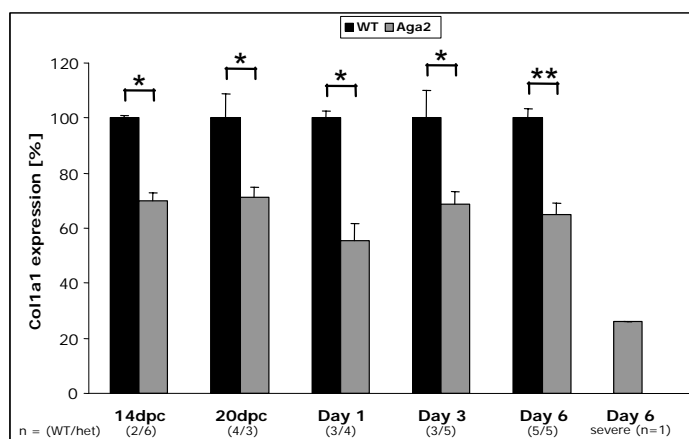
Figure 34. *Col1a1* expression in perinatal development of heterozygous *Aga2* (qRT-PCR). In all heterozygous *Aga2*, the cardiac *Col1a1* expression is significantly downregulated to 55-75% in all developmental stages compared to wild type control. Of note, the first heterozygous animal exhibiting the severe phenotype like strong *Col1a1* reduction to 25% appears at day 6 postnatal. * = p ≤ 0.05, ** = p ≤ 0.01, *** = p ≤ 0.001.

Since *Aga2^mild^* and *Aga2^severe^* are both heterozygous mutants possessing the same genetic background, we finally tried to figure out possible molecular reasons underlying the different *Col1a1* expression in the heart of both mutant groups. We designed two allele specific *Col1a1* primer pairs, consisting of the same forward primer but different reverse sequences, to discriminate the normal *Col1a1* wild type allele (*Col1a1^WT^*) and the mutated *Col1a1* allele (*Col1a1^Aga2^*) within heterozygous RNA samples. Efficiency testing revealed similar amplification efficiencies (data not

shown) and the qRT-PCR study was conducted with the same RNA samples from the 14dpc to 6 day old heterozygous animals previously used for the determination of the onset of the *Col1a1* downregulation described above.

Compared to the expression of the *Col1a1^{WT}* alleles in wild type mice, the amount of the *Col1a1^{WT}* allele was about 50%-60% in all heterozygous animals of all developmental stages, beginning with 14dpc (figure 35). This value equates the expression of a single copy gene, as it is the case in heterozygous animals possessing one WT allele.

Striking, the expression of the mutated *Col1a1^{Aga2}* allele did not match these 50% but was strongly decreased in all heterozygous mice to average 10% compared to the *Col1a1^{WT}* alleles in the wild type littermates (figure 35). Concomitantly, the combined expression of the *Col1a1^{WT}* and *Col1a1^{Aga2}* allele in heterozygous animals yield in about 60%-70% compared to the *Col1a1^{WT}* alleles in wild type littermates – the value already obtained for the overall *Col1a1* expression in the heart fibroblast cultures of *Aga2^{mild}*.

Astonishingly, one 6 day old heterozygous mouse also showed a dramatic downregulation of even the healthy *Col1a1^{WT}* allele to about 20% instead of the single copy value of 50%-60% seen in the other heterozygous animals (figure 35). Also the *Col1a1^{Aga2}* allele of this mouse was further decreased to about 5%. Since this heterozygous mouse already showed the severe phenotype with an overall collagen Col1a1 expression of 25% in the previous experiment (see above and figure 34), the tremendous reduction of the type I collagen in *Aga2^{severe}* hearts seems to be caused by an additional silencing of the healthy *Col1a1^{WT}* allele in these mutants.
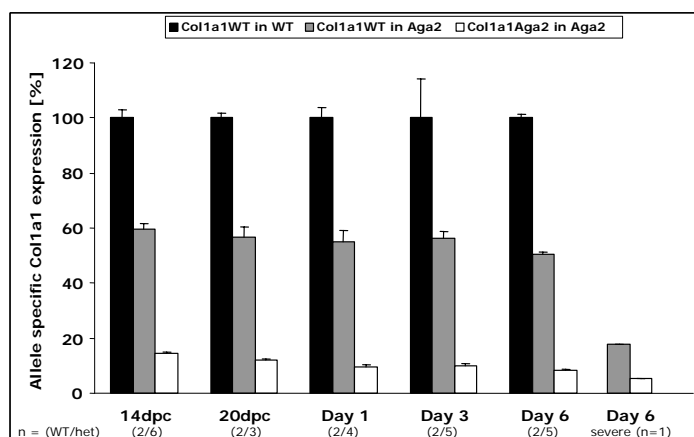
Figure 35. Allele specific *Col1a1* expression in perinatal development of heterozygous *Aga2* (qRT-PCR). Compared to the expression of the wild type *Col1a1* allele in wild type mice (■), the wild type *Col1a1* allele is reduced to 50% in all heterozygous animals (▣), corresponding to a single gene copy. In contrast, the mutated *Col1a1* allele is downregulated to 10% in all heterozygous animals (□).

Intriguing, in one 6 day old heterozygous animal the wild type allele is also silenced to 20%. This mouse showed the severe phenotype. Statistical analysis was not performed as the number of wild type mice was n=2.

To confirm this hypothesis, we performed additional qRT-PCR with both allele specific primers at 11day old mutant mice classified in *Aga2^{mild}* and *Aga2^{severe}* (figure 36).

As expected, all *Aga2^{mild}* expressed the *Col1a1^{WT}* allele to about 50% compared to the *Col1a1^{WT}* allele in the littermates, and the mutated *Col1a1^{Aga2}* allele was reduced to about 10%. However, we again obtained the strong downregulation of the *Col1a1^{WT}* allele in the *Aga2^{severe}* to 20% accompanied by a further decrease of the *Col1a1^{Aga2}* allele to about 5%. This confirms our hypothesis of the healthy *Col1a1^{WT}* allele also being silenced in hearts of severely affected mutants.
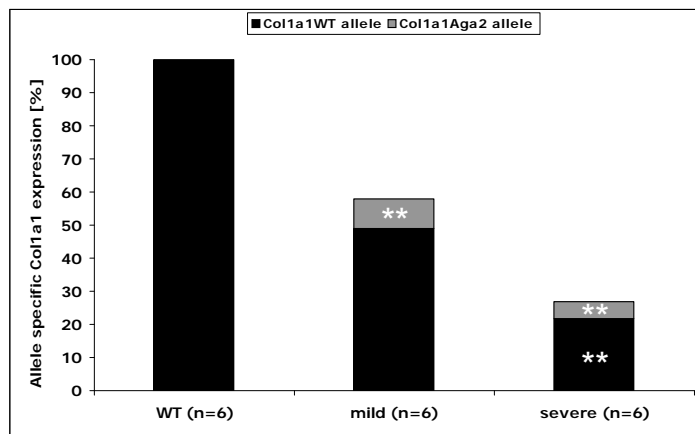
Figure 36. Allele specific *Col1a1* expression in *Aga2^{mild}* and *Aga2^{severe}* (qRT-PCR). In *Aga2^{mild}*, the wild type *Col1a1* allele (■) is expressed to 50% and the mutated *Col1a1* allele (▨) to 10%, resulting in 60% overall *Col1a1* expression. However, in *Aga2^{severe}* the mutated *Col1a1* allele is further decreased to 5% and also the wild type allele is silenced to 20%, yielding in 25% overall *Col1a1* expression. Statistical analysis was performed assuming the *Col1a1^{WT}* allele is only expressed to 50% in wild type mice (corresponding to a single gene copy). * = p ≤ 0.05, ** = p ≤ 0.01, *** = p ≤ 0.001.

4. Discussion

4.1. *In vitro* analysis of osteoblasts

4.1.1. Establishment of the cell culture system

4.1.1.1. Growth and differentiation of the osteoblasts

In vitro cell culture is the most appropriate way to study the behavior and phenotype as well as biochemical pathways and molecular mechanisms of cells independent from systemic influences of the whole organism. For bone cells, the first method to isolate and cultivate osteoblasts was based on explant cultures with outgrowth of cells from bone fragments [91-93]. However, cell migration first occurs several days after incubation, is slow and the quantity of isolated cells is often insufficient for many experimental needs. Therefore, a new method for osteoblast isolation was presented by Peck, Birge and Fedak in 1964 using enzymatic digestion of rat calvariae via crude collagenase solution to obtain a high quantity of morphological intact and viable cells that contained alkaline phosphatase [94]. The isolation protocol was further refined by several researchers to obtain a homogeneous population of the isolated bone cells with improved osteoblastic character [95].

For the cell culture system presented here, the enzymatic isolation of bone cells from neonatal calvariae has been chosen as the method of choice for several reasons. (1) Fetal rat or immature mouse calvariae are suitable for enzymatic digestion because they possess a high surface to volume ratio (large surface area compared to small volume), they are not heavily mineralized at that stage of development and there is a substantial amount of collagen in the matrix that can be disaggregated by collagenase [96]. (2) A recent study has compared osteoblastic cells from different sources (long bones vs. calvaria), ages (adult vs. fetal) and isolation techniques (explant vs. enzymatic digestion). They demonstrated that enzymatic released fetal calvaria cells are the most suitable cells concerning proliferative capacity and osteogenic potential [97]. (3) The calvaria as flat bone is formed by intramembranous ossification like most bones of the craniofacial skeleton whereas most of the vertebrate appendicular and axial skeleton is formed by endochondral ossification [30]. However, the actual process of bone formation is the same in both cases and

they only differ in the material that is replaced during the bone formation (embryonic mesenchymal condensation vs. hyaline cartilage model). The cells and the chemical reactions that are involved are identical and the osteoblasts originate from mesenchymal progenitors in both ossification types. For example, mechanosensitivity of bone cells was investigated *in vitro* and no differences were found in responsiveness of osteoblasts from adult mouse calvaria or long bones suggesting that both cell cultures can be used for these kind of experiments [95]. On the other hand, a few restrictions have to be taken into account when working with calvarial cells that will be discussed below (see Concluding remarks and further directions 4.1.1.4.).

Given these facts and the high number of cells needed for the cell culture system, we applied the enzymatic digestion method with an optimized protocol for maximum recovery of viable cells within a short preparation time. Two factors determined the isolation efficiency. (1) The age of the mice deployed for the isolation protocol was crucial for cell preparation, as with increasing age the mineralization of the calvaria proceeds [98], thus impeding the disintegration of the ECM and accordingly reducing the yield of cells released from the matrix. (2) The quantity and viability of isolated cells was further determined by the quality of the collagenase used for the isolation procedure. There is a high variability of the commercial product and the effectiveness varies between different lots [96]. The quality is mainly defined by the formulation of the mixture that determines the proportion of protease activity and the amount of cytotoxic enzymes like clostripain that can also be found in crude collagenase. Therefore it has been recommended to screen several lots to identify one that is suitable and then purchasing a larger quantity to continue the work for an extended period [96].

The calvarial cells that were isolated possessed the typical cuboidal morphology of osteoblasts [95] and differentiation of the cells was initiated by application of ascorbic acid and β-glycerophosphate. Ascorbic acid induces collagen synthesis necessary for development of the ECM by increasing the proline hydroxylation of intracellular procollagens, stimulating the cleavage of type I collagen propeptides and enhancing the rate of procollagen secretion from the cell layers to the culture media. It furthermore enhances the synthesis of several osteoblast-related proteins like ALP and osteocalcin [99]. ALP in turn is necessary for hydroxyapatite formation by providing P_i and concomitantly reducing the amount of inhibitory pyrophosphate

molecules [22-24]. Since appropriate levels of organic phosphate are further required for mineralization to occur, β-glycerophosphate can induce mineralization *in vitro* [100] and provide a substrate for ALP that hydrolyzes the organic phosphate to supply P_i [23, 24, 100]. The supplementation considerably enhanced the osteogenic potential of the culture, seen by increased ALP activity, expression of bone relevant marker genes, mineralization and formation of nodule-like structures as well as secretion and matrix deposition of collagen (see below).

Our findings that the degree of differentiation is markedly determined by the cell density and the quality of the FCS used as media supply are consistant with previous observations. It has been reported that mineralization in primary cultures only occurs in multilayer areas [101] and that the number of mineralized nodules is correlated with the density of plated cells [102]. Furthermore, micromass cultures possess a higher ALP activity per DNA than monolayer cultures and promote the differentiation of osteoblast-like cells [102]. It has been suggested that compaction and cell interactions are required to obtain an adequate environment at mineralizing sites [101] and cell-cell contacts and cell-cell communication are important for the differentiation process [102]. Micromass inoculation corresponds to the mesenchymal condensations during the process of intramembranous ossification and cells in the condensation exhibit a dramatically increased cell-cell communication, cell-cell contact and increase the number of gap junctions [102]. Also the quality of FCS has been shown to affect nodule formation, the level of ALP activity, osteocalcin synthesis and total mineral accumulation concerning the onset and amount of differentiation [103]. The concentration of endogenous factors which differ between various serum lots may be important for osteoblast differentiation like glucocorticoids which initially promote osteoprogenitor differentiation *in vitro* or EGF that inhibits ALP activity and decreases collagen synthesis as well as nodule formation [103].

4.1.1.2. Cellular assays for the characterization of the osteoblast phenotype

To allow for a comprehensive investigation of the osteoblast phenotype, nine different assays have been designed comprising methods to assess common features of cell growth and function as well as bone specific parameters.

Proliferative capacity, metabolic activity and protein content are determined to receive an overall impression of the cellular viability and behavior under culture

conditions. As the parameters are obtained within the same biological sample, the DNA amount can be used to normalize the metabolic activity and protein content. The applicability of each assay could be verified by a linear correlation between cell number and assay values (DNA / RFU / μg protein), whereas increasing cell numbers yield in increasing values but similar values are obtained for all cell number after normalization to the DNA amount of each samples.

The determination of ALP, mineralization and nodule formation has been included as widely used indicators and accepted markers for the osteogenic potential of calvarial cell cultures [97, 103]. The ALP assay based on the colorimetric detection of PNPP turnover [24, 95] and mineralization was assessed by colorimetric measurement of calcium deposits using Alizarin Red S [104]. Both methods could be verified by comparison of the respective parameter between unstimulated vs. stimulated cells over a cultivation period, that result in a strong increase of the ALP activity as well as the matrix mineralization in stimulated cells with time, whereas in unstimulated cells no activity nor staining was detectable. Nodules appear in stimulated cultures and possess morphological, ultrastructural and biochemical features of embryonic/woven bone [105]. Osteocyte-like cells are embedded within these three-dimensional structures [106, 107]. To assess the nature of the nodules in our cell culture system, we performed ICC for E11 in stimulated cultures. E11 (gp38) was described as a marker that binds selectively to cells of the late osteogenic cell lineage and was exclusively found on cell membranes of osteocytes in calvaria specimen and not at those of osteoblasts [108, 109]. Given the defined expression pattern of E11 with exclusively staining of the nodules in stimulated cultures, we confirmed the occurrence of osteocyte-like cells being embedded in the nodule structures. Therefore we investigated the nodule formation to assess the ability of functional osteoblasts to differentiate to a more mature (osteocyte-like) phenotype in our culture system. The strong increase of total nodule area in stimulated cultures with time verified the established method for investigating the nodule formation.

Given that collagen is the most abundantly expressed protein of the ECM and isolated osteoblasts in culture synthesize primarily type I collagen (~ 95%) [101], the measurement of collagen secretion and deposition based on colorimetric determination with Sirius Red [87] has been implemented to further assess the osteogenic capacity of the cell culture. Comparable to the verification of the ALP, mineralization and nodule assay, we have proven the established method for

detection of secreted and deposited collagen by comparing both parameters between unstimulated and stimulated cultures. The overall collagen synthesis increases in stimulated cultures with time and during this process, the ratio of secreted and deposited collagen gets reversed. This might be explained by the enhanced incorporation of collagen into the matrix during formation and maturation of the ECM. In contrast, neither collagen secretion nor deposition could be detected by the developed assays in unstimulated cultures.

To further characterize the molecular phenotype of the bone cells, gene expression analysis has been implemented in the cell culture system. Several studies have been conducted using comprehensive microarray-based expression profiling to unravel changes in gene expression during *in vitro* differentiation of osteoblasts and to find marker genes for certain developmental stages [110-113]. However, to limit cost and time intensive experiments, we have developed a qRT-PCR based expression assay limited to 13 important bone marker genes. The repertoire of marker genes was chosen to cover all developmental stages of *in vitro* osteoblast culture with 1) proliferation 2) differentiation and extracellular matrix maturation and 3) mineralization [114] as briefly discussed below.

1) Proliferation

The first period is characterized by expression of mitotic active genes important for regulation of cell cycle and cell growth as well as several genes associated with the formation of the extracellular matrix [114, 115].

***Fos* (c-fos)** is a nuclear phosphoprotein (Fos family) that after dimerization with c-jun (Jun family) forms a transcription factor (AP-1). It is considered to be important for the regulation of skeletal development and highly expressed in proliferating cells. Since AP-1 can prevent differentiation by inhibition of tissue-specific genes like osteocalcin (*Bglap1*), c-fos is downregulated when cells switch to differentiation [115].

Twist1 is a transcription factor involved in the negative regulation of cellular determination and differentiation of several lineages including myogenesis, neurogenesis and osteogenesis. As inhibitor of osteoblast differentiation, overexpression leads to reduced levels of ALP, whereas repression leads to increased levels of ALP, osteopontin (*Spp1*) and type I collagen [112, 116]. Therefore, *Twist1* must be repressed for osteoblast differentiation to occur [111].

Col1a1 is part of the type I collagen heterotrimer - the most abundant expressed protein of the extracellular matrix fundamental for the development of the osteoid. It is expressed in the late proliferative phase at the beginning of the differentiation / extracellular matrix maturation and therefore considered as a marker for the transition between both developmental stages [117]. Furthermore, mineralization is not observed if collagen is not produced properly [118].

2) Differentiation and extracellular matrix maturation

During the second developmental stage, genes associated with osteoblast and matrix maturation are detected and the ECM undergoes a series of modification that renders it competent for mineralization [114, 115].

Runx2 (*Cbfa1*) is a transcription factor essential for skeletal morphogenesis and maturation of osteoblasts in intramembranous and endochondral ossification. It binds to numerous enhancers and promoters including osteocalcin, osteopontin and bone sialoprotein. *Runx2* performs an antiproliferative function by suppression of cell cycle progression through G1 and supporting the transition from active cell growth to quiescence (G0/G1) in osteoblasts [119].

ALP (*Akp2*) is an important enzyme for matrix calcification by providing P_i for hydroxyapatite formation and hydrolyzing inhibitory pyrophosphate as mentioned above [22-24]. It is a widely used marker for the mature osteoblast phenotype and indicates the late proliferative and early matrix maturation stage [116]. *ALP* peaks at the maturation period and decreases to baseline levels in the mineralization phase [118].

Osterix (*Sp7*) is a transcription factor that is specifically expressed in all developing bones. It decreases osteoblast proliferation and is required for the differentiation of preosteoblasts into functional osteoblasts. Osterix inhibits Wnt pathway activity and acts downstream of *Runx2* [120, 121].

3) Mineralization

The third period is characterized by expression of late stage marker genes for the mature osteoblast phenotype and by mineralization of the extracellular matrix [115].

Spp1 (osteopontin) is an ECM protein involved in ossification and cell adhesion that binds tightly to hydroxyapatite and is important to cell-matrix interactions. *Spp1* expression reaches peak levels during the initial mineralization period [114] and has

therefore been considered as marker of late osteoblastic maturation [111] and pre-osteocytic stage of ECM mineralization [116].

Fosl2 **(Fra2)** is an important factor in the development of the mature osteoblast phenotype. Fra2 (Fos family) dimerizes with JunD (Jun family) to build up a transcription factor (AP-1). In contrast to c-fos and c-jun which show highest expression during proliferation, Fra2 and JunD reach highest expression during mineralization and are involved in the development of the mature osteoblast phenotype [122].

Bglap1 **(osteocalcin)** is an ECM protein that constitutes 1-2% of total bone protein, binds strongly to hydroxyapatite and is involved in ossification and regulation of bone mineralization. *Bglap1* is a marker of mature osteoblasts [115, 117] and its expression was found to be correlated with the formation of bone nodules [118].

Cst3 **(cystatin C)** is an ECM protein and member of the cystatin family of proteinase inhibitors. Cst3 has been found to inhibit bone resorption and it has been postulated that Cst3 maintains the integrity of newly formed bone matrix by inhibiting the action of ECM degradating enzymes [113].

Mmp13 **(Collagenase 3)** is a matrix metallopeptidase that degrades type I collagen and is involved in bone mineralization and cartilage development (collagen catabolism). Osteoblast-derived matrix metalloproteinases are key mediators of bone resorption during the initial stage of osteoid removal prior to osteoclast attachement. The expression of *Mmp13* has been reported to increase during osteoblast differentiation and mineralization in vitro and is controlled by *Runx2* [110].

Ibsp **(bone sialoprotein)** is a noncollagenous glycoprotein that stimulates cell attachment and its distribution is restricted to bone and mineralized tissues in vivo. It is a marker for osteoblast differentiation and overexpression of Ibsp has been shown to increase osteoblast-related gene expression as well as calcium incorporation and nodule formation in osteoblast cultures. Thus, *Ibsp* promotes osteoblast differentiation and it has been furthermore considered to be an initial center of hydroxyapatite crystal precipitation [123, 124].

E11 (Gp38) is described as a marker of the late osteogenic cell lineage and was found to be expressed exclusively on osteocytes and not osteoblasts within calvaria specimen [108, 109]. Since we confirmed its expression in nodule-like structures, *E11* has been included in the expression analysis as a marker for terminally differentiated osteoblasts / osteocyte-like cells.

The established qRT-PCR gene expression assay and the developed primer pairs could be verified by a high accordance of the expression values for each marker gene between single biological replicates (separate cell cultures from individual calvariae).

To achieve a reasonable and significant comparison of the osteoblast phenotype between two biological groups, all assays have been designed to allow for a quantification of the measured parameters and to assess the development of the cellular phenotype by means of a kinetic collection of the data throughout the whole culture period.

4.1.1.3. Validation of the cell culture system

To validate the established cell culture system, two mutant lines were investigated to assess the biological significance of the system and further examine the practicability of the developed SOP for an entire analysis of the cells comprising all developed assays. *Aga2* and *ABE2* were chosen as mutant lines possessing strong alterations of the bone phenotype previously identified and described within the primary and secondary screening in the Dysmorphology, Bone and Cartilage module of the GMC.

1. Wild type osteoblasts

If the behavior of the wild type control cells of both analyses are compared to each other, a similar picture of the cellular development and osteoblast differentiation is obtained. As revealed by the proliferation assay, cell growth is highest during the initial phase of development and afterwards decreases to the end of the culture period. The course of cell growth reflects three distinct proliferation periods during the *in vitro* culture. The exponential growth at the beginning supports the expansion of the osteoblast population. Postconfluent proliferation supports focal multilayering of bone forming cells and biosynthesis of type I collagen to establish a bone tissue-like organization with developing nodules. Compensatory proliferation occurs in a limited extent in mature, mineralizing bone nodules accompanying collagenase-mediated apoptotic restructuring of the nodules [8]. Given that replication and cell growth are energy-expensive processes, the metabolic activity of the culture is highest at the beginning of the culture period and decreases during matrix maturation and mineralization when the initial proliferation phase is restricted for differentiation to

occur [8, 125]. In contrast, protein synthesis is low during the initial proliferation stage but increases when the ECM is produced and remains high for maintaining and restructuring of the matrix.

The osteogenic potential of the culture markedly increases at the end of the growth period, according to the reciprocal and functionally coupled relationship between the decline in proliferative activity and the subsequent induction of genes associated with matrix maturation and mineralization [114, 125]. For example: the *ALP* gene was expressed as previously described reaching the maximum mRNA-level during the stage of differentiation and extracellular matrix maturation (about T15) [125], whereas the enzyme activity increased until the end of the cultivation period [102, 103]. Although *Col1a1* mRNA already peaked during the proliferative stage [8, 125], the overall synthesis and ECM incorporation of collagen increased during the culture time [125]. That shifting of mRNA level and collagen incorporation has previously been reported and it was shown that type I collagen synthesis and collagen accumulation are uncoupled in the developing osteoblast [126]. Accompanied by an strong increase of *Spp1* (osteopontin) and *Bglap1* (osteocalcin) - two markers for mature osteoblasts that bind to hydroxyapatite, regulate ossification and peak during the beginning of mineralization [125] - matrix mineralization and nodule formation starts at the late stage of exponential growth and proceed by the end of the culture period [103, 107, 125].

Taken together, the wild type cells recapitulate the aforementioned developmental sequence of 1) proliferation, 2) differentiation and extracellular matrix maturation and 3) mineralization [114].

Aga2 osteoblasts

In comparison to the wild type culture, calvarial cells from *Aga2* mutants depict a different characteristic of osteoblast development and maturation. No obvious differences where found in the metabolic activity and overall protein synthesis. It has been reported that, although the amount of collagen was significantly reduced (see below), the amount of total protein synthesized by OI bone cells in culture was unchanged compared to controls [127]. In contrast, the proliferation of mutant cells was significantly changed. After a slightly reduced exponential growth phase, the proliferation plateaued and again increased during the end of the culture period. This

goes well with the previously described decrease of the maximal growth rate of human osteoblasts from OI patients *in vitro* [127, 128].

Strikingly, the development of the osteogenic phenotype was completely disordered. The reduction of the ALP activity is due to the almost unchanged *ALP* gene expression throughout the culture period with a 3-fold lower peak expression compared to wild type cells. As previously described for bone cells from human OI patients [127, 129], the overall collagen synthesis (secreted and deposited) was decreased in accordance with the lower expression of the *Col1a1* gene. The matrix mineralization assay revealed higher values of calcium incorporation in the *Aga2* matrix compared to controls. Recent findings indicate a relation between collagen structure and mineralization pattern [130, 131]. Thus, it is conceivable that – although the overall secretion of collagen is decreased in *Aga2* – structural changes in the matrix by incorporation of mutated *Col1a1* chains entail alterations in nucleation sites leading to higher calcium incorporations. However, our findings are in correlation to studies showing higher mineralization in human OI patients [132], but further investigations regarding this matter are needed. Finally, the diminished osteogenic potential of the *Aga2* calvarial cells was further indicated and morphological discernable by a strong reduction of nodule formation.

The alterations on the protein and functional level could be confirmed with the expression analysis. Beside the already mentioned alteration of the *ALP* and *Col1a1* transcript level, the expression of almost all bone marker genes were changed. In most cases, the changes comprise three or more time points during the culture period in a manner that indicates diminished differentiation and matrix maturation. For example, the decrease in *Runx2* and *Osterix* after the exponential growth phase are in accordance to the observed secondary rise of the proliferative activity and the reduced osteogenic potential of the *Aga2* osteoblasts, since both transcription factors have anti-proliferative functions and are important for the transition from cell growth to the differentiation of the osteoblasts [119-121]. The downregulation of *Bglap1*, *Spp1* and *Ibsp* at the end of the cultivation period also indicate a disordered osteoblast differentiation in *Aga2*, since these ECM proteins are considered as markers of late osteoblastic maturation and found to be correlated with bone nodule formation [111, 118, 123].

The results obtained within the *Aga2* cell culture might be explained by the interaction between proliferation, ECM maturation and osteoblast differentiation in bone development. The *Col1a1* mutation in *Aga2* leads to structural alterations of the type I collagen protein with reduced extracellular secretion causing impairment of structural and functional ECM integrity [55]. Since a proper matrix is necessary for cellular differentiation and function [30], and a critical role of type I collagen in mediating the expression of a mature osteoblast phenotype has been proposed [133], the decreased collagen expression and failing ECM in *Aga2* cultures prevent appropriate osteoblast development. Furthermore, there is a reciprocal correlation between proliferation and matrix maturation, hence proliferation needs to be decreased for differentiation to occur [114, 125]. Thus, the secondary increase in proliferation during the end of the culture in *Aga2* cells might impede or delay the transition between the proliferation stage and the phase of differentiation and extracellular matrix maturation.

The course of cell growth with reduced proliferation at the beginning and the secondary increase towards the end of the culture period might be explained by the previously reported link between type I collagen synthesis and cellular proliferation, whereas destabilized collagen triple helix formation and altered collagen secretion also decreases the maximal growth rate [128]. Thus, the reduced extracellular secretion of type I collagen in *Aga2* diminish the proliferation at the beginning and after a basal level of collagen has incorporated in the matrix, proliferation might increase a second time. In wild type cells such a second growth phase does not occur, as the transition point towards extracellular matrix maturation and differentiation has been exceeded after the first phase of proliferation.

Given that the osteoblasts are cultivated under identical conditions independent from systemic influences *in vitro*, the differences in the cellular behavior and development between mutant cells and wild type control refer to a primary defect of the *Aga2* osteoblasts, whereas inappropriate collagen synthesis and secretion yield in a diminished or at least delayed extracellular matrix maturation and osteoblast differentiation in *Aga2*.

ABE2 osteoblasts

In contrast to *Aga2*, no significant differences were obtained in the cell culture system between osteoblasts from *ABE2* mice and wild type control animals in the assays performed and parameters analyzed. The differences in the expression of some marker genes are not considered as biological significant, since the alterations only occurred at one out of five measurement days except for *Mmp13* and *Ibsp* - but these two markers already showed the highest variability in the validation experiment with biological replicates (see Gene expression (A5) 3.1.1.6. and table 8). Only the expression of osteocalcin (*Bglap1*) differed from the wild type control over the complete cultivation period with elevated values observed in *ABE2* osteoblasts. One possibility for the elevated osteocalcin expression might be a failing of Notch activation in the osteoblasts by the mutated Jagged1 ligand. Since Notch normally inhibits osteoblastogenesis and impairs osteoblast differentiation [134], the insufficient Notch activation in *ABE2* bone cells promotes osteoblast differentiation and thus, osteocalcin as differentiation marker is elevated.

This alteration in the Jagged1 - Notch interaction might also explain the overall bone phenotype with more cortical bone and a higher trabecular bone mineral density in *ABE2* mice, as previous studies with transgenic mice lacking Notch signaling reveal increases of osteoblastogenesis and bone parameter in the mutants [135]. However, the effect is reversed in older mice and long term inhibition of Notch results in osteoporotic mice [135], which to our knowledge has never been observed in *ABE2*. Moreover, Notch1/2 mutants have increased trabecular bone volume but *ABE2* mice possess strong alterations of the cortical bone. Finally, although Notch and Jagged1 are expressed in osteoblasts [134] and could therefore influence themselves in culture, no alterations (except for osteocalcin gene expression) were observed in the analyzed cellular parameters. In contrast, *in vitro* cultivation under identical conditions without systemic influences reveals identical behavior and development of *ABE2* calvarial cultures compared to wild type control. Thus, we assume a secondary effect occurs in the *ABE2* mutants leading to the bone phenotype rather than a disordered Jagged1 - Notch interaction in bone cells.

A possible explanation for the alteration of the bone structure in *ABE2* might be the increased angular velocity and forward locomotor activity in mutant mice, which was revealed in the Behavior Screen of the GMC (unpublished data) and might be related to the vestibular defect in these mutants [90]. Previous studies have shown that

enhanced locomotor activity in laboratory mice markedly increased bone mineral content, bone mass and density as well as cortical area and concomitantly enhances bone mechanical properties [136, 137]. Therefore, the increased bone parameters might be explained as a secondary effect due to elevated physical activity that positively effects bone homeostasis and remodeling [32].

It should be emphasized, that the aforementioned speculation about the unaffected Notch signaling is not a general consideration for the mutants. In contrast, given that the mutation of Jagged1 resides in the second EGF-like repeat of the extracellular domain important for Notch binding [90], a disordered Jagged1 - Notch signaling is actually likely but might be unrecognized in bone development, since osteoblasts also express Delta-like1 which may rescue the Jagged1 mutation with regards to Notch activation [134]. Further studies concerning this matter are necessary that might also elucidate the observed alterations in the osteocalcin expression in primary calvarial osteoblasts of *ABE2*.

4.1.1.4. Concluding remarks and further directions

A comprehensive and multifaceted cell culture system has been established to unravel and describe the cellular phenotype of *in vitro* cultivated osteoblasts isolated from mice with bone alterations in a quick and timely fashion. The combination of nine different assays - each performed at multiple time points during a 3 week culture period - allows for the assessment of general properties of cell growth and function as well as concurrently the determination of bone specific parameters on functional-, protein- and RNA-level. As the cells are cultivated and investigated independently from systemic influences of the whole organism under identical and well known conditions, it is possible to assess whether a primary cell autonomous or a secondary systemic effect is responsible for the observed bone phenotype [138].

However, the system should be regarded as a first line investigation and important considerations have to be taken into account for the interpretation of the results.

1) Variation in isolation, initial plating and cultivation of the cells can occur between different days and replicated cultures. Since the osteoblast differentiation is determined by the culture conditions as shown in initial experiments, wild type control cells have to be isolated, cultivated and analyzed in parallel to every mutant line. This ensures identical treatment of wild type and mutant cells which is the basic

requirement for a reliable comparison of both cultures and the assessment of the mutant phenotype.

2) Given that the mutant and wild type cultures each arise from a single pool of cells, biological replicates are not performed within the culture system and therefore, statistical predications are not feasible. Thus, it should be kept in mind that only trends in the differences between mutant and wild type cells can be obtained, but the development and course of each single parameter during the culture period provide valuable information to assess possible differences between both cultures.

3) It has been mentioned above, that neonatal calvarial cells are the most suitable cells concerning proliferative capacity and osteogenic potential. However, this means that osteoblasts from different sources (e.g. long bones) possess changes in their *in vitro* development and indeed, differences in ALP activity and mineralization between cultures from calvaria and long bones were found [97]. In contrast, for other parameters like mechanosensitivity no differences were found [95]. As aforementioned, the actual process of bone formation is the same between intramembranous and endochondral ossification with the same cells and chemical reactions being involved. However, the intramembranous origin of the calvaria should always been taken into account when correlating the result from the culture system to bone alterations observed in the long bones (endochondral). Furthermore, it has been noted that neonatal cell cultures behave differently and contain more immature, rapidly growing cells than cultures from adult bone [95]. Therefore, the age of the calvaria also has to be considered when explaining the result of the cell culture system in association to a bone disease with late onset in adult mice.

4) The established system enables the analysis of osteoblasts. However, the skeletal system is maintained by a precisely regulated interaction between bone formation (osteoblasts) and bone resorption (osteoclasts) in the process of remodeling (homeostasis). Thus, the investigation of osteoblasts allows for assessing the formation process but alterations in bone resorption cannot be disclosed. Therefore, *in vitro* analysis of osteoclasts can be implemented to broaden the phenotyping options of the cell culture system. TRAP staining and pit formation assays could be performed to evaluate osteoclast development and function [139]. To further extend the cellular analysis and unravel possible dysregulations in cell-cell communication, coculture systems can be applied combining osteoblasts and MSC [140], osteoblasts and osteoclasts [141] or osteoblasts and chondrocytes [142] for example.

4.2. Heart and lung investigation in the *Aga2* OI mouse model

Although primarily described as a bone disorder, alterations in other organ systems are known associated symptoms in *Osteogenesis imperfecta* and in the most severe cases, pulmonary and cardiovascular impairments are described as the main causes for lethality. However, there is no direct association between the underlying collagen mutation and the pathological tissue alterations leading to death so far. Moreover, the malfunctions in lung and heart are considered as secondary effects due to bone deformities and fractures, respectively.

Comparable to clinical heterogeneity in human *Osteogenesis imperfecta*, heterozygous *Aga2* mice possess two different phenotypes concerning symptoms and lethality. *Aga2^mild^* possess a moderate phenotype and survive to adulthood, while *Aga2^severe^* exhibit a serious onset of symptoms and succumb to postnatal lethality. To elucidate the pathological differences and molecular reasons leading to death in the severe affected mice, comprehensive investigation of the *Aga2* mutant line was performed. Functional, morphological and molecular-genetical analyses were conducted concentrating on heart and lung as the most affected organs in lethal human OI cases.

4.2.1. Downregulation of cardiac type I collagen in *Aga2*

In *Aga2^severe^*, we observed a tremendous downregulation of the type I collagen protein in heart tissue and cardiac fibroblasts, both *in vivo* and *in vitro*. The result was confirmed independently on protein level by IHC and ICC as well as transcript level using expression profiling and qRT-PCR. On the RNA level we found a 4 fold decrease in the *Col1a1* expression (to 25%) in *Aga2^severe^* compared to wildtpye tissue. To our knowledge, such strong reduction of the collagen content in hearts of lethal OI has not been shown before. There is one study describing a downregulation of collagen in hearts of the *oim* mouse model for OI [49]. However, the investigation was done in surviving animals at the age of 16 weeks which do not succumb to earlier lethality [143] and the mutation affects the *Col1a2* gene, which can be partially rescued by the formation of homotrimers composed of *Col1a1* [144]. Furthermore, echocardiograms showed no differences and the collagen concentration was only about 1.8 fold reduced - comparable to the downregulation of the collagen in *Aga2^mild^*

animals which as well survive to adulthood. Only one study hints to a downregulation of the collagen content in the lethal form of type II OI by investigating the hearts of two deceased fetuses using SEM and TEM analysis. However, they did not relate the collagen alterations with the onset of heart failure [50].

To explain the strong downregulation of type I collagen in hearts of $Aga2^{severe}$, we have to consider two important facts regarding cardiac fibroblasts. First, as one of the pivotal organs in the body, the maintenance of heart function during stress situations is essential for survival of the organism and therefore, mechanisms of resistance against stress-induced cell death in this organ have been evolved [145]. Since cardiac fibroblasts play an essential role for heart physiology by producing the ECM as well as angiogenic and cardioprotective factors, they possess the most enhanced survival potential in cases of serious insults in the heart [146]. Space left by dead myocytes is filled by several cell types including fibroblasts and newly synthesized extracellular matrix [147, 148]. It has been shown that cardiac fibroblasts have decreased apoptosis and sustained proliferation in case of hypoxia, alcohol exposure and oxidative stress, for example [149-151]. On the other hand it is known, that unfolded or misfolded collagens triggers the activation of ER stress related genes such as *BiP*, *CHOP* and *HSP47* in affected cells like chondrocytes and fibroblasts [152, 153]. Furthermore, the expression and intracellular retention of mutant collagen is accompanied by ER stress in OI [154]. Additionally, we have recently shown that the expression of the mutated *Col1a1* in our *Aga2* OI model also causes ER stress-associated unfolded protein response in osteoblasts and induces apoptosis in the cells [55]. Considering both issues - the necessity for ECM production while avoiding apoptosis and the increased cell death after expression of malformed collagen - the cardiac fibroblasts, in the case of OI, run into a dilemma if they express the mutated collagen. The observed collagen reduction might therefore be the only escape to circumvent cell death in cardiac fibroblasts. Indeed, we found no signs for apoptosis in the heart, neither on protein nor on RNA level. In contrast, *Cox6a1* which has been recently described as a novel suppressor of Bax-mediated cell death was elevated [155], strengthening our hypothesis that decreased collagen expression prevents apoptosis.

Moreover, the *Col1a2* allele as the binding partner for the collagen I heterotrimer was as well downregulated together with *Dpt* and *Mfap4*, two important proteins for collagen fibrillogenesis and matrix assembly [156-159]. Thus, the collagen reduction

seems to be a well-regulated cellular process. And since the decreased collagen expression was additionally verified in cultivated heart fibroblasts of *Aga2^severe^* in vitro, the downregulation appears to be primarily caused and intrinsic to the fibroblasts, independent from systemic influences and pathological tissue alterations.

4.2.2. Structural alterations and dysfunction of the heart in *Aga2*

The downregulation of type I collagen as the major ECM protein entail structural alterations and impair the integrity of the heart connective tissue in *Aga2^severe^*. IHC points out the collagen meshwork as fundamentally disordered with interrupted collagen distribution throughout the extracellular matrix. SEM analysis further discloses considerable alterations in structure, organization and spatial arrangement of the collagen fibrils. The reduced thickness, stronger bending and increased ratio of smaller fibrils is similar to the observation made in the two studies which showed a slight collagen downregulation mentioned above [49, 50]. Finally, expression profiling hint to an increased remodeling of the ECM showing upregulation of *Col8a1*, *Ctgf* and *Tgm2*, which might simultaneously indicate a possible rescue mechanism for maintenance and stabilisation of the heart connective tissue [160-162]. Additionally, reduced PECAM staining indicates impairments in cardiac vessel integrity. This is confirmed by the upregulation of *Col8a1* that was shown to be elevated after vessel injury in hearts [163].

An appropriate collagen scaffold is needed for attachment, connection and orientation of myocytes and muscle fibers, confers myocardial stiffness and biomechanical strength to resist contraction force and is required for adequate diastolic and systolic ventricular function [164, 165]. Furthermore, since a broad decrease of the collagen amount results in a dilated ventricle with increased compliance [166], the disordered collagen matrix in *Aga2^severe^* leads to impaired cardiac function and the development of heart failure in these lethal OI mice.

Indeed, histological examination clearly depicts the expected morphological alterations in hearts of *Aga2^severe^*. Given the huge differences in the body constitution between severe mutants and wild type littermates, the even heart size is pathological and caused by enlarged septum and right ventricular hypertrophy. Expression profiling confirmed the morphological findings with upregulation of *Nppa*, *Tgm2* and *Slc25a4* as marker for hypertrophy and stress. Nppa is a hormone exclusively

secreted by heart cells in response to stress, high blood pressure and atrial stretch to modulate cardiac growth and hypertrophy [167, 168]. *Tgm2* was shown to be markedly increased during transition to heart failure and development of hypertrophy [169] and *Slc25a4* (*Ant1*) activation is involved in cardioprotective program to improve myocardial functions in failing hearts [170]. Furthermore, the combined strong upregulation of *Mt1* with decreased *D0H0S114* (*P311*) expression hints at muscular atrophy of the heart [171], which might argue for an alteration of the cellular tissue composition with reduced myocyte fraction.

The accompanied functional impairments could be clearly disclosed by ultrasound analysis. Left ventricular end-systolic internal diameter (LVESD) is significant elevated in the lethal *Aga2^severe^* and the fractional shortening and ejection fraction accordingly decreased. This alludes to an impaired mechanical property of the cardiac ECM and restricted ability of the ventricular muscle to contract, which might be due to the collagen deterioration [164, 165] and/or a diminished myocyte fraction which decreases brawniness and muscle strength. The hypertrophic tissue accompanied by the impaired cardiac function might be referred to as hypertrophic cardiomyopathy [172].

4.2.3. Hemorrhagic lungs and impaired pulmonary function in *Aga2*

Consistent with the literature [46], we also observed a strong lung phenotype in *Aga2^severe^* with hemorrhagic lungs accompanied by pneumonia and pleurisy as the most distinctive features. These morphological observations could be affirmed by the significant regulation of markers for injury and inflammation within the expression profiling. *Tgfbi* and *Ltbp3* – both associated with TGF beta and marker for wound healing and inflammatory response [173, 174] are upregulated as well as *Tnc*, which reappears in adult tissue during injury and wound healing [175]. Furthermore, the elevation of *Wnt11*, which has been shown to be involved in inflammation of joints and the intestine further hint to inflammatory processes in the lungs of *Aga2^severe^* [176, 177]. In addition, the Wnt pathway has also been associated with lung diseases such as interstitial lung disease (ILD) and asthma [178].

Intriguingly, comparison of the ribcage morphology and the blood gas analysis revealed the bleedings in *Aga2^severe^* are not caused by bone fractures, since *Aga2^mild^* exhibit the same strong fracture rate as *Aga2^severe^* but concurrently possess a normal lung phenotype without bleedings and normal blood gas parameter. The ubiquitous distribution of the bleedings over the lung parenchyma argues for an intrinsic onset of the hemorrhages. Therefore, most important and contrary to the published literature describing lung problems due to bone alterations [40, 47], we found that the bleedings are primarily caused and bone-independent not due to ribcage fractures.

Concomitantly with the hemorrhagic lungs, vessel problems shown by reduced PECAM staining in lung capillaries might be related to the bleedings. Moreover, the upregulation of *Agt* as an antiangiogenic factor can prevent neovascularization [179] and the simultaneous decrease of some angiogenesis supporting markers like *Ang*, *Cxcl12* or *Ctgf* hint to a diminished angiogenesis in lungs of *Aga2^severe^* [180-182].

Bleedings prevent adequate respiration. Therefore, as expected from the hemorrhagic lungs, molecular markers inducible by hypoxemia and hypoxia were upregulated in the lung of *Aga2^severe^*, like *Pltp*, *Cd248*, *AR* and *Gdf10* [183-186]. Furthermore, *Prkce* which contributes to pulmonary vasoconstriction in case of hypoxia was elevated [187]. Importantly, various markers indicating low oxygen supply were as well upregulated in the heart tissue, like *Aldoa*, *Eno*, *Ldha* or *Egln3* [188, 189], thus confirming our hypothesis of hypoxic conditions in *Aga2^severe^*. Indeed, electrochemical analysis of blood gas parameter discloses a tremendous reduction of the pO_2 arterial pressure and corresponding low oxygen saturation in the blood of *Aga2^severe^*, confirming our hypothesis and referring to hypoxemic hypoxia in lethal mutants. Beside, the equal blood gas parameter in *Aga2^mild^* with strong rib fractures and wild type littermates possessing healthy ribcages, strengthen our assumption for a bone-independent incidence of the lung alterations. Since hypoxia has shown to cause greater injury and cell death in myocytes compared with cardiac fibroblasts [149], the hypoxic conditions might also explain the aforementioned speculated decrease in the myocyte fraction of the heart.

4.2.4. Pulmonary ECM in *Aga2*

In contrast to the heart tissue, we obtained no hints for a substantial remodeling of the extracellular matrix in lungs of *Aga2^severe^* and *Col1a1* was not found to be significantly altered. This was confirmed independently on the protein level using histology and in vitro cultivation of pulmonary fibroblasts as well as on the transcript level applying expression profiling and qRT-PCR. We found a negligible tendency of *Col1a1* downregulation to about 75% as compared to the wild type situation. The morphological absence of fibrotic tissue in the lung was further supported by the downregulation of *Ctgf* as a transcription factor responsible for enhanced tissue assembly and fibrotic processes [190-192], that was upregulated in the heart. Concomitantly, *Fli1* as a negative regulator of *Ctgf* was upregulated, explaining the decrease of the Ctgf transcript [193].

Contrary to the *Col1a1*, some other ECM related markers showed a significant alteration on the expression level. For example, *Mfap2* as an elastin binding microfibrillar glycoprotein important for the formation of elastic fibers [194] was upregulated in *Aga2^severe^* as were type III and type V collagens. Concurrently, we observed an upregulation of *Dpt* as an important protein for the fibrillation of the collagen molecules, that was downregulated in the heart [157, 158]. Another upregulated ECM molecule was tenascin C (*Tnc*). Beside its function in wound healing described above, it is known to be induced in pulmonary vascular disease affecting vascular remodeling [195]. Importantly, it has been shown that denatured collagen increases the activity of the *Tnc* promoter [195] and moreover, nonmodified native type I collagen suppresses its activity [196]. Therefore, although the quantity of the type I collagen was only marginal changed in the lungs, this might be a slight hint for possible structural alterations of the mutated collagen which is able to induce the *Tnc* promoter. Accordingly, the upregulation of type III and V collagens as interaction partner of type I collagen and some other ECM proteins could be seen as a rescue mechanism, to support the constitution of a functioning matrix in presence of the mutated and therefore structural altered type I collagen.

Surprisingly, no signs for augmented apoptosis could be obtained in lungs of *Aga2^severe^*. Contrariwise, the proapoptotic factors *Bnip3*, *Hey1* and *Dusp6* were even slightly downregulated as shown in expression profiling [197-199] whereas *Prkce*, an anti-apoptotic PKC isoform was upregulated [200].

4.2.5. Pathological linkage between heart and lung dysfunction in *Aga2*

To explain the correlation between the heart and lung alterations seen in lethal *Aga2^severe^*, we have to consider the pathological interactions between lung function and cardiovascular disease, whereas pulmonary hypertension and hypoxia contribute to cardiac remodeling and heart failure, and vice versa [201-205].

Indeed, besides the described structural and functional impairments in the heart and the hypoxic conditions, we found an upregulation of marker for hypertension within the expression profiling of *Aga2^severe^*. *Tgm2* has been shown to contribute to the development of hypertension [206] and beside its antiangiogenic effects mentioned above, *Agt* increases blood pressure due to vasoconstriction [207]. Additionally, tenascin c - already mentioned above - has also been implicated to be expressed upon mechanical stress and in clinical pulmonary hypertension [208-210]. All these markers are elevated in heart and lung, respectively, alluding to hypertension in the cardiopulmonary system of *Aga2^severe^*.

Consequently, we assume a vicious cycle of heart failure, pulmonary hypertension and hypoxia is enforced in *Aga2^severe^* and the vast abatement of the oxygen supply finally leads to death in severely affected mice. It is important to mention that an increase and progressive remodeling of cardiac type I collagen has been found to occur in failing myocardium as a kind of reparative myocardial fibrosis, to at least partially ameliorate life-threatening consequences [146, 150, 211]. But as explained before, the upregulation of mutated type I collagen in cardiac fibroblasts would cause cellular deterioration in this pivotal organ [212], precluding this adaptive mechanism, thereby fortifying the pathological cycle leading to death.

4.2.6. Origin and molecular onset of the cardiopulmonary disorder in *Aga2*

The early onset of the *Col1a1* downregulation during the embryonic development allude to the heart as the origin of the pathological changes. Since downregulation and structural alterations of the cardiac type I collagen lead to the functional impairments [164, 165], we assume this as the initial point for the pathological alterations in terms of an intrinsic cardiomyopathy in *Aga2^severe^* mice. The heart dysfunction might entail a secondary pulmonary hypertension [213], which triggers the bleedings and the emerging hypoxia, additionally favored by vessel problems and

an impaired angiogenesis in the lungs. Furthermore, the in vitro observed collagen I downregulation in cardiac fibroblasts under normoxic conditions independent from further systemic influences argue for the cardiac origin of the pathological cycle in *Aga2^{severe}*.

Admittedly, the downregulation of the type I collagen in the embryonic heart tissue was not that strong as in *Aga2^{severe}* but yield the values obtained in *Aga2^{mild}* that survive to adulthood. Therefore, we also have to consider further mechanisms occur in parallel to the heart alterations and trigger simultaneously the onset of the pathological changes in the cardiopulmonary system. It might be conceivable that the hypertension occurs first or in parallel as idiopathic (primary) pulmonary hypertension [214] and the accompanied bleedings are fostered by vessel alterations. Indeed, an upregulation of *Wnt11* has previously been shown in idiopathic pulmonary arterial hypertension [215]. The resulting hypoxia then entails the cardiac hypertrophy as an extrinsic cardiomyopathy which in turn fortifies the pathological cycle. To clarify this issue, additional investigations have to be done. However, several reasons discussed above argue for a bone-independent primary nature of the pathological alterations in heart and lung that finally lead to premature death in severely affected *Aga2* mice.

To finally explain the molecular mechanism for the strong collagen I downregualtion in hearts of *Aga2^{severe}* and to reveal the differences in the type I collagen expression between both mutant groups, allele specific *Col1a1* expression was investigated in heart tissue of heterozygous animals. In *Aga2^{mild}*, the wild type *Col1a1^{WT}* allele was expressed to about 50%-60% compared with wild type littermates, corresponding to the amount of a single copy gene. The downregulation of the mutated *Col1a1^{Aga2}* allele to about 10% is likely to avoid the formation of malformed collagen heterotrimers, which might cause cellular stress [55, 154]. Intriguingly, in *Aga2^{severe}* the mutated *Col1a1^{Aga2}* allele is further silenced down to 5% and most strikingly and unexpectedly, even the wild type *Col1a1^{WT}* allele is dramatically decreased to about 20% in severely affected *Aga2* mice. In *Osteogenesis imperfecta*, such downregulation of the wild type *Col1a1* allele has not been shown before or allele specific differences of the *Col1a1* expression could not be detected [154].

A possible explanation for this phenomenon was obtained in the expression profiling with the strongest upregulation of *Mt1* in the hearts of *Aga2^severe^*. Beside its expression as a cell protective factor in cases of stress and hypoxia [216], *Mt1* has also been found to be expressed in cardiac injury [217, 218]. But most importantly, *Mt1* positively regulates the cellular level and activity of the transcription factor NF-kappaB [219, 220], which in turn inhibits the expression of *Col1a1* [221]. Given that NFkappaB is also known to inhibit the *Col1a2* allele [222], the concomitantly strong decrease of the *Col1a2* allele in *Aga2^severe^* hearts point further to the assumed Mt1 - NFkappaB induced downregulation of the type I collagen. Additionally, the downregulation of *Rabgef1* as a potent inhibitor of NF-kappaB activation [223] strengthen our hypothesis of NF-kappaB mediated collagen reduction. Since NFkappaB affects the promoter activity, this might explain the downregulation of the mutant as well as the wild type *Col1a1* allele in *Aga2^severe^*. In contrast, the slight type I collagen reduction in *Aga2^mild^* seems to be a more epigenetic regulation of allele specific silencing, only inhibiting the mutated *Col1a1^Aga2^* allele. Beside the supposed Mt1 - NFkappaB mechanism, also *Nppa*, which is strongly upregulated in hearts of *Aga2^severe^*, has been described to reduce the collagen expression [224, 225].

However, this assumption is hypothetical and the precise molecular mechanism for the strong collagen downregulation in *Aga2^severe^* remains to be further elucidated and the molecular switch determining the mild and severe phenotype in heterozygous *Aga2* has yet to be identified.

4.2.7. Concluding remarks

To date, various clinical studies have been performed showing pathological alterations in combination with pulmonary and cardiac dysfunction in Osteogenesis imperfecta. However, the impact of abnormal collagen is poorly understood and lung disease and heart failure are thought to be secondary due to fractures and bone deformities. Therefore, lethality in OI patients suffering from cardiovascular and pulmonary disorders has been seen as asymptomatic subjects.

Within this work, bone-independent and primary pathological alterations of heart and lung in the case of OI have been described for the first time using a new mouse model for this severe bone disorder. A strong downregulation of cardiac type I collagen was shown to occur in severely affected mice and related to structural as

well as functional impairments of the heart causing cardiac disorder. The hemorrhagic lungs were found to be primarily caused and not due to rib fractures as previously assumed. Furthermore, mice suffer from serious hypoxia and a vicious cycle of heart hypertrophy, hypertension and hypoxia finally lead to death. Figure 37 illustrates the pathological mechanisms evoked in heart and lung by the collagen alterations in the *Aga2* OI mouse model independent of the somewhat different processes detected in bone [55].
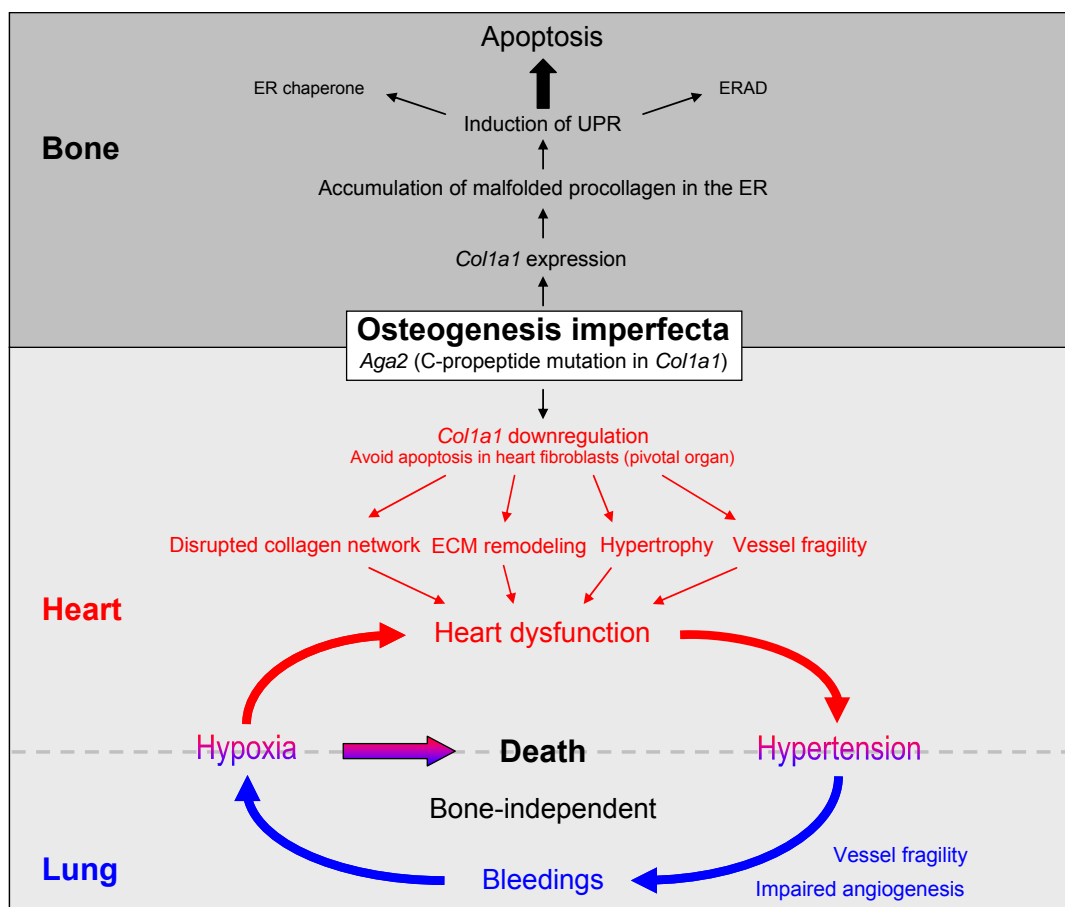
Figure 37. The pathological mechanisms in heart, lung and bone tissue of *Aga2^{severe}*. In bone, the expression of the mutated *Col1a1* leads to accumulation of malformed collagen molecules in the ER that causes the induction of UPR and triggers apoptosis [55]. In contrast, *Col1a1* gets downregulated in heart fibroblasts to avoid apoptosis in this pivotal organ. The accompanying cardiac alterations cause a bone-independent vicious cycle of heart dysfunction, hypertension, bleedings and hypoxia that finally leads to death in *Aga2^{severe}* mutant mice.

Given the new insights of the bone-independent phenotype, these results might also provide a new basis to reassess the current treatment of OI using bisphosphonates or RANKL inhibitors. The primary nature of the heart and lung alterations might require further therapeutic strategies to be considered for a successful treatment of *Osteogenesis imperfecta*.

5. Supplement

Figure S 1. B-mode pictures from the ultrasound analysis of *Aga2^severe^*. The dotted line represents the border of the septum. Compared to the wild type situation (A - diastole / B - systole), severely affected animals (C - diastole / D - systole) show a clear deformation of the septum during contraction (D). The conved bulge into the left ventricle hints to a right ventricular hypertrophy in *Aga2^severe^* animals.

Figure S2. TEM analysis of *in vitro* cultivated heart and lung fibroblasts. **A,B,C** Heart fibroblasts. Wild type cells depict a normal cellular morphology and produce a huge amount of ECM (A). *Aga2^mild^* samples exhibit few structural differences (B), but enormous alterations are seen within the *Aga2^severe^* culture in terms of disordered cytoplasm, bullous structures, changes in ER and Golgi amongst others (C). Of note, there is no sign for an ECM in the cultures of *Aga2^severe^* heart fibroblasts. **D,E,F** Lung fibroblasts. Compared to wild type cells (D), *Aga2^mild^* (E) and *Aga2^severe^* (F) fibroblasts possess a more pronounced rER and Golgi while the ECM is almost normally developed. Scale bars in A-C = 500 nm; D-F = 200 nm.

-2.0 0.0 2.0				
Mean ratio	severe 1 / severe 2 / severe 3		Gene Symbol	Comment
1.60			Rbm3	RNA binding motif protein 3
1.48			Pgm2	phosphoglucomutase 2
1.51			Egln3	EGL nine homolog 3
1.73			Lpl	lipoprotein lipase
1.53			Gorasp1	golgi reassembly stacking protein 1
1.62			Gapdh	glyceraldehyde-3-phosphate dehydrogenase
1.46			Mgll	monoglyceride lipase
1.68			3110006E14Rik	
1.69			Fabp5	fatty acid binding protein 5
3.11			Mt1	metallothionein 1
1.45			Clic5	chloride intracellular channel 5
1.59			2310056P07Rik	
1.53			Atp4a	ATPase, H+/K+ exchanging, gastric, alpha polypeptide
1.59			Slc25a4	solute carrier family 25, member 4
1.46			Utp11l	UTP11-like, U3 small nucleolar ribonucleoprotein
1.70			CR516017	
1.78			Rad17	RAD17 homolog
1.47			CR519105	
1.54			Tgm2	transglutaminase 2, C polypeptide
1.55			Eno1	enolase 1
1.94			Glul	glutamate-ammonia ligase
1.73			Aldoart1	aldolase 1, A isoform, retrogene 1
1.71			CR518500	
3.10			Ctgf	connective tissue growth factor
1.70			Gapd	similar to glyceraldehyde-3-phosphate dehydrogenase
1.68			Aldoa	aldolase 1, A isoform
1.78			CR516862	
1.58			Cox6a1	cytochrome c oxidase, subunit VI a, polypeptide 1
1.78			Slc5a10	solute carrier family 5, member 10
1.86			Aldoart1	aldolase 1, A isoform, retrogene 1
1.82			Ldh1	lactate dehydrogenase A
2.03			Aldoa	aldolase 1, A isoform
2.04			Col8a1	collagen, type VIII, alpha 1
1.75			Ldha	lactate dehydrogenase A
2.07			Nppa	natriuretic peptide precursor type A
-2.51			Col1a1	collagen, type I, alpha 1
-2.23			Mfap4	microfibrillar-associated protein 4
-1.86			Col1a2	collagen, type I, alpha 2
-1.82			Col1a2	collagen, type I, alpha 2
-2.31			Tbk1	TANK-binding kinase 1
-2.25			Psmc1	protease 26S subunit, ATPase 1
-2.32			Col3a1	collagen, type III, alpha 1
-1.85			Atoh8	atonal homolog 8
-2.18			Col1a1	collagen, type I, alpha 1
-1.74			Ptger1	Prostaglandin E receptor 1
-1.66			Col1a2	collagen, type I, alpha 2
-2.14			Dpt	dermatopontin
-2.02			Col2a1	collagen, type II, alpha 1
-1.50			Rabgef1	RAB guanine nucleotide exchange factor 1
-2.01			Col1a1	collagen, type I, alpha 1
-1.57			Gas1	growth arrest specific 1
-1.82			Mlf1	myeloid leukemia factor 1
-1.78			Tinf2	Terf1 (TRF1)-interacting nuclear factor 2
-1.69			Col1a2	collagen, type I, alpha 2
-1.45			Cdgap	Cdc42 GTPase-activating protein
-2.56			D0H4S114	DNA segment, human D4S114

Figure S3. Expression profiling of heart tissue. red - upregulation; green - downregulation.

Mean ratio	severe 1	severe 2	severe 3	Gene Symbol	Comment
1.74				Rgs9	regulator of G-protein signaling 9
2.20				Col5a1	collagen, type V, alpha 1
1.88				Raver2	ribonucleoprotein, PTB-binding 2
1.62				Ar	androgen receptor
2.61				Adh1	alcohol dehydrogenase 1
1.58				Anks1	ankyrin repeat and SAM domain containing 1
2.10				Cyp26b1	cytochrome P450, 26b1
1.67				St3gal2	ST3 beta-galactoside alpha-2,3-sialyltransferase 2
2.39				Lhfpl2	lipoma HMGIC fusion partner-like 2
1.61				CR519726	
1.77				Prdm6	PR domain containing 6
2.40				Col3a1	collagen, type III, alpha 1
1.84				Yeats4	YEATS domain containing 4
1.74				Pltp	phospholipid transfer protein
1.70				Clip3	CAP-GLY domain containing linker protein 3
1.83				Al256396	
2.03				Gap43	growth associated protein 43
1.77				Nsg2	neuron specific gene family member 2
1.66				CR518478	
1.83				Faim3	Fas apoptotic inhibitory molecule 3
2.46				Tgfbi	transforming growth factor, beta induced
2.13				Hmgn2	high mobility group nucleosomal binding domain 2
1.84				Cklfsf3	Chemokine-like factor super family 3
1.75				Scyl1	SCY1-like 1
1.95				Fscn1	fascin homolog 1, actin bundling protein
2.33				Lypd2	Ly6/Plaur domain containing 2
1.79				1810015C04Rik	
1.64				E430002G05Rik	
2.60				Fcgbp	Fc fragment of IgG binding protein
1.83				Scn3b	sodium channel, voltage-gated, type III, beta
1.89				Vash2	vasohibin 2
2.64				Gdf10	growth differentiation factor 10
2.63				Tnc	tenascin C
1.94				Serpine2	serine peptidase inhibitor, clade E, member 2
1.71				Prkce	protein kinase C
1.74				Tppp	tubulin polymerization promoting protein
1.72				Car2	carbonic anhydrase 2
2.29				1200009O22Rik	
2.18				Dpt	dermatopontin
1.73				Nfix	nuclear factor I/X
2.03				Cd248	CD248 antigen, endosialin
1.91				Antxr2	anthrax toxin receptor 2
1.69				Cbx2	chromobox homolog 2
2.36				Ltbp3	latent transforming growth factor beta binding protein 3
3.41				Agt	angiotensinogen
1.83				Plcd1	phospholipase C, delta 1
2.48				Dnahc8	dynein, axonemal, heavy chain 8
1.90				Rnf144a	ring finger protein 144A
1.75				2700081O15Rik	
3.37				Cpxm1	carboxypeptidase X 1
2.04				Zfp536	zinc finger protein 536
2.26				Cd19	CD19 antigen
3.53				Wnt11	wingless-related MMTV integration site 11
2.20				Prom1	prominin 1
2.69				Igsf10	immunoglobulin superfamily, member 10
1.99				Dclre1a	DNA cross-link repair 1A, PSO2 homolog
2.08				Elovl5	ELOVL family member 5, elongation of long chain fatty acids
2.11				Prom1	prominin 1
3.15				Igh-6	immunoglobulin heavy chain 6
2.36				Itih2	inter-alpha trypsin inhibitor, heavy chain 2
4.41				Mdk	midkine
2.54				Mfap2	microfibrillar-associated protein 2
3.18				Thbs2	thrombospondin 2
2.69				Mfap2	microfibrillar-associated protein 2
6.80				Fli1	Friend leukemia integration 1

Figure S4. Expression profiling of lung tissue (1). red - upregulation.

Mean ratio	severe 1	severe 2	severe 3	Gene Symbol	Comment
-4.41				Pf4	platelet factor 4
-3.03				Serpina3k	serine peptidase inhibitor, clade A, member 3K
-2.76				Cxcl12	chemokine (C-X-C motif) ligand 12
-2.97				Eltd1	EGF, latrophilin transmembrane domain containing 1
-2.86				C3	complement component 3
-3.34				Lyz2	lysozyme 2
-2.38				St3gal1	ST3 beta-galactoside alpha-2,3-sialyltransferase 1
-6.88				Lcn2	lipocalin 2
-2.29				Meg3	maternally expressed 3
-2.51				Tmem49	transmembrane protein 49
-2.73				Msln	mesothelin
-2.67				Dusp6	dual specificity phosphatase 6
-2.04				Clu	Clusterin
-1.93				Tacstd2	tumor-associated calcium signal transducer 2
-2.63				Ddi1	DDI1, DNA-damage inducible 1, homolog 1
-1.96				H6pd	hexose-6-phosphate dehydrogenase
-4.76				Rabgap1l	RAB GTPase activating protein 1-like
-1.84				Tspan2	tetraspanin 2
-2.24				D130051D11Rik	
-2.55				Fbp2	fructose bisphosphatase 2
-2.05				3110006E14Rik	
-2.26				S100a6	S100 calcium binding protein A6
-1.78				Lrrc8c	leucine rich repeat containing 8 family, member C
-1.93				Npc2	Niemann Pick type C2
-2.40				Aldoart1	aldolase 1, A isoform, retrogene 1
-2.08				Ctgf	connective tissue growth factor
-2.05				Aldoart1	aldolase 1, A isoform, retrogene 1
-2.10				Sfrs11	splicing factor, arginine/serine-rich 11
-3.85				Ntrk2	neurotrophic tyrosine kinase, receptor, type 2
-3.92				Cchcr1	coiled-coil alpha-helical rod protein 1
-2.05				Junb	Jun-B oncogene
-2.17				Sat1	Spermidine/spermine N1-acetyl transferase 1
-2.30				Nfasc	neurofascin
-1.93				Cdkn1c	cyclin-dependent kinase inhibitor 1C
-1.94				Sv2a	synaptic vesicle glycoprotein 2 a
-1.88				Ldha	lactate dehydrogenase A
-1.94				Fasn	fatty acid synthase
-2.23				CR515738	
-1.65				S100g	S100 calcium binding protein G
-2.58				Sparcl1	SPARC-like 1
-2.03				Treml1	triggering receptor expressed on myeloid cells-like 1
-3.54				A130040M12Rik	
-1.93				LOC100047129	similar to Glyceraldehyde-3-phosphate dehydrogenase
-1.73				S1pr1	sphingosine-1-phosphate receptor 1
-1.88				Itga2b	integrin alpha 2b
-4.37				Bnip3	BCL2/adenovirus E1B interacting protein 1
-1.75				Bcl3	B-cell leukemia/lymphoma 3
-3.71				Amd-ps7	S-adenosylmethionine decarboxylase, pseudogene 7
-1.79				Gapdh	glyceraldehyde-3-phosphate dehydrogenase
-2.16				Fabp5	Fatty acid binding protein 5
-4.08				Fabp4	fatty acid binding protein 4
-1.89				4930447K04Rik	
-1.83				Ldha	lactate dehydrogenase A
-1.80				Uhrf1bp1l	UHRF1 (ICBP90) binding protein 1-like
-2.13				Cp	ceruloplasmin
-2.82				S100a4	S100 calcium binding protein A4
-1.81				Utp11l	UTP11-like, U3 small nucleolar ribonucleoprotein
-2.00				Cd300a	CD300A antigen
-1.79				Gm22	gene model 22
-1.96				Clip4	CAP-GLY domain containing linker protein family, 4
-2.11				4930563F15Rik	
-1.97				Npc2	Niemann Pick type C2
-1.80				C1qb	complement component 1q beta polypeptide
-1.66				Pgk1	phosphoglycerate kinase 1
-1.63				Pgm2	phosphoglucomutase 2
-1.74				Ttf2	transcription termination factor, RNA polymerase II
-1.95				Mgll	monoglyceride lipase
-1.76				Ang	angiogenin, ribonuclease, RNase A family, 5
-1.85				Scnn1a	sodium channel, nonvoltage-gated, type I, alpha
-1.77				Klf6	Kruppel-like factor 6
-2.06				Mgll	monoglyceride lipase
-1.67				Npc2	Niemann Pick type C2
-1.73				Glrx	glutaredoxin
-1.70				Tpd52	tumor protein D52
-2.17				Tinagl	tubulointerstitial nephritis antigen-like
-1.73				Pkm2	pyruvate kinase
-2.14				Hey1	hairy/enhancer-of-split related with YRPW motif 1
-1.74				Btg2	B-cell translocation gene 2
-1.69				Hspb8	heat shock protein 8
-1.75				Lcp1	lymphocyte cytosolic protein 1
-2.01				Wipf3	WAS/WASL interacting protein family, member 3
-1.70				Smoc2	SPARC related modular calcium binding 2
-2.60				Hsd11b1	hydroxysteroid 11-beta dehydrogenase 1
-2.12				AA986860	
-3.66				Lpl	lipoprotein lipase
-1.61				Avpi1	arginine vasopressin-induced 1
-1.71				AW554918	
-1.67				Prdx6-rs1	peroxiredoxin 6, related sequence 1
-2.15				Gpx1	glutathione peroxidase 1
-1.52				CR516647	
-1.91				Atp1a1	ATPase, Na+/K+ transporting, alpha 1 polypeptide

Figure S5. Expression profiling of lung tissue (2).
green - downregulation.

GO-term	Gene symbol
Cell communication	*Col1a2, Col2a1, Col8a1, Ctgf, Dpt, Glul, Gorasp1, Mfap4, Ptger1, Tbk1, Tgm2*
Cell growth and / or maintenance	*Apt4a, Cdgap, Clic5, Ctgf, Fabp5, Gas1, Lpl, Rad17, Scl25a4, Tinf2*
Organogenesis	*Col1a1, Col1a2, Col2a1, Col3a1, Col8a1, Ctgf, Fabp5*
Cell adhesion	*Col1a2, Col2a1, Col8a1, Ctgf, Dpt, Mfap4*
Energy pathways	*Aldoa, Cox6a1, Eno1, Gapd, Ldha, Scl25a4*
Carbohydrate metabolism	*Aldoa, Eno1, Gapd, Ldha, Pgm2*
Protein metabolism	*Egln3, Lpl, Psmc1, Tbk1, Tgm2*
Response to stress	*Ctgf, Mgll, Rad17, Tinf2*
Skeletal development	*Col1a1, Col1a2, Col2a1, Ctgf*
Epidermal differentiation	*Col1a1, Ctgf, Fabp5*
Lipid metabolism	*Fabp5, Lpl, Mgll*
Apoptosis	*Egln3, Tgm2*
Signal transduction in Golgi apperatus	*Clic5, Gorasp1*
Hormone activity	*Nppa*

Table S1. GO-Term analysis of differentially expressed genes in hearts of *Aga2severe*.

GO-term	Gene symbol
Cell growth and / or maintenance	*Ar, Atp1a1, Bcl3, Btg2, Cbx2, Cdkn1c, Cp, Ctgf, Cxcl12, Dusp6, Fabp4, Fli1, Fscn1, Gap43, Hmgn2, Junb, Lcn2, Lpl, Mdk, Nfix, Pgm2, Pltp, S100A6, scn3b, Scnn1a, Sv2a, Tacstd2, Tgfb1*
Cell surface receptor linked signal transduction	*Agt, C3, Cd19, Ctgf, Cxcl12, Eltd1, Gap43, Gdf10, Itga2b, Ltbp3, Ntrk2, Pf4, RgS9, Tacstd2, Wnt11*
Organogenesis	*Ang, Ar, Col3a1, Ctgf, Fabp5, Fli1, Gap43, Gdf10, Hey1, Mdk, Ntrk2, Pf4, S100a6*
Response to stress	*Btg2, C1qb, C3, CD19, Clu, Ctgf, Cxcl12, Dclre1a, Gap43, Gpx1, Mgll, Pf4*
Protein metabolism	*Bcl3, Col5a1, Dusp6, Itih2, Lpl, Ntrk2, Prkce, Scyl1, Serpine2*
Immune response	*C1qb, C2, Cd19, Clu, Cxcl12, Fcgbp, Mgll, Pf4*
Lipid metabolism	*Clu, Fabp5, Fasn, Hsd11b1, Lpl, Mgll, Plcd1, Pltp*
Oxidoreductase activity	*Cp, Fasn, Glrx, Gpx1, H6Pd, Hsd11b1, Ldha, Msln*
Response to wounding	*C3, Cd19, Ctgf, Cxcl12, Gap43, Mgll, Pf4*
Energy pathway	*Fbp2, H6pd, Ldha, Pgk1, Pkm2*
Neurogenesis	*Gap43, Hey1, Mdk, Ntrk2, S100a6*
Apoptosis	*Bnip3, Clu, Dusp6, Prkce*
Inflammatory response	*C3, Cxcl12, Mgll, Pf4*
Angiogenesis	*Ng, Ctgf, Pf4*
Embryogenesis and morphogenesis	*Tpd52, Wnt11*
Epidermal differentiation	*Gtgf. Fabp5*

Table S2. GO-Term analysis of differentially expressed genes in lungs of *Aga2severe*.

6. References

1. Cohen, M.M., Jr., *The new bone biology: pathologic, molecular, and clinical correlates.* Am J Med Genet A, 2006. **140**(23): p. 2646-706.
2. Bryan, G.J., Johnson, W.H., Davies, E.R., , *Skeletal Anatomy.* 3, illustrated ed. 1996: Elsevier Health Sciences.
3. Buckwalter, J.A., et al., *Bone biology. I: Structure, blood supply, cells, matrix, and mineralization.* Instr Course Lect, 1996. **45**: p. 371-86.
4. Hillier, M.L. and L.S. Bell, *Differentiating human bone from animal bone: a review of histological methods.* J Forensic Sci, 2007. **52**(2): p. 249-63.
5. Buckwalter, J.A. and R.R. Cooper, *Bone structure and function.* Instr Course Lect, 1987. **36**: p. 27-48.
6. Forriol, F. and F. Shapiro, *Bone development: interaction of molecular components and biophysical forces.* Clin Orthop Relat Res, 2005(432): p. 14-33.
7. Marks, S.C., Jr. and S.N. Popoff, *Bone cell biology: the regulation of development, structure, and function in the skeleton.* Am J Anat, 1988. **183**(1): p. 1-44.
8. Stein, G.S., et al., *Transcriptional control of osteoblast growth and differentiation.* Physiol Rev, 1996. **76**(2): p. 593-629.
9. Komori, T., *Regulation of osteoblast differentiation by transcription factors.* J Cell Biochem, 2006. **99**(5): p. 1233-9.
10. Ducy, P., T. Schinke, and G. Karsenty, *The osteoblast: a sophisticated fibroblast under central surveillance.* Science, 2000. **289**(5484): p. 1501-4.
11. Harada, S. and G.A. Rodan, *Control of osteoblast function and regulation of bone mass.* Nature, 2003. **423**(6937): p. 349-55.
12. Bonewald, L., *Osteocytes as multifunctional cells.* J Musculoskelet Neuronal Interact, 2006. **6**(4): p. 331-3.
13. Bonewald, L.F., *Mechanosensation and Transduction in Osteocytes.* Bonekey Osteovision, 2006. **3**(10): p. 7-15.
14. Miller, S.C. and W.S. Jee, *The bone lining cell: a distinct phenotype?* Calcif Tissue Int, 1987. **41**(1): p. 1-5.
15. Vignery, A., *Macrophage fusion: the making of osteoclasts and giant cells.* J Exp Med, 2005. **202**(3): p. 337-40.
16. Cappellen, D., et al., *Transcriptional program of mouse osteoclast differentiation governed by the macrophage colony-stimulating factor and the ligand for the receptor activator of NFkappa B.* J Biol Chem, 2002. **277**(24): p. 21971-82.
17. Boyle, W.J., W.S. Simonet, and D.L. Lacey, *Osteoclast differentiation and activation.* Nature, 2003. **423**(6937): p. 337-42.
18. Karsenty, G. and E.F. Wagner, *Reaching a genetic and molecular understanding of skeletal development.* Dev Cell, 2002. **2**(4): p. 389-406.
19. Young, M.F., et al., *Structure, expression, and regulation of the major noncollagenous matrix proteins of bone.* Clin Orthop Relat Res, 1992(281): p. 275-94.
20. Robey, P.G., et al., *Structure and molecular regulation of bone matrix proteins.* J Bone Miner Res, 1993. **8 Suppl 2**: p. S483-7.
21. Boskey, A.L. and A.S. Posner, *Bone structure, composition, and mineralization.* Orthop Clin North Am, 1984. **15**(4): p. 597-612.
22. Anderson, H.C., et al., *Impaired calcification around matrix vesicles of growth plate and bone in alkaline phosphatase-deficient mice.* Am J Pathol, 2004. **164**(3): p. 841-7.
23. Balcerzak, M., et al., *The roles of annexins and alkaline phosphatase in mineralization process.* Acta Biochim Pol, 2003. **50**(4): p. 1019-38.
24. Addison, W.N., et al., *Pyrophosphate inhibits mineralization of osteoblast cultures by binding to mineral, up-regulating osteopontin, and inhibiting alkaline phosphatase activity.* J Biol Chem, 2007. **282**(21): p. 15872-83.
25. Garimella, R., J.B. Sipe, and H.C. Anderson, *A simple and non-radioactive technique to study the effect of monophosphoesters on matrix vesicle-mediated calcification.* Biol Proced Online, 2004. **6**: p. 263-267.
26. Shapiro, F., *Bone development and its relation to fracture repair. The role of mesenchymal osteoblasts and surface osteoblasts.* Eur Cell Mater, 2008. **15**: p. 53-76.
27. Ornitz, D.M. and P.J. Marie, *FGF signaling pathways in endochondral and intramembranous bone development and human genetic disease.* Genes Dev, 2002. **16**(12): p. 1446-65.
28. Hartmann, C., *A Wnt canon orchestrating osteoblastogenesis.* Trends Cell Biol, 2006. **16**(3): p. 151-8.

29. Goldring, M.B., K. Tsuchimochi, and K. Ijiri, *The control of chondrogenesis.* J Cell Biochem, 2006. **97**(1): p. 33-44.

30. Ortega, N., D.J. Behonick, and Z. Werb, *Matrix remodeling during endochondral ossification.* Trends Cell Biol, 2004. **14**(2): p. 86-93.

31. Marx, R.E. and A.K. Garg, *Bone structure, metabolism, and physiology: its impact on dental implantology.* Implant Dent, 1998. **7**(4): p. 267-76.

32. Benjamin, M. and B. Hillen, *Mechanical influences on cells, tissues and organs - 'Mechanical Morphogenesis'.* Eur J Morphol, 2003. **41**(1): p. 3-7.

33. Boyce, B.F. and L. Xing, *Osteoclasts, no longer osteoblast slaves.* Nat Med, 2006. **12**(12): p. 1356-8.

34. Hill, P.A., *Bone remodelling.* Br J Orthod, 1998. **25**(2): p. 101-7.

35. Superti-Furga, A., L. Bonafe, and D.L. Rimoin, *Molecular-pathogenetic classification of genetic disorders of the skeleton.* Am J Med Genet, 2001. **106**(4): p. 282-93.

36. Fuchs, H., Lisse, T., Abe, K., Hrabé de Angelis, M., *Screening for bone and cartilage phenotypes in mice.* In Standards of Mouse Model Phenotyping, ed. M. Hrabé de Angelis, Chambon, P., Brown, S. 2006, Weinheim: Wiley-VCH. 35-85.

37. Reeder, J. and E. Orwoll, *Images in clinical medicine. Adults with osteogenesis imperfecta.* N Engl J Med, 2006. **355**(26): p. e28.

38. Martin, E. and J.R. Shapiro, *Osteogenesis imperfecta:epidemiology and pathophysiology.* Curr Osteoporos Rep, 2007. **5**(3): p. 91-7.

39. Glorieux, F.H., *Osteogenesis imperfecta.* Best Pract Res Clin Rheumatol, 2008. **22**(1): p. 85-100.

40. Rauch, F. and F.H. Glorieux, *Osteogenesis imperfecta.* Lancet, 2004. **363**(9418): p. 1377-85.

41. Kocher, M.S. and F. Shapiro, *Osteogenesis imperfecta.* J Am Acad Orthop Surg, 1998. **6**(4): p. 225-36.

42. Marini, J.C., et al., *Components of the collagen prolyl 3-hydroxylation complex are crucial for normal bone development.* Cell Cycle, 2007. **6**(14): p. 1675-81.

43. Roughley, P.J., F. Rauch, and F.H. Glorieux, *Osteogenesis imperfecta--clinical and molecular diversity.* Eur Cell Mater, 2003. **5**: p. 41-7; discussion 47.

44. Ralston, S.H. and B. de Crombrugghe, *Genetic regulation of bone mass and susceptibility to osteoporosis.* Genes Dev, 2006. **20**(18): p. 2492-506.

45. Singer, R.B., S.A. Ogston, and C.R. Paterson, *Mortality in various types of osteogenesis imperfecta.* J Insur Med, 2001. **33**(3): p. 216-20.

46. McAllion, S.J. and C.R. Paterson, *Causes of death in osteogenesis imperfecta.* J Clin Pathol, 1996. **49**(8): p. 627-30.

47. Widmann, R.F., et al., *Spinal deformity, pulmonary compromise, and quality of life in osteogenesis imperfecta.* Spine, 1999. **24**(16): p. 1673-8.

48. Shapiro, J.R., et al., *Pulmonary hypoplasia and osteogenesis imperfecta type II with defective synthesis of alpha I(1) procollagen.* Bone, 1989. **10**(3): p. 165-71.

49. Weis, S.M., et al., *Myocardial mechanics and collagen structure in the osteogenesis imperfecta murine (oim).* Circ Res, 2000. **87**(8): p. 663-9.

50. Wheeler, V.R., N.R. Cooley, Jr., and W.R. Blackburn, *Cardiovascular pathology in osteogenesis imperfecta type IIA with a review of the literature.* Pediatr Pathol, 1988. **8**(1): p. 55-64.

51. Perkins, A.S., *Functional genomics in the mouse.* Funct Integr Genomics, 2002. **2**(3): p. 81-91.

52. Darling, S., *Mice as models of human developmental disorders: natural and artificial mutants.* Curr Opin Genet Dev, 1996. **6**(3): p. 289-94.

53. Soewarto, D., M. Klaften, and I. Rubio-Aliaga, *Features and strategies of ENU mouse mutagenesis.* Curr Pharm Biotechnol, 2009. **10**(2): p. 198-213.

54. Hrabe de Angelis, M.H., et al., *Genome-wide, large-scale production of mutant mice by ENU mutagenesis.* Nat Genet, 2000. **25**(4): p. 444-7.

55. Lisse, T.S., et al., *ER stress-mediated apoptosis in a new mouse model of osteogenesis imperfecta.* PLoS Genet, 2008. **4**(2): p. e7.

56. Fuchs, H., et al., *The German Mouse Clinic: a platform for systemic phenotype analysis of mouse models.* Curr Pharm Biotechnol, 2009. **10**(2): p. 236-43.

57. Fuchs, H., et al., *Phenotypic characterization of mouse models for bone-related diseases in the German Mouse Clinic.* J Musculoskelet Neuronal Interact, 2008. **8**(1): p. 13-4.

58. Harrison, R.G., *Observations on the living developing nerve fibre.* Anat Rec, 1907. **1**: p. 116-118.

59. Carrel, A., *On the permanent life of tissues outside of the organism.* J Exp Med, 1912. **15**: p. 516-528.

60.   Freshney, R.I., *Culture of animal cells: a manual of basic techniques*. 4th ed. 2000: Wiley-Liss.

61.   Gailus-Durner, V., et al., *Introducing the German Mouse Clinic: open access platform for standardized phenotyping.* Nat Methods, 2005. **2**(6): p. 403-4.

62.   Sahn, D.J., et al., *Recommendations regarding quantitation in M-mode echocardiography: results of a survey of echocardiographic measurements.* Circulation, 1978. **58**(6): p. 1072-83.

63.   Collins, K.A., C.E. Korcarz, and R.M. Lang, *Use of echocardiography for the phenotypic assessment of genetically altered mice.* Physiol Genomics, 2003. **13**(3): p. 227-39.

64.   Teichholz, L.E., et al., *Study of left ventricular geometry and function by B-scan ultrasonography in patients with and without asynergy.* N Engl J Med, 1974. **291**(23): p. 1220-6.

65.   Ohtani, O., et al., *Collagen fibrillar networks as skeletal frameworks: a demonstration by cell-maceration/scanning electron microscope method.* Arch Histol Cytol, 1988. **51**(3): p. 249-61.

66.   Macchiarelli, G., et al., *A micro-anatomical model of the distribution of myocardial endomysial collagen.* Histol Histopathol, 2002. **17**(3): p. 699-706.

67.   Agocha, A.E. and M. Eghbali-Webb, *A simple method for preparation of cultured cardiac fibroblasts from adult human ventricular tissue.* Mol Cell Biochem, 1997. **172**(1-2): p. 195-8.

68.   Neuss, M., et al., *Isolation and characterisation of human cardiac fibroblasts from explanted adult hearts.* Cell Tissue Res, 1996. **286**(1): p. 145-53.

69.   Eghbali, M., et al., *Cardiac fibroblasts are predisposed to convert into myocyte phenotype: specific effect of transforming growth factor beta.* Proc Natl Acad Sci U S A, 1991. **88**(3): p. 795-9.

70.   Phan, S.H., J. Varani, and D. Smith, *Rat lung fibroblast collagen metabolism in bleomycin-induced pulmonary fibrosis.* J Clin Invest, 1985. **76**(1): p. 241-7.

71.   Raghow, R., A.H. Kang, and D. Pidikiti, *Phenotypic plasticity of extracellular matrix gene expression in cultured hamster lung fibroblasts. Regulation of type I procollagen and fibronectin synthesis.* J Biol Chem, 1987. **262**(17): p. 8409-15.

72.   Pardo, A., et al., *Production of collagenase and tissue inhibitor of metalloproteinases by fibroblasts derived from normal and fibrotic human lungs.* Chest, 1992. **102**(4): p. 1085-9.

73.   Horsch, M., et al., *Systematic gene expression profiling of mouse model series reveals coexpressed genes.* Proteomics, 2008. **8**(6): p. 1248-56.

74.   Edgar, R., M. Domrachev, and A.E. Lash, *Gene Expression Omnibus: NCBI gene expression and hybridization array data repository.* Nucleic Acids Res, 2002. **30**(1): p. 207-10.

75.   Hegde, P., et al., *A concise guide to cDNA microarray analysis.* Biotechniques, 2000. **29**(3): p. 548-50, 552-4, 556 passim.

76.   Quackenbush, J., *Microarray data normalization and transformation.* Nat Genet, 2002. **32 Suppl**: p. 496-501.

77.   Tusher, V.G., R. Tibshirani, and G. Chu, *Significance analysis of microarrays applied to the ionizing radiation response.* Proc Natl Acad Sci U S A, 2001. **98**(9): p. 5116-21.

78.   Dennis, G., Jr., et al., *DAVID: Database for Annotation, Visualization, and Integrated Discovery.* Genome Biol, 2003. **4**(5): p. P3.

79.   Pfaffl, M.W., *A new mathematical model for relative quantification in real-time RT-PCR.* Nucleic Acids Res, 2001. **29**(9): p. e45.

80.   Livak, K.J. and T.D. Schmittgen, *Analysis of relative gene expression data using real-time quantitative PCR and the 2(-Delta Delta C(T)) Method.* Methods, 2001. **25**(4): p. 402-8.

81.   Zhang, H.X., G.H. Du, and J.T. Zhang, *Assay of mitochondrial functions by resazurin in vitro.* Acta Pharmacol Sin, 2004. **25**(3): p. 385-9.

82.   Candeias, L.P., et al., *The catalysed NADH reduction of resazurin to resorufin.* J. Chem. Soc., Perkin Trans. 2, 1998: p. 2333-2334.

83.   Krohn, R.I., *The colorimetric detection and quantitation of total protein.* Curr Protoc Cell Biol, 2002. **Appendix 3**: p. Appendix 3H.

84.   Walker, J.M., *The bicinchoninic acid (BCA) assay for protein quantitation.* Methods Mol Biol, 1994. **32**: p. 5-8.

85.   Bessey, O.A., O.H. Lowry, and M.J. Brock, *A method for the rapid determination of alkaline phosphatase with five cubic millimeters of serum.* J Biol Cem, 1946. **164**: p. 321-329.

86.   von Schroeder, H.P., et al., *Endothelin-1 promotes osteoprogenitor proliferation and differentiation in fetal rat calvarial cell cultures.* Bone, 2003. **33**(4): p. 673-84.

87.   Tullberg-Reinert, H. and G. Jundt, *In situ measurement of collagen synthesis by human bone cells with a sirius red-based colorimetric microassay: effects of transforming growth factor beta2 and ascorbic acid 2-phosphate.* Histochem Cell Biol, 1999. **112**(4): p. 271-6.

88.   Lee, D.A., E. Assoku, and V. Doyle, *A specific quantitative assay for collagen synthesis by cells seeded in collagen-based biomaterials using sirius red F3B precipitation.* J Mater Sci Mater Med, 1998. **9**(1): p. 47-51.

89.   Puchtler, H., S.N. Meloan, and M.S. Terry, *On the history and mechanism of alizarin and alizarin red S stains for calcium.* J Histochem Cytochem, 1969. **17**(2): p. 110-24.

90.   Kiernan, A.E., et al., *The Notch ligand Jagged1 is required for inner ear sensory development.* Proc Natl Acad Sci U S A, 2001. **98**(7): p. 3873-8.

91.   Fell, H.B., *The Osteogenic Capacity in vitro of Periosteum and Endosteum Isolated from the Limb Skeleton of Fowl Embryos and Young Chicks.* J Anat, 1932. **66**(Pt 2): p. 157-180 11.

92.   Rose, G.G. and T.O. Shindler, *The cytodifferentiation of osteoblasts in tissue culture. A description of cellular emigrations from embryo chick-leg bones.* J Bone Joint Surg Am, 1960. **42-A**: p. 485-98.

93.   Jones, S.J. and A. Boyde, *The migration of osteoblasts.* Cell Tissue Res, 1977. **184**(2): p. 179-93.

94.   Peck, W.A., S.J. Birge, Jr., and S.A. Fedak, *Bone Cells: Biochemical and Biological Studies after Enzymatic Isolation.* Science, 1964. **146**: p. 1476-7.

95.   Bakker, A. and J. Klein-Nulend, *Osteoblast isolation from murine calvariae and long bones.* Methods Mol Med, 2003. **80**: p. 19-28.

96.   Hefley, T., J. Cushing, and J.S. Brand, *Enzymatic isolation of cells from bone: cytotoxic enzymes of bacterial collagenase.* Am J Physiol, 1981. **240**(5): p. C234-8.

97.   Declercq, H., et al., *Isolation, proliferation and differentiation of osteoblastic cells to study cell/biomaterial interactions: comparison of different isolation techniques and source.* Biomaterials, 2004. **25**(5): p. 757-68.

98.   Tarnowski, C.P., M.A. Ignelzi, Jr., and M.D. Morris, *Mineralization of developing mouse calvaria as revealed by Raman microspectroscopy.* J Bone Miner Res, 2002. **17**(6): p. 1118-26.

99.   Franceschi, R.T., B.S. Iyer, and Y. Cui, *Effects of ascorbic acid on collagen matrix formation and osteoblast differentiation in murine MC3T3-E1 cells.* J Bone Miner Res, 1994. **9**(6): p. 843-54.

100.   Tenenbaum, H.C. and J.N. Heersche, *Differentiation of osteoblasts and formation of mineralized bone in vitro.* Calcif Tissue Int, 1982. **34**(1): p. 76-9.

101.   Ecarot-Charrier, B., et al., *Osteoblasts isolated from mouse calvaria initiate matrix mineralization in culture.* J Cell Biol, 1983. **96**(3): p. 639-43.

102.   Gerber, I. and I. ap Gwynn, *Influence of cell isolation, cell culture density, and cell nutrition on differentiation of rat calvarial osteoblast-like cells in vitro.* Eur Cell Mater, 2001. **2**: p. 10-20.

103.   Aronow, M.A., et al., *Factors that promote progressive development of the osteoblast phenotype in cultured fetal rat calvaria cells.* J Cell Physiol, 1990. **143**(2): p. 213-21.

104.   Chang, Y.L., C.M. Stanford, and J.C. Keller, *Calcium and phosphate supplementation promotes bone cell mineralization: implications for hydroxyapatite (HA)-enhanced bone formation.* J Biomed Mater Res, 2000. **52**(2): p. 270-8.

105.   Beresford, J.N., S.E. Graves, and C.A. Smoothy, *Formation of mineralized nodules by bone derived cells in vitro: a model of bone formation?* Am J Med Genet, 1993. **45**(2): p. 163-78.

106.   Bhargava, U., et al., *Ultrastructural analysis of bone nodules formed in vitro by isolated fetal rat calvaria cells.* Bone, 1988. **9**(3): p. 155-63.

107.   Sudo, H., et al., *In vitro differentiation and calcification in a new clonal osteogenic cell line derived from newborn mouse calvaria.* J Cell Biol, 1983. **96**(1): p. 191-8.

108.   Schulze, E., et al., *Immunohistochemical investigations on the differentiation marker protein E11 in rat calvaria, calvaria cell culture and the osteoblastic cell line ROS 17/2.8.* Histochem Cell Biol, 1999. **111**(1): p. 61-9.

109.   Bonewald, L.F., *Generation and function of osteocyte dendritic processes.* J Musculoskelet Neuronal Interact, 2005. **5**(4): p. 321-4.

110.   Roman-Roman, S., et al., *Identification of genes regulated during osteoblastic differentiation by genome-wide expression analysis of mouse calvaria primary osteoblasts in vitro.* Bone, 2003. **32**(5): p. 474-82.

111.   Garcia, T., et al., *Behavior of osteoblast, adipocyte, and myoblast markers in genome-wide expression analysis of mouse calvaria primary osteoblasts in vitro.* Bone, 2002. **31**(1): p. 205-11.

112.   Beck, G.R., Jr., B. Zerler, and E. Moran, *Gene array analysis of osteoblast differentiation.* Cell Growth Differ, 2001. **12**(2): p. 61-83.

113.   Raouf, A. and A. Seth, *Discovery of osteoblast-associated genes using cDNA microarrays.* Bone, 2002. **30**(3): p. 463-71.

114.   Stein, G.S., J.B. Lian, and T.A. Owen, *Relationship of cell growth to the regulation of tissue-specific gene expression during osteoblast differentiation.* FASEB J, 1990. **4**(13): p. 3111-23.

115. Varga, F., et al., *Triiodothyronine, a regulator of osteoblastic differentiation: depression of histone H4, attenuation of c-fos/c-jun, and induction of osteocalcin expression.* Calcif Tissue Int, 1997. **61**(5): p. 404-11.
116. Billiard, J., et al., *Transcriptional profiling of human osteoblast differentiation.* J Cell Biochem, 2003. **89**(2): p. 389-400.
117. Kitching, R., et al., *Coordinate gene expression patterns during osteoblast maturation and retinoic acid treatment of MC3T3-E1 cells.* J Bone Miner Metab, 2002. **20**(5): p. 269-80.
118. Choi, J.Y., et al., *Expression patterns of bone-related proteins during osteoblastic differentiation in MC3T3-E1 cells.* J Cell Biochem, 1996. **61**(4): p. 609-18.
119. Galindo, M., et al., *The bone-specific expression of Runx2 oscillates during the cell cycle to support a G1-related antiproliferative function in osteoblasts.* J Biol Chem, 2005. **280**(21): p. 20274-85.
120. Zhang, C., et al., *Inhibition of Wnt signaling by the osteoblast-specific transcription factor Osterix.* Proc Natl Acad Sci U S A, 2008. **105**(19): p. 6936-41.
121. Nakashima, K., et al., *The novel zinc finger-containing transcription factor osterix is required for osteoblast differentiation and bone formation.* Cell, 2002. **108**(1): p. 17-29.
122. McCauley, L.K., et al., *Parathyroid hormone stimulates fra-2 expression in osteoblastic cells in vitro and in vivo.* Endocrinology, 2001. **142**(5): p. 1975-81.
123. Gordon, J.A., et al., *Bone sialoprotein expression enhances osteoblast differentiation and matrix mineralization in vitro.* Bone, 2007. **41**(3): p. 462-73.
124. Mizuno, M., et al., *Bone sialoprotein (BSP) is a crucial factor for the expression of osteoblastic phenotypes of bone marrow cells cultured on type I collagen matrix.* Calcif Tissue Int, 2000. **66**(5): p. 388-96.
125. Owen, T.A., et al., *Progressive development of the rat osteoblast phenotype in vitro: reciprocal relationships in expression of genes associated with osteoblast proliferation and differentiation during formation of the bone extracellular matrix.* J Cell Physiol, 1990. **143**(3): p. 420-30.
126. Quarles, L.D., et al., *Distinct proliferative and differentiated stages of murine MC3T3-E1 cells in culture: an in vitro model of osteoblast development.* J Bone Miner Res, 1992. **7**(6): p. 683-92.
127. Fedarko, N.S., et al., *Extracellular matrix formation by osteoblasts from patients with osteogenesis imperfecta.* J Bone Miner Res, 1992. **7**(8): p. 921-30.
128. Fedarko, N.S., et al., *Cell proliferation of human fibroblasts and osteoblasts in osteogenesis imperfecta: influence of age.* J Bone Miner Res, 1995. **10**(11): p. 1705-12.
129. Morike, M., et al., *Collagen metabolism in cultured osteoblasts from osteogenesis imperfecta patients.* Biochem J, 1992. **286 (Pt 1)**: p. 73-7.
130. Xu, P., et al., *Osteogenesis imperfecta collagen-like peptides: self-assembly and mineralization on surfaces.* Biomacromolecules, 2008. **9**(6): p. 1551-7.
131. Sweeney, S.M., et al., *Candidate cell and matrix interaction domains on the collagen fibril, the predominant protein of vertebrates.* J Biol Chem, 2008. **283**(30): p. 21187-97.
132. Boyde, A., et al., *The mineralization density of iliac crest bone from children with osteogenesis imperfecta.* Calcif Tissue Int, 1999. **64**(3): p. 185-90.
133. Lynch, M.P., et al., *The influence of type I collagen on the development and maintenance of the osteoblast phenotype in primary and passaged rat calvarial osteoblasts: modification of expression of genes supporting cell growth, adhesion, and extracellular matrix mineralization.* Exp Cell Res, 1995. **216**(1): p. 35-45.
134. Canalis, E., *Notch signaling in osteoblasts.* Sci Signal, 2008. **1**(17): p. pe17.
135. Hilton, M.J., et al., *Notch signaling maintains bone marrow mesenchymal progenitors by suppressing osteoblast differentiation.* Nat Med, 2008. **14**(3): p. 306-14.
136. Hamrick, M.W., et al., *Increased osteogenic response to exercise in metaphyseal versus diaphyseal cortical bone.* J Musculoskelet Neuronal Interact, 2006. **6**(3): p. 258-63.
137. Hoshi, A., et al., *Effects of exercise at different ages on bone density and mechanical properties of femoral bone of aged mice.* Tohoku J Exp Med, 1998. **185**(1): p. 15-24.
138. Sheng, M.H., et al., *In vivo and in vitro evidence that the high osteoblastic activity in C3H/HeJ mice compared to C57BL/6J mice is intrinsic to bone cells.* Bone, 2004. **35**(3): p. 711-9.
139. Bradley, E.W. and M.J. Oursler, *Osteoclast culture and resorption assays.* Methods Mol Biol, 2008. **455**: p. 19-35.
140. Csaki, C., et al., *Co-culture of canine mesenchymal stem cells with primary bone-derived osteoblasts promotes osteogenic differentiation.* Histochem Cell Biol, 2009. **131**(2): p. 251-66.
141. van't Hof, R.J., *Osteoclast Formation in the Mouse Coculture Assay.* Methods Mol Med, 2003. **80**: p. 145-152.
142. Jiang, J., S.B. Nicoll, and H.H. Lu, *Co-culture of osteoblasts and chondrocytes modulates cellular differentiation in vitro.* Biochem Biophys Res Commun, 2005. **338**(2): p. 762-70.

143. Chipman, S.D., et al., *Defective pro alpha 2(I) collagen synthesis in a recessive mutation in mice: a model of human osteogenesis imperfecta.* Proc Natl Acad Sci U S A, 1993. **90**(5): p. 1701-5.

144. Kuznetsova, N.V., D.J. McBride, and S. Leikin, *Changes in thermal stability and microunfolding pattern of collagen helix resulting from the loss of alpha2(I) chain in osteogenesis imperfecta murine.* J Mol Biol, 2003. **331**(1): p. 191-200.

145. Marin-Garcia, J. and M.J. Goldenthal, *Mitochondria play a critical role in cardioprotection.* J Card Fail, 2004. **10**(1): p. 55-66.

146. Mayorga, M., et al., *Bcl-2 is a key factor for cardiac fibroblast resistance to programmed cell death.* J Biol Chem, 2004. **279**(33): p. 34882-9.

147. Frangogiannis, N.G., C.W. Smith, and M.L. Entman, *The inflammatory response in myocardial infarction.* Cardiovasc Res, 2002. **53**(1): p. 31-47.

148. Schaper, J. and B. Speiser, *The extracellular matrix in the failing human heart.* Basic Res Cardiol, 1992. **87 Suppl 1**: p. 303-9.

149. Long, X., et al., *p53 and the hypoxia-induced apoptosis of cultured neonatal rat cardiac myocytes.* J Clin Invest, 1997. **99**(11): p. 2635-43.

150. Li, P.F., R. Dietz, and R. von Harsdorf, *Superoxide induces apoptosis in cardiomyocytes, but proliferation and expression of transforming growth factor-beta1 in cardiac fibroblasts.* FEBS Lett, 1999. **448**(2-3): p. 206-10.

151. Zhang, X., et al., *Differential vulnerability to oxidative stress in rat cardiac myocytes versus fibroblasts.* J Am Coll Cardiol, 2001. **38**(7): p. 2055-62.

152. Tsang, K.Y., et al., *Surviving endoplasmic reticulum stress is coupled to altered chondrocyte differentiation and function.* PLoS Biol, 2007. **5**(3): p. e44.

153. Kojima, T., et al., *The retention of abnormal type I procollagen and correlated expression of HSP 47 in fibroblasts from a patient with lethal osteogenesis imperfecta.* J Pathol, 1998. **184**(2): p. 212-8.

154. Forlino, A., et al., *Differential expression of both extracellular and intracellular proteins is involved in the lethal or nonlethal phenotypic variation of BrtlIV, a murine model for osteogenesis imperfecta.* Proteomics, 2007. **7**(11): p. 1877-91.

155. Eun, S.Y., et al., *Identification of cytochrome c oxidase subunit 6A1 as a suppressor of Bax-induced cell death by yeast-based functional screening.* Biochem Biophys Res Commun, 2008. **373**(1): p. 58-63.

156. Okamoto, O. and S. Fujiwara, *Dermatopontin, a novel player in the biology of the extracellular matrix.* Connect Tissue Res, 2006. **47**(4): p. 177-89.

157. MacBeath, J.R., D.R. Shackleton, and D.J. Hulmes, *Tyrosine-rich acidic matrix protein (TRAMP) accelerates collagen fibril formation in vitro.* J Biol Chem, 1993. **268**(26): p. 19826-32.

158. Takeda, U., et al., *Targeted disruption of dermatopontin causes abnormal collagen fibrillogenesis.* J Invest Dermatol, 2002. **119**(3): p. 678-83.

159. Toyoshima, T., et al., *Differential gene expression of 36-kDa microfibril-associated glycoprotein (MAGP-36/MFAP4) in rat organs.* Cell Tissue Res, 2008. **332**(2): p. 271-8.

160. Chen, M.M., et al., *CTGF expression is induced by TGF- beta in cardiac fibroblasts and cardiac myocytes: a potential role in heart fibrosis.* J Mol Cell Cardiol, 2000. **32**(10): p. 1805-19.

161. Griffin, M., R. Casadio, and C.M. Bergamini, *Transglutaminases: nature's biological glues.* Biochem J, 2002. **368**(Pt 2): p. 377-96.

162. Chau, D.Y., et al., *The cellular response to transglutaminase-cross-linked collagen.* Biomaterials, 2005. **26**(33): p. 6518-29.

163. Sibinga, N.E., et al., *Collagen VIII is expressed by vascular smooth muscle cells in response to vascular injury.* Circ Res, 1997. **80**(4): p. 532-41.

164. Janicki, J.S. and G.L. Brower, *The role of myocardial fibrillar collagen in ventricular remodeling and function.* J Card Fail, 2002. **8**(6 Suppl): p. S319-25.

165. de Simone, G. and O. de Divitiis, *Extracellular matrix and left ventricular mechanics in overload hypertrophy.* Adv Clin Path, 2002. **6**(1): p. 3-10.

166. Janicki, J.S., *Myocardial collagen remodeling and left ventricular diastolic function.* Braz J Med Biol Res, 1992. **25**(10): p. 975-82.

167. Mori, T., et al., *Volume overload results in exaggerated cardiac hypertrophy in the atrial natriuretic peptide knockout mouse.* Cardiovasc Res, 2004. **61**(4): p. 771-9.

168. Houweling, A.C., et al., *Expression and regulation of the atrial natriuretic factor encoding gene Nppa during development and disease.* Cardiovasc Res, 2005. **67**(4): p. 583-93.

169. Iwai, N., H. Shimoike, and M. Kinoshita, *Genes up-regulated in hypertrophied ventricle.* Biochem Biophys Res Commun, 1995. **209**(2): p. 527-34.

170. Walther, T., et al., *Accelerated mitochondrial adenosine diphosphate/adenosine triphosphate transport improves hypertension-induced heart disease.* Circulation, 2007. **115**(3): p. 333-44.

171. Lecker, S.H., et al., *Multiple types of skeletal muscle atrophy involve a common program of changes in gene expression.* FASEB J, 2004. **18**(1): p. 39-51.

172. Towbin, J.A. and N.E. Bowles, *The failing heart.* Nature, 2002. **415**(6868): p. 227-33.

173. Thapa, N., B.H. Lee, and I.S. Kim, *TGFBlp/betaig-h3 protein: a versatile matrix molecule induced by TGF-beta.* Int J Biochem Cell Biol, 2007. **39**(12): p. 2183-94.

174. ten Dijke, P. and H.M. Arthur, *Extracellular control of TGFbeta signalling in vascular development and disease.* Nat Rev Mol Cell Biol, 2007. **8**(11): p. 857-69.

175. Chiquet-Ehrismann, R. and M. Chiquet, *Tenascins: regulation and putative functions during pathological stress.* J Pathol, 2003. **200**(4): p. 488-99.

176. Nakamura, Y., M. Nawata, and S. Wakitani, *Expression profiles and functional analyses of Wnt-related genes in human joint disorders.* Am J Pathol, 2005. **167**(1): p. 97-105.

177. You, J., et al., *Wnt pathway-related gene expression in inflammatory bowel disease.* Dig Dis Sci, 2008. **53**(4): p. 1013-9.

178. Van Scoyk, M., et al., *Wnt signaling pathway and lung disease.* Transl Res, 2008. **151**(4): p. 175-80.

179. Corvol, P., et al., *Inhibition of angiogenesis: a new function for angiotensinogen and des(angiotensin I)angiotensinogen.* Curr Hypertens Rep, 2003. **5**(2): p. 149-54.

180. Gao, X. and Z. Xu, *Mechanisms of action of angiogenin.* Acta Biochim Biophys Sin (Shanghai), 2008. **40**(7): p. 619-24.

181. Li, M. and R.M. Ransohoff, *The roles of chemokine CXCL12 in embryonic and brain tumor angiogenesis.* Semin Cancer Biol, 2008.

182. Brigstock, D.R., *Regulation of angiogenesis and endothelial cell function by connective tissue growth factor (CTGF) and cysteine-rich 61 (CYR61).* Angiogenesis, 2002. **5**(3): p. 153-65.

183. Jiang, X.C., et al., *Expression of plasma phospholipid transfer protein mRNA in normal and emphysematous lungs and regulation by hypoxia.* J Biol Chem, 1998. **273**(25): p. 15714-8.

184. Ohradanova, A., et al., *Hypoxia upregulates expression of human endosialin gene via hypoxia-inducible factor 2.* Br J Cancer, 2008. **99**(8): p. 1348-56.

185. Park, S.Y., et al., *Hypoxia increases androgen receptor activity in prostate cancer cells.* Cancer Res, 2006. **66**(10): p. 5121-9.

186. Lafont, J.E., et al., *Hypoxia promotes the differentiated human articular chondrocyte phenotype through SOX9-dependent and -independent pathways.* J Biol Chem, 2008. **283**(8): p. 4778-86.

187. Littler, C.M., et al., *Protein kinase C-epsilon-null mice have decreased hypoxic pulmonary vasoconstriction.* Am J Physiol Heart Circ Physiol, 2003. **284**(4): p. H1321-31.

188. Semenza, G.L., et al., *Hypoxia response elements in the aldolase A, enolase 1, and lactate dehydrogenase A gene promoters contain essential binding sites for hypoxia-inducible factor 1.* J Biol Chem, 1996. **271**(51): p. 32529-37.

189. Pescador, N., et al., *Identification of a functional hypoxia-responsive element that regulates the expression of the egl nine homologue 3 (egln3/phd3) gene.* Biochem J, 2005. **390**(Pt 1): p. 189-97.

190. Lasky, J.A., et al., *Connective tissue growth factor mRNA expression is upregulated in bleomycin-induced lung fibrosis.* Am J Physiol, 1998. **275**(2 Pt 1): p. L365-71.

191. Mori, T., et al., *Role and interaction of connective tissue growth factor with transforming growth factor-beta in persistent fibrosis: A mouse fibrosis model.* J Cell Physiol, 1999. **181**(1): p. 153-9.

192. Grotendorst, G.R., *Connective tissue growth factor: a mediator of TGF-beta action on fibroblasts.* Cytokine Growth Factor Rev, 1997. **8**(3): p. 171-9.

193. Nakerakanti, S.S., et al., *Fli1 and Ets1 have distinct roles in connective tissue growth factor/CCN2 gene regulation and induction of the profibrotic gene program.* J Biol Chem, 2006. **281**(35): p. 25259-69.

194. Jensen, S.A., et al., *Protein interaction studies of MAGP-1 with tropoelastin and fibrillin-1.* J Biol Chem, 2001. **276**(43): p. 39661-6.

195. Jones, P.L., J. Crack, and M. Rabinovitch, *Regulation of tenascin-C, a vascular smooth muscle cell survival factor that interacts with the alpha v beta 3 integrin to promote epidermal growth factor receptor phosphorylation and growth.* J Cell Biol, 1997. **139**(1): p. 279-93.

196. Jones, P.L., et al., *Altered hemodynamics controls matrix metalloproteinase activity and tenascin-C expression in neonatal pig lung.* Am J Physiol Lung Cell Mol Physiol, 2002. **282**(1): p. L26-35.

197. Yasuda, M., et al., *BNIP3alpha: a human homolog of mitochondrial proapoptotic protein BNIP3.* Cancer Res, 1999. **59**(3): p. 533-7.

198. Huang, Q., et al., *Identification of p53 regulators by genome-wide functional analysis.* Proc Natl Acad Sci U S A, 2004. **101**(10): p. 3456-61.

199. Furukawa, T., et al., *Potential tumor suppressive pathway involving DUSP6/MKP-3 in pancreatic cancer.* Am J Pathol, 2003. **162**(6): p. 1807-15.

200. Ding, L., et al., *Protein kinase C-epsilon promotes survival of lung cancer cells by suppressing apoptosis through dysregulation of the mitochondrial caspase pathway.* J Biol Chem, 2002. **277**(38): p. 35305-13.

201. Campbell, F.E., *Cardiac effects of pulmonary disease.* Vet Clin North Am Small Anim Pract, 2007. **37**(5): p. 949-62, vii.

202. Chowdhuri, S., et al., *Cardiovascular complications of respiratory diseases.* Am J Med Sci, 2007. **334**(5): p. 361-80.

203. Moraes, D.L., W.S. Colucci, and M.M. Givertz, *Secondary pulmonary hypertension in chronic heart failure: the role of the endothelium in pathophysiology and management.* Circulation, 2000. **102**(14): p. 1718-23.

204. Hoshikawa, Y., et al., *Generation of oxidative stress contributes to the development of pulmonary hypertension induced by hypoxia.* J Appl Physiol, 2001. **90**(4): p. 1299-306.

205. Bonnet, P., et al., *Chronic hypoxia induces nonreversible right ventricle dysfunction and dysplasia in rats.* Am J Physiol Heart Circ Physiol, 2004. **287**(3): p. H1023-8.

206. Sane, D.C., J.L. Kontos, and C.S. Greenberg, *Roles of transglutaminases in cardiac and vascular diseases.* Front Biosci, 2007. **12**: p. 2530-45.

207. Ohkubo, H., et al., *Cloning and sequence analysis of cDNA for rat angiotensinogen.* Proc Natl Acad Sci U S A, 1983. **80**(8): p. 2196-200.

208. Chiquet-Ehrismann, R., et al., *Tenascin-C expression by fibroblasts is elevated in stressed collagen gels.* J Cell Biol, 1994. **127**(6 Pt 2): p. 2093-101.

209. Chiquet, M., et al., *Regulation of extracellular matrix synthesis by mechanical stress.* Biochem Cell Biol, 1996. **74**(6): p. 737-44.

210. Jeffery, T.K. and N.W. Morrell, *Molecular and cellular basis of pulmonary vascular remodeling in pulmonary hypertension.* Prog Cardiovasc Dis, 2002. **45**(3): p. 173-202.

211. Agocha, A., H.W. Lee, and M. Eghbali-Webb, *Hypoxia regulates basal and induced DNA synthesis and collagen type I production in human cardiac fibroblasts: effects of transforming growth factor-beta1, thyroid hormone, angiotensin II and basic fibroblast growth factor.* J Mol Cell Cardiol, 1997. **29**(8): p. 2233-44.

212. Bateman, J.F., R.P. Boot-Handford, and S.R. Lamande, *Genetic diseases of connective tissues: cellular and extracellular effects of ECM mutations.* Nat Rev Genet, 2009. **10**(3): p. 173-83.

213. Shah, R.V. and M.J. Semigran, *Pulmonary hypertension secondary to left ventricular systolic dysfunction: contemporary diagnosis and management.* Curr Heart Fail Rep, 2008. **5**(4): p. 226-32.

214. Runo, J.R. and J.E. Loyd, *Primary pulmonary hypertension.* Lancet, 2003. **361**(9368): p. 1533-44.

215. Laumanns, I.P., et al., *The Non-canonical WNT-pathway Is Operative in Idiopathic Pulmonary Arterial Hypertension.* Am J Respir Cell Mol Biol, 2008.

216. Wang, G.W., et al., *Inhibition of hypoxia/reoxygenation-induced apoptosis in metallothionein-overexpressing cardiomyocytes.* Am J Physiol Heart Circ Physiol, 2001. **280**(5): p. H2292-9.

217. Adeghate, E., *Molecular and cellular basis of the aetiology and management of diabetic cardiomyopathy: a short review.* Mol Cell Biochem, 2004. **261**(1-2): p. 187-91.

218. Liang, Q., et al., *Overexpression of metallothionein reduces diabetic cardiomyopathy.* Diabetes, 2002. **51**(1): p. 174-81.

219. Butcher, H.L., et al., *Metallothionein mediates the level and activity of nuclear factor kappa B in murine fibroblasts.* J Pharmacol Exp Ther, 2004. **310**(2): p. 589-98.

220. Abdel-Mageed, A.B. and K.C. Agrawal, *Activation of nuclear factor kappaB: potential role in metallothionein-mediated mitogenic response.* Cancer Res, 1998. **58**(11): p. 2335-8.

221. Rippe, R.A., et al., *NF-kappaB inhibits expression of the alpha1(I) collagen gene.* DNA Cell Biol, 1999. **18**(10): p. 751-61.

222. Novitskiy, G., et al., *Identification of a novel NF-kappaB-binding site with regulation of the murine alpha2(I) collagen promoter.* J Biol Chem, 2004. **279**(15): p. 15639-44.

223. Diatchenko, L., et al., *Identification of novel mediators of NF-kappaB through genome-wide survey of monocyte adherence-induced genes.* J Leukoc Biol, 2005. **78**(6): p. 1366-77.

224. Franco, V., et al., *Atrial natriuretic peptide dose-dependently inhibits pressure overload-induced cardiac remodeling.* Hypertension, 2004. **44**(5): p. 746-50.

225. Cao, L. and D.G. Gardner, *Natriuretic peptides inhibit DNA synthesis in cardiac fibroblasts.* Hypertension, 1995. **25**(2): p. 227-34.

7. Summary

7.1. In vitro analysis of osteoblasts

The German Mouse Clinic (GMC) provides a large scale phenotyping platform for standardized and comprehensive analysis of mouse mutants in various clinical and biological fields. The Dysmorphology screen of the GMC comprises the analysis of the bone and cartilage phenotype. DXA measurements, X-ray analysis, µCT and pQCT analysis amongst others provide a comprehensive picture of morphological and structural alterations of the skeletal system in mutant mice. However, as the screen is of a descriptive nature, the cellular and molecular causes of the observed bone alterations cannot be defined. To broaden the phenotyping options of the GMC Dysmorphology screen to the cellular level, a comprehensive and multifaceted cell culture system for primary calvarial osteoblasts has been established. Nine different assays have been developed to assess general properties of cell growth and to investigate the cells concerning bone specific parameters at the functional-, protein- and RNA-level. As the cells are cultivated and investigated independently from systemic influences of the whole organism, it is possible to assess whether direct alterations of the bone cells (primary effect) or systemic influences in terms of hormonal / metabolic dysreguations (secondary effect) are responsible for the bone phenotype of the mutants. The culture system has been validated by the investigation of two mutant lines that have shown strong alterations in their bone parameters within the Dysmorphology screen. Osteoblasts of *Aga2* mice - a new mouse model for *Osteogenesis imperfecta* - showed strong differences within the cell culture system compared to wild type control cells. The cellular behavior and development indicates a primary defect of the osteoblasts, whereas inappropriate collagen synthesis causes diminished and delayed extracellular matrix maturation and osteoblast differentiation in *Aga2*. In contrast, no significant differences were found between osteoblasts from *ABE2* mutants and wild type littermates, arguing for a secondary effect as the cause of the bone alterations that might be due to the hyperactive phenotype where elevated physical activity in the mutants positively effects bone homeostasis and remodeling.

7.2. Heart and lung investigation in the *Aga2* OI mouse model

Osteogenesis imperfecta (OI) is a group of inherited connective tissue disorders, predominantly caused by mutations in the collagen I genes (*Col1a1*/*Col1a2*). It is characterized by brittle bones, fractures and osteoporosis and is associated with increased mortality reaching 100% perinatal lethality in the most severe type II OI. Cardiovascular and pulmonary diseases have been described as the main causes of death in OI patients. However, the pathological alterations in heart and lung tissues are generally considered as secondary effects due to skeletal deformities and the bone disorders. Comparable to human cases, heterozygous *Aga2* mice - a new mouse model for OI - vary in their etiopathology and severely affected mutants (*Aga2^{severe}*) die shortly after birth. To explain the postnatal lethality in *Aga2^{severe}* and to elucidate the pathological and molecular reasons, comprehensive analysis of *Aga2* mice were performed. Given the cardiopulmonary complication in human OI patients, heart and lung have been chosen as the most relevant and reasonable organs to be examined and investigations were performed on the functional, morphological and molecular level. In cardiac tissue of *Aga2^{severe}*, a strong downregulation of *Col1a1* on mRNA and protein level was found both *in vivo* and *in vitro*. Histological and SEM analysis revealed disordered collagen fibers in the ECM and right ventricular hypertrophy. In addition, echocardiography depicts functional impairments with decreased fractional shortening of the hearts in severely affected mutants. In lungs of *Aga2^{severe}*, pronounced pulmonary hemorrhages were found and it could be demonstrated, that these bleedings are not due to rib fractures. Blood gas analysis indicated hypoxia with significantly reduced pO_2 (hypoxemic hypoxia). Finally, gene-expression analysis verified all pathological observations by significant misregulation of respective marker genes. These results provide clear evidence to support the hypothesis that the cardiac collagen alterations represent the primary cause of the OI lethality. Taken together, a vicious cycle of heart dysfunction, pulmonary hypertension and hypoxia is thought to provoke early death in severely affected *Aga2* mice - independently from the bone phenotype.

8. Zusammenfassung

8.1. *In vitro* Analyse von Osteoblasten

Die „Deutsche Maus Klinik" (GMC - German Mouse Clinic) ermöglicht auf Grundlage einer umfangreichen Phänotypisierungsplattform eine standardisierte und umfassende Analyse von Mausmutanten in verschiedenen klinischen und biologischen Bereichen. Untersuchungen des Knochen- und Knorpelapparates werden im Dysmorphologie-Modul der GMC durchgeführt. Durch den Einsatz von u.a. Knochendichtemessungen (DXA), Röntgenanalysen, µCT als auch pQCT Untersuchungen kann ein umfassendes Bild morphologischer und struktureller Veränderungen des Skelettsystems von mutanten Mäusen gewonnen werden. Da diese Untersuchungstechniken jedoch einen überwiegend diagnostischen und beschreibenden Charakter besitzen, können die zellulären und molekularen Ursachen der beobachteten Knochenveränderungen nicht bestimmt werden. Um die Phänotypisierungmöglichkeiten des Dysmorphologie-Modules auf zellulärer Ebene zu erweitern, wurde ein umfangreiches und vielfältiges Zellkultursystem für primäre Osteoblasten entwickelt. Die Kombination von 9 verschiedenen Assays ermöglicht dabei das Abschätzen von allgemeinen Eigenschaften des Zellwachstums und die Untersuchung von knochenspezifischen Parametern auf funtioneller-, Protein- und RNA-Ebene. Da die Kultivierung und Untersuchung der Zellen unabhängig von systemischen Einflüssen des Organismus erfolgt, kann anhand der Ergebnisse eine Aussage darüber getroffen werden, ob eine direkte Veränderung der Knochenzellen (primärer Effekt) oder systemische Einflüsse in Form von beispielsweise hormonellen oder metabolischen Störungen (sekundärer Effekt) die Knochenveränderungen bedingt. Das Kultursystem wurde anhand von zwei Mutantenlinien validiert, bei denen zuvor Veränderungen der Knochenparameter im Dysmorphologie-Modul beobachtet wurden. Die Untersuchung von Osteoblasten aus *Aga2* Mäusen - einem neuen Modellsystem für *Osteogenesis imperfecta* - ergaben große Unterschiede im Zellkultursystem im Vergleich zu wildtypischen Kontrollzellen. Das Verhalten und die Entwicklung der Zellen deutet auf einen primären Defekt in den Osteoblasten hin, wobei eine unzureichende Kollagensynthese eine verminderte und verzögerte extrazelluläre Matrix Reifung und Osteoblastendifferenzierung in den *Aga2* Mutanten verursacht. Im Gegensatz dazu zeigte die Untersuchung von Osteoblasten aus *ABE2*

Mäusen keine signifikanten Unterschiede zu Zellen aus gesunden Kontrolltieren. Dies deutet auf einen sekundären Effekt als Ursache der Knochenveränderung hin, wobei der hyperaktive Phenotyp in Verbindung mit der gesteigerten körperlichen Aktivität der *ABE2* Mutanten die Homöostase und das Remodelling der Knochen positiv beeinflusst.

8.2. Herz- und Lungenuntersuchung beim *Aga2* OI Mausmodell

Osteogenesis imperfecta (OI) bezeichnet eine Gruppe von vererbbaren Bindegewebserkrankungen, die vorwiegend von Mutationen in den Genen für Kollagen Typ I (*Col1a1*/*Col1a2*) verursacht werden. Brüchigen Knochen (engl. „brittle bone disease"), häufigen Frakturen und Osteoporose sind typische krankheitsassoziierte Symptome. In Abhängigkeit des Schweregrades der Erkrankung ist eine erhöhte Mortalität unter OI Patienten beschrieben, wobei die Sterblichkeit bei der schwerste Verlaufsform 100% im perinatalen Stadium beträgt (Typ II OI). Als Haupttodesursache bei OI Patienten sind kardiovaskuläre und pulmonale Erkrankungen bekannt, wobei die pathologischen Veränderungen im Herz- und Lungengewebe bis heute als sekundäre Effekte durch Knochenveränderungen und skelettale Deformitäten beschrieben sind. Vergleichbar zu humanen Erkrankungsfällen, variieren heterozygote *Aga2* Mäuse - ein neues Mausmodell für OI - in ihrer Ätiopathologie und schwer erkrankte Tiere (*Aga2^severe^*) sterben kurz nach der Geburt. Um die Gründe für die postnatale Sterblichkeit der *Aga^severe^* Mutanten aufzuklären und die pathologischen und molekularen Ursachen dafür zu beschreiben, wurde eine umfangreiche Analyse von *Aga2* Mäusen durchgeführt. Basierend auf den cardiopulmonären Störungen bei OI Patienten, wurden Herz und Lunge als wichtigste krankheitsassoziierte Organe für die Untersuchungen ausgewählt und funktionell, morphologischer und molekular analysiert. Im Herzgewebe von *Aga2^severe^* wurde sowohl *in vivo* als auch *in vitro* eine starke Herunterregulierung von *Col1a1* auf mRNA- und Proteinebene nachgewiesen. Histologische Untersuchungen ergaben eine rechtsventrikuläre Hypertrophie des Herzens und Rasterelektronenmikroskopische Analysen zeigten eine gestörte Anordnung kollagener Fibrillen in der extrazellulären Matrix des Herzgewebes in *Aga2^severe^* Mäusen. Durch den Einsatz von Echokardiographie konnte weiterhin eine Funktionsstörung des Herzens mit einer verminderten Kontraktionsfähigkeit des

linken Herzventikels während der Systole in den mutanten Mäusen nachgewiesen werden. Die Lungen von *Aga2severe* Tieren sind durch das Auftreten von exzessiven Hämorrhagien gekennzeichnet, wobei der Nachweis erbracht werden konnte, dass diese Blutungen nicht auf die zahlreich vorkommenden Frakturen im Bereich des Brustkorbes zurückzuführen sind. Blutgas-Untersuchungen weisen auf einen hypoxischen Zustand mit stark vermindertem Sauerstoffpartialdruck (pO_2) in *Aga2severe* Mäusen hin (Hypoxämische Hypoxie). Alle pathologischen Veränderungen in Herz- und Lungengewebe konnten mittels Genexpressionsstudien durch die signifikante Regulation entsprechender Markergene verifiziert werden. Die gewonnenen Untersuchungsergebnisse sind Grundlage für die Hypothese, dass die kardialen Kollagenveränderungen die primäre Ursache für die OI assoziierte Lethalität darstellen. Zusammenfassend wird ein pathologischer Kreislauf aus Herzinsuffizienz, pulmonärer Hypertonie und Hypoxie vermutet, welcher die postnatale Sterblichkeit der *Aga2severe* Tiere unabhängig vom Knochenphänotyp der Mutanten verursacht.

IV. Publications

Poster

<u>Frank Thiele</u>, Thomas S. Lisse, Gerhard K.H. Przemeck, Helmut Fuchs, Martin Hrabé de Angelis. "In vitro and molecular characterization of bone related phenotypes". 20th IMGC conference, 2006. Charleston, USA.

Thomas S. Lisse, <u>Frank Thiele</u>, Koichiro Abe, Wolfgang Hans, Matthias Klaften, Michael Schulz, Helmut Fuchs, Martin Hrabé de Angelis. "Characterization and mapping of ALI34: A new ENU-derived murine model for osteoarthritis". 20th IMGC conference, 2006. Charleston, USA.

Wolfgang Hans, Helmut Fuchs, Koichiro Abe, Thomas S. Lisse, <u>Frank Thiele</u>, Valerie Gailus-Durner, Martin Hrabé de Angelis. "The German Mouse Clinic – Dysmorphology, Bone and Cartilage Screen". 3rd EUMORPHIA meeting, 2007. Barcelona, Spain.

<u>Frank Thiele</u>, Thomas S. Lisse, Gerhard K.H. Przemeck, Helmut Fuchs, Valerie Gailus-Durner, Martin Hrabé de Angelis. "Cellular Screening of bone related disease in mice". 34th European Symposium on Calcified Tissues, 2007. Kopenhagen, Denmark.

Thomas S. Lisse, <u>Frank Thiele</u>, Koichiro Abe, Wolfgang Hans, Stuart Ralston, Helmut Fuchs, Martin Hrabé de Angelis. "ER stress induced apoptosis in a new murine model for type II Osteogenesis imperfecta". 34th European Symposium on Calcified Tissues, 2007. Kopenhagen, Denmark.

Thomas S. Lisse, Christian Cohrs, <u>Frank Thiele</u>, Wolfgang Hans, Matthias Klaften, Helmut Fuchs, Martin Hrabé de Angelis. "Characterization and mapping of ALI34: A new ENU-derived murine model for Osteoarthritis and Chondrodysplasia". 34th European Symposium on Calcified Tissues, 2007. Kopenhagen, Denmark.

Wolfgang Hans, Thomas S. Lisse, Helmut Fuchs, Koichiro Abe, <u>Frank Thiele</u>, Valeria Gailus-Durner, Martin Hrabé de Angelis. "New models and mechanisms for bone and cartilage disorders". 19th annual meeting on mouse molecular genetics, 2007. Hinxton, GB.

Thomas S. Lisse, <u>Frank Thiele</u>, Helmut Fuchs, Wolfgang Hans, Koichiro Abe, Gerhard K.H. Przemeck, Martin Hrabé de Angelis. "ER stress-mediated apoptosis in a new mouse model of osteogenesis imperfecta". 22th IMGC conference, 2008. Prag, Czech Republik.

Wolfgang Hans, Thomas Lisse, Helmut Fuchs, Koichiro Abe, <u>Frank Thiele</u>, Christian Cohrs, Valerie Gailus-Durner, Martin Hrabé de Angelis. "New mouse models and mechanisms for bone and cartilage disorders". 35th European Symposium on Calcified Tissues, 2008. Barcelona, Spain.

Cohrs C.M., <u>Thiele F.</u>, Lisse T.S., Przemeck G.K.H., Fuchs H., Hans W. and Hrabé de Angelis M. "Molecular and functional characterization of Aga2 – a mouse model for osteogenesis imperfecta". 36th European Symposium on Calcified Tissues, 2009. Vienna, Austria.

W. Hans, T. Lisse, H. Fuchs, K. Abe, <u>F. Thiele</u>, C.M. Cohrs, V. Gailus-Durner, M. Hrabé de Angelis. „New mouse models and mechanisms for bone and cartilage disorders".36th European Symposium on Calcified Tissues, 2009. Vienna, Austria.

Oral presentations

"In vitro and molecular characterization of bone related phenotypes". 20th IMGC conference, 2006. Charleston, USA.

"Aga2, OI and collagen: considerations beyond the bone". 8th NGFN workshop, 2007. Grassau/Chiemgau, Germany.

"Aga2 and osteogenesis imperfecta - more than a bone disease ?". 9th NGFN workshop, 2008. Grassau/Chiemgau, Germany.

Paper

Fuchs H., Lisse T., Hans W., Abe K., Thiele F., Gailus-Durner V., Hrabe de Angelis M. "Phenotypic characterization of mouse models for bone-related disease in the German Mouse Clinic". J Musculoskelet Neuronal Interact. 2008 Jan-Mar; 8(1):13-4.

Lisse T.S., Thiele F., Fuchs H., Hans W., Przemeck G.K., Abe K., Rathkolb B., Quintanilla-Martinez L., Hoelzlwimmer G., Helfrich M., Wolf E., Ralston S.H., Hrabé de Angelis M. "ER stress-mediated apoptosis in a new mouse model of osteogenesis imperfecta". PLoS Genet. 2008 Feb; 4(2):e7.

Fuchs, H., Gailus-Durner, V., Adler, T., Pimentel, J. A., Becker, L., Bolle, I., Brielmeier, M., Calzada-Wack, J., Dalke, C., Ehrhardt, N., Fasnacht, N., Ferwagner, B., Frischmann, U., Hans, W., Holter, S. M., Holzlwimmer, G., Horsch, M., Javaheri, A., Kallnik, M., Kling, E., Lengger, C., Maier, H., Mossbrugger, I., Morth, C., Naton, B., Noth, U., Pasche, B., Prehn, C., Przemeck, G., Puk, O., Racz, I., Rathkolb, B., Rozman, J., Schable, K., Schreiner, R., Schrewe, A., Sina, C., Steinkamp, R., Thiele, F., Willershauser, M., Zeh, R., Adamski, J., Busch, D. H., Beckers, J., Behrendt, H., Daniel, H., Esposito, I., Favor, J., Graw, J., Heldmaier, G., Hofler, H., Ivandic, B., Katus, H., Klingenspor, M., Klopstock, T., Lengeling, A., Mempel, M., Muller, W., Neschen, S., Ollert, M., Quintanilla-Martinez, L., Rosenstiel, P., Schmidt, J., Schreiber, S., Schughart, K., Schulz, H., Wolf, E., Wurst, W., Zimmer, A., Hrabe de Angelis, M. "The German Mouse Clinic: A platform for systemic phenotype analysis of mouse models". Curr Pharm Biotechnol. 2009 10, 236-243.

Gailus-Durner, V., Fuchs, H., Adler, T., Aguilar Pimentel, A., Becker, L., Bolle, I., Calzada-Wack, J., Dalke, C., Ehrhardt, N., Ferwagner, B., Hans, W., Holter, S. M., Holzlwimmer, G., Horsch, M., Javaheri, A., Kallnik, M., Kling, E., Lengger, C., Morth, C., Mossbrugger, I., Naton, B., Prehn, C., Puk, O., Rathkolb, B., Rozman, J., Schrewe, A., Thiele, F., Adamski, J., Aigner, B., Behrendt, H., Busch, D. H., Favor, J., Graw, J., Heldmaier, G., Ivandic, B., Katus, H., Klingenspor, M., Elisabeth Kremmer, T. K., Ollert, M., Quintanilla-Martinez, L., Schulz, H., Wolf, E., Wurst, W., de Angelis, M. H. "Systemic first-line phenotyping". Methods Mol Biol. 2009 530, 1-47.

Thiele, F., Cohrs, C.M., Lisse T.S., Przemeck, G.K., Horsch, M., Schrewe, A., Fuchs, H., Hans, W., Beckers, J., Hrabé de Angelis, M. "Col1a1 mutation triggers early lethality in a mouse model for Osteogenesis imperfecta due to bone-independent primary defects in heart and lung". Manuscript in preparation.

Thiele, F., Cohrs, C.M., Przemeck, G.K., Fuchs, H., Hrabé de Angelis, M. „Comprehensive in vitro analysis of bone phenotypes in mice using osteoblast cell culture". Manuscript in preparation.

V. Curriculum Vitae

Personal Data

Name	Frank Thiele
Date of birth	February 4th 1979
Place of birth	Borna
Citizenship	German

Highschool

1992 - 1997	"Heinrich Pestalozzi" Secondary School in Borna
1997	Abitur / finale grade: 2,3

Military Service

1997 - 1998	Soldier at basic military service / Military Police at 4.FJgBtl 740

University

1998 - 2003	University of Leipzig Faculty of Life Science, Pharmacy and Psychology Subject: Biology Main focus: Genetics / Immunology / Microbiology / Molecular Medicine
2003 - 2005	Diploma thesis Institute of Virology at the Medical School Leipzig Topic: Investigation of the infectivity of Measles Virus RNA between neuronal cells
2005	Degree: certified biologist / final grade: 1,6

Dissertation

2005 - 2009	Helmholtz Zentrum Munich Institute of Experimental Genetics Topic: Development of an osteoblast cell culture system for functional characterization and comparative analyses of mouse models with bone phenotypes and systemic investigation of an Osteogenesis imperfecta disease model

VI. Affirmation

- XII -

Ich erkläre hiermit an Eides statt, dass ich die vorliegende Arbeit selbstständig, ohne unzulässige fremde Hilfe und ausschließlich mit den angegebenen Quellen und Hilfsmitteln angefertigt habe.

Die verwendeten Literaturquellen sind im Literaturverzeichnis (References) vollsändig zitiert.

Diese Arbeit hat in dieser oder ähnlicher Form noch keiner anderen Prüfungsbehörde vorgelegen.

München, den 16.07.2009   Frank Thiele

VII. Acknowledgment